TECHNICAL REPORT S-76-4

EFFECT OF BACKFILL COMPACTION ON DESIGN CRITERIA FOR HARDENED FACILITIES: RESULTS OF SOIL-STRUCTURE INTERACTION CALCULATIONS FOR DRY TYPES I AND II BACKFILL MATERIALS

by

Jon E. Windham

Soils and Pavements Laboratory
U. S. Army Engineer Waterways Experiment Station
P. O. Box 631, Vicksburg, Miss. 39180

June 1976

Final Report

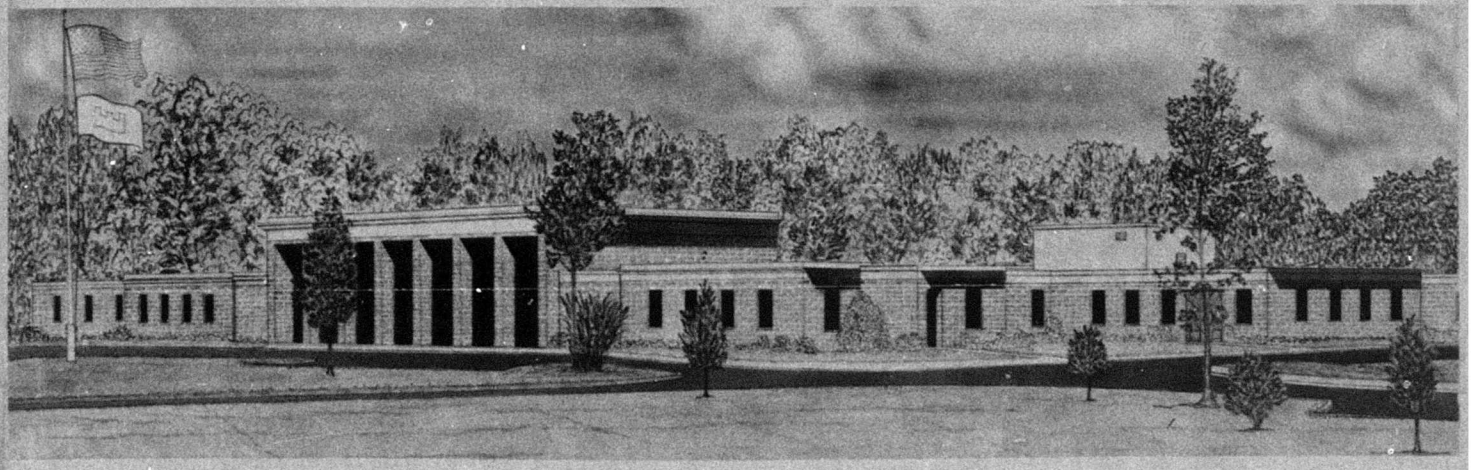

Prepared for Office, Chief of Engineers, U. S. Army
Project AT60, Task 01, Work Unit 001

T. R. S-76-4 EFFECT OF COMPACTION ON DESIGN CRITERIA FOR HARDENED FACILITIES: SOIL-STRUCTURE INTERACTION CALCULATIONS JUNE 1976

Destroy this report when no longer needed. Do not return
it to the originator.

Unclassified

SECURITY CLASSIFICATION OF THIS PAGE (When Data Entered)

REPORT DOCUMENTATION PAGE

READ INSTRUCTIONS BEFORE COMPLETING FORM

1. REPORT NUMBER: Technical Report S-76-4

2. GOVT ACCESSION NO.

3. RECIPIENT'S CATALOG NUMBER

4. TITLE (and Subtitle): EFFECT OF BACKFILL COMPACTION ON DESIGN CRITERIA FOR HARDENED FACILITIES: RESULTS OF SOIL-STRUCTURE INTERACTION CALCULATIONS FOR DRY TYPES I AND II BACKFILL MATERIALS

5. TYPE OF REPORT & PERIOD COVERED: Final report, Jul 75—Jun 75

6. PERFORMING ORG. REPORT NUMBER

7. AUTHOR(s): Jon E. Windham

8. CONTRACT OR GRANT NUMBER(s): WES-TR-S-76-4

9. PERFORMING ORGANIZATION NAME AND ADDRESS
Soils and Pavements Laboratory
U. S. Army Engineer Waterways Experiment Station
P. O. Box 631, Vicksburg, Miss. 39180

10. PROGRAM ELEMENT, PROJECT, TASK AREA & WORK UNIT NUMBERS
Project AT60, Task 01,
Work Unit 001

11. CONTROLLING OFFICE NAME AND ADDRESS
Office, Chief of Engineers, U. S. Army
Washington, D. C. 20314

12. REPORT DATE: June 1976

13. NUMBER OF PAGES: 92

14. MONITORING AGENCY NAME & ADDRESS (if different from Controlling Office): AEWES-AT60

15. SECURITY CLASS. (of this report): Unclassified

15a. DECLASSIFICATION/DOWNGRADING SCHEDULE

16. DISTRIBUTION STATEMENT (of this Report)

Approved for public release; distribution unlimited.

17. DISTRIBUTION STATEMENT (of the abstract entered in Block 20, if different from Report)

18. SUPPLEMENTARY NOTES

19. KEY WORDS (Continue on reverse side if necessary and identify by block number)

Backfills	Finite element method
Compaction (soils)	Protective structures
Constitutive properties	Soil-structure interaction
Dynamic loads	Underground structures

20. ABSTRACT (Continue on reverse side if necessary and identify by block number)

The results of a series of two-dimensional (2D) plane-strain, dynamic finite element, structure-medium interaction code calculations are presented. These calculations were made to parametrically investigate the effect of variations in constitutive properties of the backfill region around a hypothetical, shallow-buried protective structure.

Two parameter studies were conducted on this plane-strain idealization

(Continued)

DD FORM 1 JAN 73 1473 EDITION OF 1 NOV 65 IS OBSOLETE

Unclassified

SECURITY CLASSIFICATION OF THIS PAGE (When Data Entered)

038100

20. ABSTRACT (Continued)

of a simple buried structure while under a long duration local surface airblast loading. The first study investigated the differences in the dynamic response of the structure under this loading due to changing the surrounding backfill from a dense (or well-compacted) glacial till to the same material in a loose (or poorly compacted) condition; The second parameter study is identical with the first except that dense and loose clay shale materials were simulated.

The calculations performed indicated that, for the particular idealized problem investigated, the use of loose rather than dense backfill results in (a) increased deflections across backfill sections; (b) increased loads on, deflections of, and thrusts, shears, and bending moments within the structure, and (c) increased amplitudes of the shock spectra for points on the inside surface of the structure.

These results are for the case of a 50-psi overpressure loading caused by a megaton range detonation over a stiff structure. Because of the long positive phase duration, negligible stress attenuation occurs in the loose backfill in spite of its high hysteresis. This would not be the case for very short duration airblast loadings. Hence, the trends observed regarding the effect of backfill compaction on dynamic structural response should not be extrapolated to a vastly different airblast loading condition.

THE CONTENTS OF THIS REPORT ARE NOT TO BE USED FOR ADVERTISING, PUBLICATION, OR PROMOTIONAL PURPOSES. CITATION OF TRADE NAMES DOES NOT CONSTITUTE AN OFFICIAL ENDORSEMENT OR APPROVAL OF THE USE OF SUCH COMMERCIAL PRODUCTS.

PREFACE

The work reported herein was performed by personnel of the Soil Dynamics Division (SDD), Soils and Pavements Laboratory (S&PL), of the U. S. Army Engineer Waterways Experiment Station (WES) during the period July 1973-June 1975. It was sponsored by the Office, Chief of Engineers (OCE), under Project AT60, Task 01, Work Unit 001, "Effect of Backfill Compaction on Design Criteria for Advanced BMD Facilities." It supports research requirements outlined in Section XII of the Army QRR for Nuclear Weapons Effects Information. The OCE Technical Monitor for this work was Mr. D. S. Reynolds (DAEN-MCE-D).

The investigation was conducted by Dr. J. E. Windham under the direction and with the technical assistance of Dr. P. F. Hadala. Dr. G. Y. Baladi incorporated the cap model into the DUFE finite element code. Dr. N. Radhakrishnan, Special Technical Assistant, Automatic Data Processing Center, WES, assisted in many technical aspects of the computer work.

The work was conducted under the general direction of Dr. J. G. Jackson, Jr., Chief, SDD. Messrs. J. P. Sale and R. G. Ahlvin were Chief and Assistant Chief, S&PL, respectively, and COL G. H. Hilt, CE, was Director of the WES during the investigation and preparation of this report; Mr. F. R. Brown was Technical Director.

CONTENTS

CONVERSION FACTORS, U. S. CUSTOMARY TO METRIC (SI) UNITS OF MEASUREMENT

U. S. customary units of measurement used in this report can be converted to metric (SI) units as follows:

Multiply	By	To Obtain
inches	2.54	centimetres
feet	0.3048	metres
pounds (force) per square inch	6.894757	kilopascals
pounds (mass) per cubic foot	16.01846	kilograms per cubic metre
kips (force) per square inch	6894.757	kilopascals
inches per second	2.54	centimetres per second
inches per millisecond	2.54	centimetres per millisecond
feet per second	0.3048	metres per second
pounds (force) per inch	175.1268	newtons per metre
inch-pounds per inch	4.448222	newton-metres per metre
inch-kips per inch	4.448222	kilonewton-metres per metre

EFFECT OF BACKFILL COMPACTION ON DESIGN CRITERIA FOR HARDENED FACILITIES: RESULTS OF SOIL-STRUCTURE INTERACTION CALCULATIONS FOR DRY TYPES I AND II BACKFILL MATERIALS

PART I: INTRODUCTION

Background

1. Large amounts of backfill must be placed around and over ground-based advanced Ballistic Missile Defense (BMD) facilities for hardening against nuclear airblast and ground shock environments. Present specifications require the highest density practicable in a given situation to maximize the dynamic constrained modulus of the fill medium. In addition, select borrow material is often specified for use as backfill instead of the material excavated at the site. However, currently proposed modular BMD facilities may have to be installed rapidly, perhaps under adverse working conditions. Overly severe backfill density specifications would result in considerable loss of time and unnecessary additional costs; lax standards could result in intolerable hardness degradation and system failure.

2. Under Project AT60, Task 01, Work Unit 001,* the Soil Dynamics Division of the U. S. Army Engineer Waterways Experiment Station (WES) has conducted a combined experimental and analytical study designated as "Effect of Backfill Compaction on Design Criteria for Advanced BMD Facilities." The experimental portion of the study, which was completed in December 1973,** consisted of determining dynamic constitutive properties for Types I and II backfill materials obtained from the Grand Forks SAFEGUARD Missile Site Radar (MSR) site. The Type I material was a gravelly sandy clay till; the Type II material was a fragmented sandy clay shale. Each material was tested at four different compaction

---

* Formerly Project A880, Task 011, Work Unit 001.

** WES(WESSD) letter to HQDA (DAEN-MCE-D) dated 7 December 1973, Subject: Project A880, Task 11, Work Unit 001, Representative Constitutive Properties for Grand Forks Backfill (Milestone 4).

conditions, i.e., loose and dense, dry and wet. The analytical portion of the study presented herein consisted of performing a series of two-dimensional (2D), dynamic finite element, structure-medium interaction (SMI) code calculations to investigate the effect of variations in constitutive properties of surrounding backfill on the calculated dynamic response of a hypothetical thick-walled, shallow-buried, rectangular protective structure. The backfill property variations investigated were based on the test data summarized in the report referenced above.*

3. The first 2D dynamic finite element code calculation parameter study accomplished under this project has previously been outlined.** Its objective was to determine the differences in the dynamic response caused by changing the surrounding backfill from a dense, dry glacial till (material Type I at 95 percent of CE 55 maximum dry unit weight) to the same material, but placed in a loose condition (72 percent of CE 55 maximum dry unit weight) of a plane-strain idealization of a simple buried structure under local surface airblast loading. This parameter study was completed and the results were reported in Reference 1. These calculations were conducted with the DUFE finite element code using a variable moduli model and a grossly simplified structural model. Significant improvements were made in the calculation scheme (including changing the model routine to a cap model and employing an improved model of the structure) after this initial parameter study.

4. The second parameter study under this project was then conducted. This consisted of a similar parametric calculation program with the exception that the backfill was varied from a dense, dry, crushed shale (material Type II at 91 percent CE 55 maximum dry unit weight) to the same material, but placed in a loose condition (75 percent of CE 55 maximum dry unit weight). Since the improved calculational scheme produced much more realistic structural response, the loose and

---

* WES (WESSD) letter to HQDA (DAEN-MCE-D), op. cit., page 5.

** WES (WESSD) letter to HQDA (DAEN-MCE-D) dated 18 Jan 1974, Project A880, Task 11, Work Unit 001: Setup of First Structure-Medium Interaction Code Parameter Study (milestone 5).

dense till calculations were rerun using the improved constitutive model and structural idealization. This was the third parameter study.

Purpose and Scope

5. The purpose of this code calculation parameter study is to determine the effects of changes in backfill constitutive properties on the dynamic response of an idealized simple buried structure subject to surface airblast loadings typical of BMD threats. These changes in backfill constitutive properties are representative of changes in backfill compaction quality (i.e., from dense to loose). The objectives of this report are to (a) outline the plan of analysis performed for this SMI parameter study, (b) present the constitutive model fits to the loose and dense Types I and II backfill properties, (c) describe the five dynamic finite element code calculations performed, (d) present the calculation results and comparative analyses, and (e) discuss the analyses and the design implications of these results. The calculations presented herein include only those conducted using the improved calculational scheme employing a cap model, i.e., the second and third parameter studies. The results of the first parameter study conducted under this project, as reported in Reference 1, now are known to be subject to numerical problems and, therefore, are not included.

6. The calculations described herein were conducted with DUFE, a 2D, nonlinear, small-strain, axisymmetric, dynamic finite element computer code. DUFE is similar to NOFEAR[2] with the exception that the equations of motion are solved explicitly in DUFE while they are solved implicitly in NOFEAR. The DUFE code has been used for soil structure-interaction analyses of underground missile silos as described in Reference 3. The material model in DUFE was changed from a variable moduli model, which does not guarantee uniqueness in neutral loading, to a soil cap model.* This cap model is the same as that being used

---

* WES (WESSD) letter to U. S. Army SAFEGUARD System Command dated 22 December 1973, Subject: Site Defense Ground Motion Criteria Studies; Supplementary Profile and Property Information for Site 1.

in the most advanced finite difference free-field ground shock calculation codes. In this new model, mathematical uniqueness and stability are unconditionally guaranteed for all possible stress paths.

PART II: PLAN OF STUDY

7. Figure 1 illustrates the geometry of the plane-strain problem investigated and its finite element grid representation. The free-field medium is postulated as a four-layered soil profile consisting of clayey sand over clay shale (Material Nos. 1-4). The structure is a hypothetical one and is assumed to be constructed of reinforced concrete (Material No. 5) and laterally supported and covered by a bowl of backfill (Material No. 6), whose constitutive properties are the only calculation variables. As previously mentioned, in the second parameter study, loose and dense shale (Type II backfill) properties were used and in the third, loose and dense till (Type I backfill) properties were used. Stress-strain curves for the loose and dense shale backfill and loose and dense till materials in a state of uniaxial strain (UX) are given in Figures 2 and 3, respectively. As shown in the figures, the loose backfill is much less stiff than the dense for both the till and shale. The dense till backfill is slightly stiffer than the dense shale and the loose shale is much stiffer than the loose till.

Finite Element Representation

8. The problem illustrated in Figure 1 was solved using different backfill materials with the DUFE finite element code on the WES GE 635 computer. The finite element grid employed is shown in the figure and consisted of 588 uniform strain rectangular elements. The elements located in the structure ranged from 2 by 2-1/2 ft to 2 by 5 ft.* In the backfill the elements were 2 by 2-1/2 ft, 2-1/2 by 4 ft, 2-1/2 by 5 ft, and 5 by 5 ft. In the stiffer and deeper earth material, elements were larger. The largest elements were in the corners of the grid and were 20 by 20 ft. The grid was chosen as a compromise between (a) the desire for fine resolution, and (b) the need to keep computer memory

---

* A table of factors for converting U. S. customary units of measurement to metric (SI) units is presented on page 4.

and running time (and, hence, cost) requirements within reason for the particular computer used. On a larger computer, a finer resolution of the problem would have been economically feasible. The present calculations were planned to preserve frequencies up to at least 50 Hz in the dense backfill calculation* and to have a minimum of at least two elements across each structural section (in order to get at least a crude approximation of bending phenomena). Obviously, doubling both of these criteria would be highly desirable for future studies. Nevertheless, the criteria used appear to have been adequate for problems involving qualitative comparisons of the effects of the variable under study.

The Hypothetical Structure

9. The idealized structure is covered by 5 ft of backfill and is supported on undisturbed shale at a depth of 30 ft; the structure has outside dimensions of 40 by 25 ft. Its roof and floor are 5 ft thick. Its sidewalls are 4 ft thick. Each member has two constant strain elements across the section. The element size in the structure varies from 2 by 2-1/2 ft to 2 by 5 ft. The exterior structure elements are treated as fully bonded to those of the backfill and underlying shale, as no slip element capability exists in the DUFE code. The structure is treated as a linear elastic material with a bulk modulus K of 1330 ksi and a shear modulus G of 800 ksi.** The structure is assumed to have a unit weight of 145 pcf. The calculated fundamental frequency of the roof of the structure, if assumed to be a one-way slab with simple supports, is 12.4 Hz and 28.5 Hz if full fixity is assumed. The calculations to be presented show that the actual conditions are closer to those of simple support.

---

* In the case of the loose till backfill, the valid frequency response of the grid shown in Figure 1 may be as low as 25 Hz. To obtain better frequency response, the use of a much finer grid would have been necessary due to the very low loading wave velocities of the backfills.

** These values are somewhat low for typical concretes. The choice was made in order to keep the time step necessary to satisfy the stability criterion within economically acceptable limits.

Constitutive Relations

10. All of the earth materials were represented in the calculations by nonlinear hysteretic soil cap models.* The constitutive properties and soil cap model fits for the in situ materials (Material Nos. 1-4) are those of the Site Defense Ground Shock Working Group's idealized site No. 1.* The constitutive properties of the backfill materials are those for the loose and dense shale and till backfill materials, which are both assumed to be at a water content dry of optimum.** These constitutive properties are reproduced with their respective soil cap model fits in Appendix A. The constitutive model constants for the loose and dense shale and till cap model fits are also given in Appexdix A.

Surface Loading

11. The traveling surface airblast loading function employed in the calculations is shown in Figure 1. The loading portion is defined by a linear rise to peak pressure in a constant time of 10 msec; the decay portion is that for a 1-Mt weapon detonated at a zero height of burst and at a distance from ground zero which will cause a 50-psi peak surface overpressure. Appending the artificial 10-msec rise time to the 1-Mt overpressure pulse increases the impulse at the 50-psi level by 11.5 percent. Based on criteria developed for 1D elastic wave propagation problems, even longer rise times should be employed if the lowest moduli for the backfill materials are used to calculate the elastic wave speeds and the finite element grid remains as defined in Figure 1. But to append a longer rise time to the overpressure function would unrealistically distort the airblast impulse. It could be satisfied by increasing the number of finite elements used to zone the problem; but this would be cost-prohibitive. Thus, 10 msec is a compromise value which may be artificially increased by the finite element grid after it

* Op. cit., page 7.
** Op. cit., page 5.

has propagated a short distance into the backfill media. The airblast propagation velocity is 2200 ft/sec. The decay of the applied pressure with time is rather slow and is typical of that for megaton range detonations at this overpressure level. At 300 msec when the calculations were terminated, the surface airblast is about one-half of the peak overpressure.

Time Increment and Duration

12. Each calculation ran for a total of 1500 time steps of 0.2 msec each. This step was chosen to satisfy the Courant criteria* and was controlled by the minimum finite element dimension and P-wave velocity within the elastic structure. The lowest frequencies that could be fully transmitted are given by the reciprocal of the calculation pulse duration, i.e., 1/300 msec or 3.33 Hz. The highest frequencies that were fully transmitted are given by the reciprocal of the calculation rise time, i.e., 1/10 msec or 100 Hz. As a practical matter, however, credible frequencies will probably not exceed one-half this value or 50 Hz. Since the running time of these 300-msec calculations on the GE 635 computer was about 4-1/2 hr, it was impractical to extend the calculations for the full positive phase duration or to rezone the problems much finer to produce better frequency response in the loose backfill calculations.

Output Data

13. Time histories of stress and motion were saved from each calculation at numerous locations in the structure and in the earth media. These locations are shown in Figure 4. This figure also shows some of the details of the finite element grid in the vicinity of the idealized structure. Element and node numbers are identified in the figure. These numbers may prove useful to the reader, as the stress and motion time histories presented later in the report are keyed to these numbers.

---

* $\Delta t \leq \frac{\Delta x_{min}}{CP_{max}} \leq \frac{2.0 \text{ ft}}{8.76 \text{ ft/msec}} \leq 0.228 \text{ msec}.$

Artificial Viscosity

14. No problems were encountered in conducting the dense shale and dense till calculations. However, when the loose shale calculation was performed, using the same grid spacing used for the dense shale calculation, large oscillations resulted in stress- and acceleration-time output. This problem was traced to the exaggerated S-shaped nature of the UX stress-strain curve (see Figure 2). The possible solution for overcoming this problem was to reduce the grid spacing or to introduce artificial viscosity. Although the best way to solve the problem is to reduce the grid size, this alternative was determined to be impractical in terms of cost and computer time on the particular computer employed in this study. Therefore, the artificial viscosity solution was pursued. A series of 1D calculations with loose shale backfill properties and varying amounts of a linear, velocity dependent artificial viscosity were conducted. It was found that the material properties actually used during a calculation with artificial viscosity were changed. These changes were investigated (see Appendix B) and a final damping value was chosen for use in a 2D calculation for the loose shale problem. An undamped loose shale 2D run was also conducted. The results of loose shale calculations with and without artificial viscosity are compared in the subsequent analyses plots. These comparisons showed very little difference in the results of the damped and undamped calculations except, of course, that the spurious banded oscillations were reduced in the damped case. Therefore, for the loose till only one calculation (without artificial viscosity) was conducted.

PART III: PRESENTATION AND ANALYSIS OF COMPUTATIONAL RESULTS

Stress and Displacement Patterns at Selected Times

Deflection across backfill sections

15. Calculated vertical displacement patterns for sections through the loose and dense backfills at 105 and 285 msec after the start of the calculations are shown in Figures 5 and 6, respectively, for the shale backfill and in Figures 7 and 8 for the till backfill. As can be seen in Figures 5 and 7, the vertical deflections in the loose shale and till backfill, respectively, at the 5-ft depth are much larger at 105 msec than those in the dense shale and till, respectively. This appears reasonable in the light of the stress-strain relations for these materials. However, the displacements at the 15-ft depth for the dense backfill cases at this time are larger than those for the loose backfill because the higher wave velocities of the dense shale and till have allowed the peak stresses to propagate to a greater depth. At 285 msec, however, when wave propagation no longer plays a major role and the peak free-field stress has occurred at all depths of interest, the vertical displacements are everywhere larger in the loose shale and till calculations than they are in those for the dense materials, as shown in Figures 6 and 8, respectively. At 285 msec, the vertical displacements of the loose and dense shale backfill differ by nearly a factor of 5 near the structure, i.e., the maximum deflection for the dense shale calculation is 3 in. and the maximum deflection for the loose shale calculation is 15 in. At the same time, the maximum deflection for the loose till is 25 in. and is greater by a factor of 8 than the 3-in. deflection calculated for the dense till. The maximum deflections for the two dense backfills are almost identical, while the deflections for the loose till are almost a factor of 2 higher than those for the loose shale. An examination of Figures 2 and 3 indicates that this trend is reasonable, as shown below:

Backfill	Axial Strain at 50-psi Vertical Stress in UX %	Max Deflection at 5-ft Depth at 285 msec in.
Dense shale	0.91	3
Dense till	0.89	3
Loose shale	6.10	15
Loose till	9.90	25

16. The interface of the backfill and structure should have been treated computationally by some type of slip element so that the relatively compressible backfill could deflect vertically with respect to the concrete structure which is founded on undisturbed clay shale. This type of element was not available. Since the structure and backfill were "welded" together, it is inevitable that very little deflection would occur near the structure walls. Of course, this is not the case in the real world. However, the backfill vertical deflections did maximize at a distance of approximately 15 ft from the structure (see Figures 5 through 8) for all cases. Deflections close to but perhaps less than the maximum shown for the backfill (because of wall friction) should be expected close to the structure. The deflections calculated in the backfill from the loose till and shale calculations would be considered very severe for cables or pipes which might be connected to the structure at some point along the sidewall. Therefore, these figures indicated that the design of cable or pipe connections which permit as much as 2 ft of relative vertical displacement at the soil-structure interface must be considered if expedient backfill is used.

Stresses on the exterior surfaces of the structure

17. The instantaneous distribution of normal stress on the structure at 105 and 235 msec is shown in Figures 9 and 10, respectively, for the shale backfill calculations. The normal stress on the structure at 115 and 230 msec for the loose and dense till calculations are shown in Figures 11 and 12, respectively. In actuality, these stresses are the horizontal stresses in the middle of the soil "cells" adjacent to the structure. The 105- and 115-msec times represent the time at which

the maximum deflection at the center of the roof of the structure is realized for the shale and till calculations, respectively. The 230- and 235-msec times represent times at which the structure undergoes the maximum clockwise (away from ground zero, GZ) rotation for the loose till and shale calculations, respectively. The roof loads shown in these figures are qualitatively similar. Although the loads are somewhat variable with position, they are fairly uniform, except in the region immediately above the stiff sidewalls where "negative" arching has caused the loading to be concentrated. The normal stresses on the blastward sidewall from the dense shale and dense till calculations at 105 (Figure 9) and 115 msec (Figure 11), respectively, are higher than those for the loose shale and till, respectively; the higher wave velocity of the dense backfill materials has permitted significant stress amplitude to propagate further down into the backfill.

18. At 230 and 235 msec for the shale and till backfill calculations, respectively, wave propagation no longer plays a major role in the loading. The sidewall stresses near the top of the leeward side of the structure, in the loose backfill calculations, are considerably larger than those at the same location in the dense backfill calculations. On the blastward side, the stresses in the loose and dense backfill calculations are roughly comparable.

19. The normal load on the base of the structure for the loose shale calculations at 105 msec, shown in Figure 9, and for the loose till calculation at 115 msec, shown in Figure 11, is concentrated under the sidewalls and is a minimum under the center of the structure. However, the stresses under the blastward sidewall in the cases of the loose backfill are approximately a factor of 2 higher than are the comparable stresses for the dense backfill cases. At these times, for the cases of both the loose and dense backfill, the normal stresses under the blastward sidewall are higher than those under the leeward sidewall. This indicates a possible counterclockwise rotation of the structure. That is probably due to the fact that the loose backfill cannot offer as much resistance to the rotation as does the dense backfill. Therefore, the foundation is required to supply a larger

restoring moment in the loose till cases.

20. At 235 msec, as shown in Figure 10, the blastward portion of the base tends to pull away from the soil, causing a tension cutoff to occur in the loose shale calculations. This, coupled with the buildup in stress on the upper part of the leeward sidewall and on the base under the leeward sidewall, indicates that the structure is tending to rotate in a clockwise direction at 235 msec. These same trends are noted at 230 msec in the loose till backfill calculation, as shown in Figure 12. The data suggest that rotation is occurring to a much greater extent for the loose backfill cases, and this appears reasonable, since the loose backfills would offer less resistance to rotation than would the dense backfills.

Deflections of the
structure at selected times

21. The deflected shapes of the outside of the structure at 105 and 235 msec after the start of the calculations are shown in Figures 13 and 14, respectively, for the shale backfill. The deflections of the structure at 115 and 230 msec for the till backfill calculations are shown in Figures 15 and 16, respectively. The deflection patterns from all the calculations are similar. At 105 msec, as shown in Figure 13, the downward deflections of the center of the roof and the outward deflections of the midpoints of the sidewalls are approximately 50 percent larger in the case of the loose shale than are those for the dense shale. The deflections of the structure floor are at maximum under the highly stressed sidewalls and at minimum under the center. At 115 msec, as shown in Figure 15, the downward deflections of the center of the roof and the outward deflection of the sidewalls in the case of the loose till are 50 percent higher than those for the dense till. As shown by the sidewall deflections in Figures 14 and 16 at 235 msec and 230 msec, respectively, the structure has moved downrange slightly more in the loose backfill than it did in the dense backfill.

Rotation of the structure

22. The maximum rotations of the chord formed by the two bottom outside corners of the structure are shown in Table 1, for all

calculations. As shown by the data, the structures undergo similar initial counterclockwise rotations during all calculations. Later, the structure, in both loose shale and loose till, undergoes a clockwise rotation; the structure in the dense shale and till does not. These rotations appear fully compatible with the structure loadings and do not appear to threaten the structure's integrity; 0.001 radian, the maximum rotation depicted during this series of calculations, represents only 1/2 in. of differential displacement over the length of the structure.

Thrusts, shear forces, and bending moments within the structure

23. Axial thrust, shear force, and bending moment per unit width of the structure were calculated from the output data for the 12 structure sections shown in Figure 17. These quantities, at 105 and 210 msec, are shown in Tables 2 and 3, respectively, for the shale calculations. Agreement of these values for the loose shale with and without artificial viscosity was good. As can be seen by examining the tables, the shear forces, axial thrusts, and bending moments for the loose backfill are higher at most sections than are those for the dense backfill calculations. On the average, the shear forces for the loose shale calculations without artificial viscosity were approximately 2.8 and 3.5 times the shear forces for the dense shale at 105 and 210 msec, respectively. The shear forces for the loose till calculation averaged approximately 4.8 and 2.5 times those for the dense till at 105 and 210 msec, respectively. Axial thrust for the undamped loose shale calculations averaged 1.5 times those for the dense shale at both times studied. Axial thrusts for the loose till calculations averaged 3.5 and 2.0 times those for the dense till at 105 and 210 msec, respectively. Bending moments for the loose shale calculations averaged 1.8 and 1.3 times those for the dense shale at 105 and 210 msec, respectively, and bending moments for the loose till at 105 and 210 msec, respectively. These tables show conclusively that the loose backfill tends to significantly increase the thrust, shear, and bending moments at most sections within the structure over those which are experienced with dense backfill.

24. For the structure examined here (see Figure 17) it can be shown that even the largest of these shears, thrusts, and moments do not pose any real threat to structural integrity if one assumes reasonable strength properties for the reinforced concrete* and determines the available resistance of the sections according to the methods of Section 8.3 of ASCE Manual 42.[4] Figure 18 shows a thrust-moment interaction diagram for yielding a structural section that could be considered typical of those in the idealized structure. Also shown in the figure are data from Table 2 which show the thrusts and moments on sections AA, GG, DD, and JJ for the loose and dense shale calculations. A change from dense to loose shale backfill caused both the thrust and moments to increase. The same was true for the till backfill except at section DD as indicated by the data in Table 4 which have also been plotted in the figure.

25. What do the increases in thrusts, moments, and shears, which have been shown to occur as backfill quality decreases, mean in terms of structural integrity, changes in strength design criteria, and resulting costs? For the structure studied here there is no criterial impact because it is clearly "overdesigned." However, if the structure were assumed to be fabricated from lower strength materials and/or if its section thicknesses had been reduced, it appears likely from the trends in the data shown in Figure 19 that structural integrity would have been threatened by a decrease in backfill quality. Poorer quality backfill material or reduced compaction effort may be considered in an effort to reduce construction time or cost or as a rapid deployment concept. This consideration, however, must be balanced against changes in design loadings which would cause increased safe minimum section thicknesses or increased strengths of construction materials (steel and concrete). These design changes will, of course, have their own time and cost penalties.

---

* For example, 1 percent of intermediate grade reinforcing steel in each face and a 28-day concrete strength of 4000 psi.

Selected Time Histories

26. Figures 19-42 present comparisons of selected stress or motion time histories from the 2D calculations for the loose and dense shale and till backfill cases. In each figure, the element and/or node number locations are sketched. The sign convention for these figures is as follows: upward and outward movement and tensile stresses are considered positive. Wave forms for the loose shale calculations, with and without artificial viscosity, are shown in these figures along with wave forms for the single dense shale calculation, which employed no artificial viscosity. In the figures and in the subsequent text, the loose shale calculation with artificial viscosity is referred to as "damped" and that without the artificial viscosity as "undamped." Generally, there were only small differences between the wave forms for the two loose shale calculations. However, there were appreciable differences between the wave forms from the loose backfill and the dense backfill calculations. These differences will be discussed in the following paragraphs.

27. Figures 19 and 20 show the vertical velocity and displacement time histories for the center of the roof span for the shale and till calculations, respectively. Slightly larger maximum vertical displacements and maximum downward velocities which were approximately a factor of 2 higher are shown to occur for the loose backfill cases. The period of the oscillation in the motion at this point which occurs after the first relative maximum displacement ranged from 67 to 89 msec. This corresponds to a frequency range of 11 to 15 Hz. As indicated in paragraph 9, a simply supported one-way slab with the same section as the roof would have a fundamental frequency of 12.4 Hz, while the same slab with complete end fixity would have a natural frequency of 28.5 Hz. If the mass of the 5 ft of earth cover is assumed to act with the slab, each of these calculated numbers would be reduced to 70 to 80 percent of the values cited above. The observed range of frequencies indicates that the roof is behaving almost as if it were simply supported. This is also substantiated by the data for sections BB and LL in Tables 2

through 5 which indicate moments that are only a few percent of the values which would be expected for a fixed-ended slab under a 50-psi uniform load (i.e., $WL^2/12$).

28. Figures 21 and 22 show the horizontal stresses at a point midway from the neutral axis to the top and bottom fibers of the roof for the shale and till backfill calculations, respectively. As can be seen, the peak stresses above and below the axis are of opposite sign and are notably higher for the loose backfill cases. The stresses shown in Figures 21 and 22 are reasonable when compared with the deflections shown in Figures 15 and 16; the top fiber is in compression and the bottom in tension.

29. Figures 23 and 24 show the vertical and horizontal velocity time histories for the upper blastward corner of the structure for the shale and till calculations, respectively. The peak downward velocity of this point is slightly greater for the dense shale than for the loose shale and slightly higher for the loose till than for the dense till.

30. Significant upward and outward velocities occur at approximately 140 to 150 msec for the loose backfill calculations. These components are believed to be related to the tendency of the structure to rotate in a clockwise direction at this time. These calculations further support the trends in other calculation results presented earlier in this report. The radial velocities for this point (node 219) are higher for the loose shale and till calculations than for the dense shale and till calculations, respectively. Vertical and radial displacement time histories for a point (node 258) near the midheight of the blastward sidewall of the structure are shown in Figures 25 and 26 for the shale and till calculations, respectively. The deflections for all the backfill cases are very similar. The maximum vertical deflections are on the order of 1 in. and the radial deflections are less than 1/2 in. for all backfill cases.

31. Figures 27-30 compare vertical deflection time histories of points on the blastward face of the structure with those for adjacent points in the backfill. As can be seen, the maximum vertical deflections of points on the structure are similar (i.e., range from 0.7 to

1.1 in.) for all backfill cases. The reason for this is that the vertical deflection of the structure is mainly controlled by the relatively incompressible clay shale material upon which it rests. The purpose of these figures is to examine the vertical deflections of the backfill with respect to the structure as a function of time. While the comparisons show that the relative displacements of the loose backfills are much greater than for the dense backfills, the quantitative values of deflections for the backfill materials are not believed to be correct. The points in the backfill were only 10 ft from the structure and the deflections indicated by these points are influenced by the welding of the backfill elements to the structural elements at the soil-structure interface (see discussion in paragraph 16).

32. Figures 27 and 28 compare the vertical deflection for a point (node 219) on the blastward sidewall of the structure at a depth of 5 ft below the ground surface with that for a point (node 183) in the adjacent backfill (a distance of 10 ft horizontally from the structure) for the shale and till backfill cases, respectively. Figures 29 and 30 compare the vertical deflections for a point on the structure at a depth of 20 ft (node 223) with those for a point in the backfill (node 187) (10 ft horizontally from the structure) for the shale and till backfill cases, respectively. As shown in Figures 27-30, the vertical deflections of the backfill and structure are downward in all cases until the maximum deflection is reached and then remain fairly constant. At the 5-ft depth, as shown in Figures 27 and 28, the vertical downward displacement of the backfill for all cases is always greater than is the downward displacement for the structure. However, for the 20-ft depth, as shown in Figures 29 and 30, the structure moves down with respect to the backfill at early times. This phenomenon occurs because at early times a significant stress has not propagated to a depth of 20 ft through the backfill materials while significant stress has been applied to the roof of the structure, which is only 5 ft below the ground surface. (See similar discussion in paragraph 15.) The maximum downward displacements of the structure relative to the backfill for the 20-ft depth and the times at which they occur are tabulated below:

Backfill	Max Downward Displacement of Structure Relative to Backfill, in.	Time at Which Max Occurs msec
Dense shale	0.25	72
Loose shale (damped)	0.35	95
Loose shale (undamped)	0.50	100
Loose till	0.70	115
Dense till	0.10	70

As shown in Figures 29 and 30, the downward displacement of the dense backfill for the till and shale cases catches up with that for the structure at a time of 80 msec, while the loose backfill materials catch up at a time of 150 to 160 msec. This results because the wave velocities of the dense backfill materials are greater than those for the loose backfills. After these times the total downward displacements of the backfills are always greater than that for the structure. The maximum downward displacements of the backfill relative to the structure for the 20-ft depth are tabulated below:

Backfill	Max Downward Displacement of Backfill Relative to Structure, in.	Time at Which Max Occurs msec
Dense shale	0.25	115
Loose shale (damped)	3.9	195
Loose shale (undamped)	3.3	200
Loose till	6.0	260
Dense till	0.5	125

33. The fact that for certain cases the structure has been shown to deflect downward with respect to the backfill at early times could be a very significant consideration when designing cable or pipe connections to protective structures. As shown in the first tabulation in paragraph 32, the relative downward displacement of the structure with respect to that for the loose shale and till backfill is a factor of 2 to 7 higher than the relative downward displacement of the structure with respect to that for the dense shale and till backfill, respectively. The second tabulation in paragraph 32 shows that the relative downward

vertical displacements of the backfill with respect to the structure (for the 20-ft depth) represent a worse environment for designing cable or pipe connections to a structure. The expedient backfill case presents the most severe conditions, from a design standpoint, for relative displacement of the structure-backfill system in either vertical direction.

34. Figures 31 and 32 show the time histories of horizontal stress at two points on the blastward sidewall* for the shale and till calculations, respectively. The horizontal stress arrives sooner in the dense shale and till backfills than in the respective loose backfills due to the higher wave speeds in the dense backfills. Figures 33-35 present selected stress time histories of stress components in the blastward sidewall for the shale calculations, and Figures 36-38 present stress time histories for the same locations for the till calculations. In all cases, except for the horizontal stress at element 207, the loose backfill represents the most severe condition. Figure 35 shows the vertical stress time histories from the shale calculations in the blastward sidewall at the midheight (elements 210 and 227). Initially, both elements experience compressive loadings for both the loose and dense shale cases; however, as the blastward sidewall begins to bow outward, the stress in element 210 for both cases becomes tensile and element 227 remains in compression. The stress in element 227 is relieved for both loose and dense backfill cases and reaches a minimum at approximately 140 to 150 msec in time. This relief of stress is greater for the loose backfill case and probably is due to rotation of the structure in a clockwise direction that is occurring at this time (see Table 2). This same trend is also depicted in the results for the till backfill calculations as shown in Figure 38.

35. Examination of the time histories of stress and motion shows the presence of frequencies of up to 200 Hz in the wave forms for points in the structure. The calculated cutoff frequency in the structure is

---

* Actually in the middle of a cell of backfill immediately adjacent to the structure.

at least 300 Hz. However, the cutoff frequency of the backfill is much lower. It is roughly 25 or 50 Hz depending on whether the backfill is loose or dense. The rise time of stress on the surface was artificially lengthened to 10 msec to minimize artificial lengthening of the rise time due to the frequency transmission limitation of the backfill. In view of these factors, it appears that, for points within the structure, frequencies up to 50 Hz should be represented in a fairly faithful manner for the idealized problem calculated and that some creditability can be given to components as high as 100 Hz. Clearly, because the duration of the calculation is only 300 msec, frequencies below 6 Hz are also suspected and those below 3 Hz are, of course, absent. The results presented appear to be a reasonable approximation of the effect of local airslap on the structure-backfill system in the frequency range cited. However, in the actual nuclear blast and shock environment at the 50-psi overpressure level, considerable low-frequency ground roll, which is not present in the calculated motion wave forms presented here, should be expected.

Shock Spectra Analyses

36. The effects of backfill variations on the response of possible equipment mounting points on the roof, sidewalls, and on the floor can be considered by examining the shock spectra for the motion wave forms calculated for these locations. Figures 43-50 present 2 percent damped shock spectra calculated for the velocity wave forms in Figures 19 and 20 and 39-42. The inside of the roof of the structure (node 323) has the most severe calculated shock environment of those points examined. As shown in Figure 44 for the shale and in Figure 48 for the till, the loose backfill cases yield the higher shock spectra for each of the locations examined through almost all of the credible range of frequencies. The only exception to this statement is shown in Figure 50 where, for a very limited frequency range, the dense backfill case produced the more severe environment. The center of the floor of the structure has the smallest shock environment, as shown in

Figures 45 and 49. This is probably due to the fact that the floor rests on the undisturbed stiff clay shale and is shielded from the direct effects of airblast-induced ground shock.

PART IV: SUMMARY, DESIGN IMPLICATIONS, AND RECOMMENDATIONS

Generalized Results

37. The results of the calculations for loose and dense shale and till backfill demonstrate that for megaton range detonations and overpressures less than 100 psi, loose backfill tends to increase the load on, the thrusts, shears, and bending moments within, and the deflection of the particular, rather stiff, rectangular, shallow-buried structure considered. This indicates that a trade-off between expedient backfill and structural loadings should be considered in design of structures where rapid backfill with limited quality control appears to be a desirable alternative. The nature of this trade-off may not always be the one qualitatively illustrated here (namely, that decreased compaction results in increased loading) because the phenomena are highly dependent on (a) the positive phase duration of the airblast, which influences stress attenuation, and (b) the degree of rigidity of the structure. For very short duration airblast loadings or for more flexible structures, the trend conceivably could be opposite to that shown. The main point to be made from the results of this study is that decisions that influence backfill quality also have a significant effect on the levels of dynamic load for which a structure should be designed. For the case shown here, in many instances, a variation in loading of a factor of two or more resulted from the variation from well compacted to loose backfill.

The Specific Problem Considered

38. The calculated maximum deflections across the backfill section at a depth of 5 ft below the ground surface were approximately 3 in. for the dense till and shale and 15 and 25 in. for the loose shale and till, respectively. Deflections of 15 to 25 in. would represent very severe conditions for cable or pipe connections to this structure unless special connectors were used. Comparisons of displacement time histories

of points on the structure at a depth of 20 ft below the ground surface with adjacent points in the backfill showed that at early times the structure was moving down with respect to the backfill. The maximum relative displacements of the structure, with respect to the dense shale and till backfills, were 0.25 and 0.1 in. at 80 msec and, with respect to the loose shale and till backfills, were 0.5 and 0.7 in. at 100 msec and 115 msec, respectively. Relative downward displacements of the structure of 0.5 and 0.7 in. with respect to the backfill could be an important consideration in the design of cable and pipe connections to protective structures.

39. The loads on the structure for the loose backfill calculations were generally higher than those for the dense backfill calculations. Stresses under the sidewalls were a factor of 2 higher for loose backfill conditions at 105 msec. Several sections through the structure were examined in detail. In these sections, at respective times of 105 and 210 msec for the undamped loose shale calculation, the shear in the structure averaged 2.8 and 3.5, the axial thrust averaged 1.5 and 1.5, and the bending moment averaged 1.8 and 1.3 times the values for the dense shale calculations. In the loose till calculations at these same times, the average shears in the structure were 4.8 and 2.5, the axial thrusts averaged 3.5 and 2.0, and the bending moment averaged 1.9 and 2.6 times the comparable values from the dense till calculations. These data show that the shears, thrusts, and moments within the structure are considerably higher with loose backfill than with the dense backfill. The expedient backfill cases appear to present the more severe conditions from a structural design standpoint, although in all of the cases considered here, the structure was nowhere near structural failure under the dynamic loading.

40. The rotation analysis showed that, for dense backfill, the structure rotated in a counterclockwise direction at early times. As the airblast passed to the leeward side at a time of 150 msec, the structure rotated in a clockwise direction to its original position and remained approximately in this position for the remainder of the calculation (i.e. 300 msec). For loose backfill, the structure also

underwent counterclockwise rotation at early times. However, at late times the structure rotated in a clockwise position past its original position. This is reasonable, because the loose backfills offered less resistance to rotation. The maximum rotations were small, representing only 1/2-in. relative displacement over the 40-ft width of the structure, and presented no threat to the structure. However, this physically reasonable calculated behavior of the structure adds to the level of confidence in the calculation results.

41. Maximum deflections of the center of the roof and sidewalls were 50 percent higher for the loose backfill cases than for the dense backfill. Thus, the loose backfill cases presented the worst case as far as the deflections are concerned.

42. The results of the shock spectra analyses show that the shock environments for the roof, sidewalls, and floor of the structure within the credible frequency range are higher when expedient backfill is used. The point at the center of the roof presented the highest shock spectra for both of the loose backfill conditions; the point at the center of the floor of the structure experienced the least severe shock environment.

Recommendations

43. The capability of the DUFE computer code could be enhanced by several modifications. The addition of a type of slip element that could be used at interfaces of materials with greatly varying material properties, such as structure-backfill interfaces, would improve the calculation results in the areas of such interfaces. A method for applying initial gravity loading and correctly treating separations that occur as a result of tension failures should be added. Finally, a technique to drive the boundaries with motion time histories taken from large free-field computer calculations should be added to DUFE so that "soil-island" problems can be calculated.

44. The combination of the S-shaped nature of the loose shale UX stress-strain curves, a fairly coarse grid, and low moduli appears to be responsible for large oscillations in stress and acceleration time

output during the loose shale calculation. As discussed in paragraph 15, the best way, from a theoretical standpoint, to reduce the oscillations to within acceptable bounds is to reduce the grid spacing within this type of material. This was not done for the problems investigated here because of the increased cost and computer time which would be required.

45. However, if the code were put on a faster computer and if a restart capability were added so that the problem could be solved in segments, these problems could be reduced to the point where finer grid calculations would be practical for a problem of this size. It is recommended that these steps be taken. The introduction of artificial viscosity or damping as was done in one of the calculations for loose shale is not an entirely satisfactory way of handling this problem because the introduction of artificial viscosity has been shown to change the properties of the material being modeled. The occurrence, in nature, of materials with S-shaped UX stress-strain curves is very common and presents a real problem in dynamic analyses of this type. A study should be performed in which the grid size is varied within a material of this type and the effect of varying the grid on the calculated dynamic response should be evaluated.

46. Additional parameter studies should be conducted for other backfill and loading conditions. As discussed in paragraph 2, material properties were determined for loose and dense Grand Forks shale and till in wet conditions as well as for the dry conditions investigated herein. More parameter studies could be conducted for the "wet" case. Additional studies should be conducted to determine the effect of weapon yield and overpressure on the response of buried structures. The above-mentioned parameter studies should also be conducted with the soil-island technique, using input from large free-field computer calculations, and compared with calculations using boundary loadings and conditions, as described in this report.

REFERENCES

1. Hadala, P. F. and Windham, J. E., "Effect of Backfill Compaction on Design Criteria for Advanced BMD Facilities: Preliminary Results from SMI Calculation Series for Dry Type I Backfill Material," Interim Report, Jun 1974, U. S. Army Engineer Waterways Experiment Station, CE, Vicksburg, Miss.

2. Farhoomand, I. and Wilson, E., "A Nonlinear Finite Element Code for Analyzing the Blast Response of Underground Structures," Contract Report N-70-1, Jan 1970, U. S. Army Engineer Waterways Experiment Station, CE, Vicksburg, Miss; prepared by Structural Engineering Laboratory, University of California, Berkeley, Calif., under Contract No. DACA 39-67-0020.

3. Pace, Carl E. and Walker, Robert E., "Investigation of Idealized Silo Motion," Technical Report N-74-8, Dec 1974, U. S. Army Engineer Waterways Experiment Station, CE, Vicksburg, Miss.

4. Anderson, Ferd E., Jr., et al, "Design of Structures to Resist Nuclear Weapons," Manuals of Engineering Practice No. 42, 1961, Prepared by the Committee on Structural Dynamics of the Engineering Mechanics Division Through its Manual Subcommittee, Headquarters, American Society of Civil Engineers, New York.

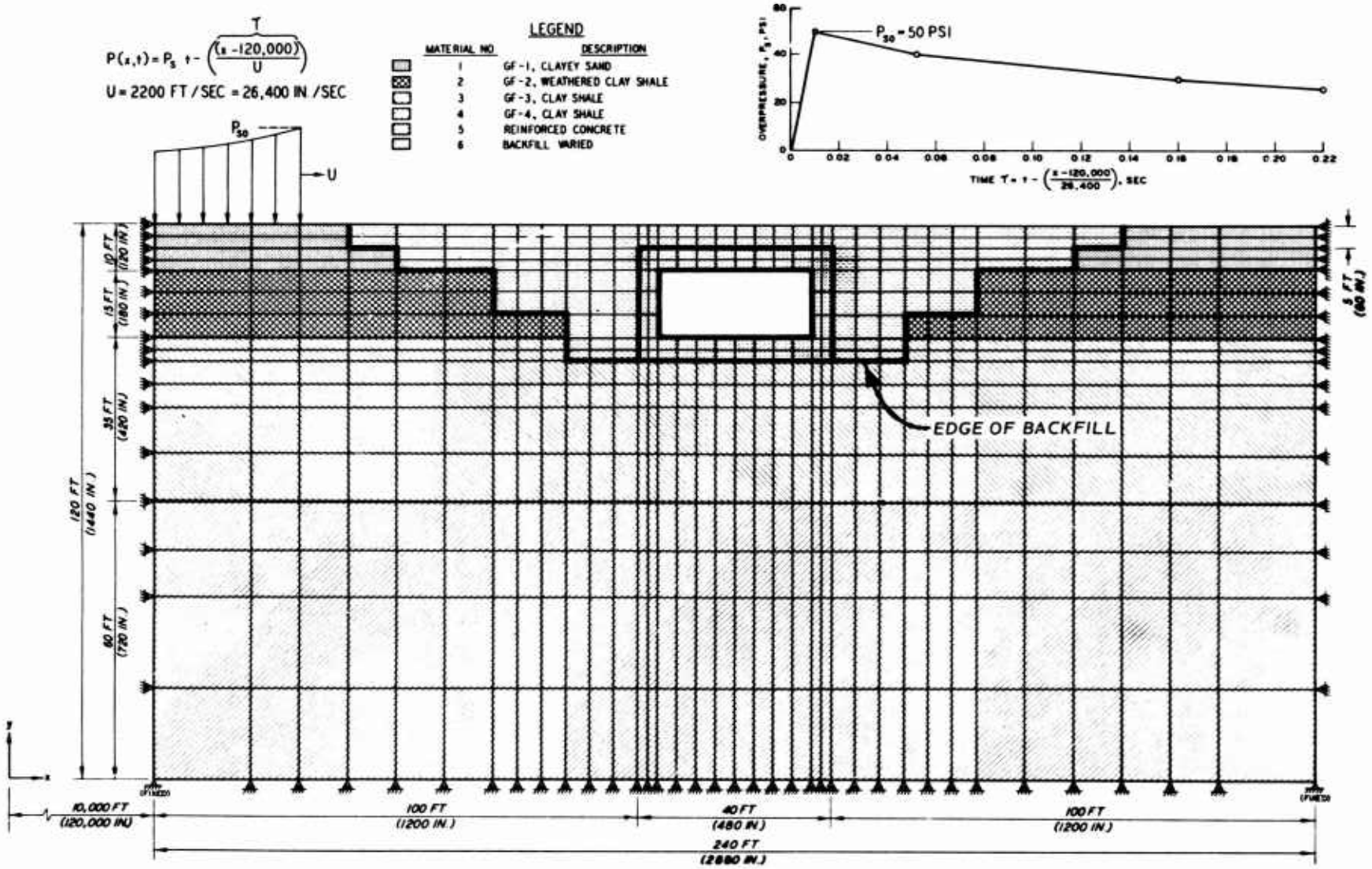

Figure 1. Geometry of and surface loading for the parameter study

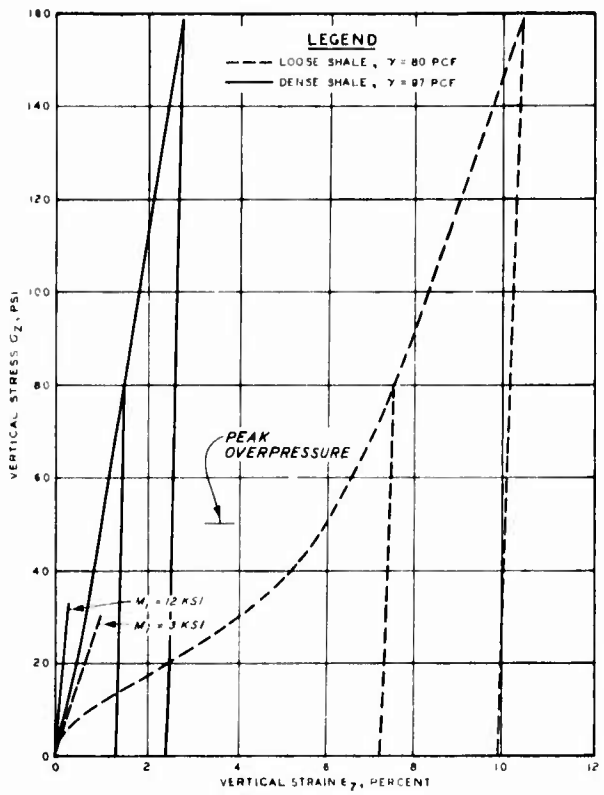

Figure 2. Comparison of UX stress-strain curves for loose and dense shale represented in the constitutive models

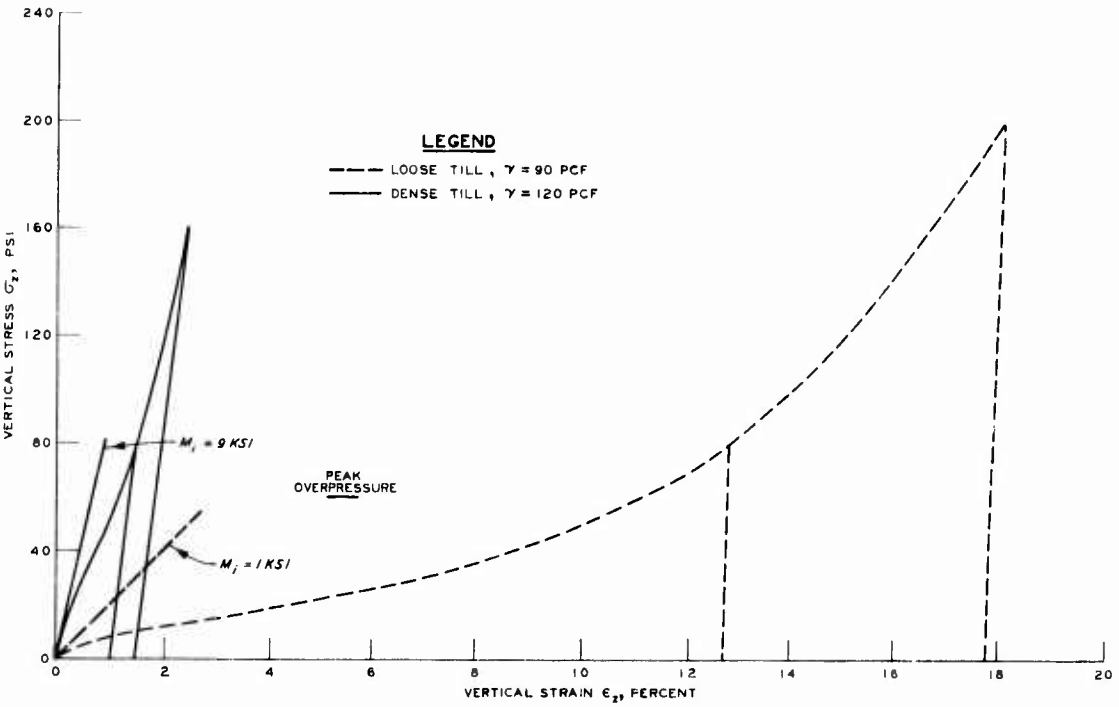

Figure 3. Comparison of UX stress-strain curves for loose and dense till represented in the constitutive models

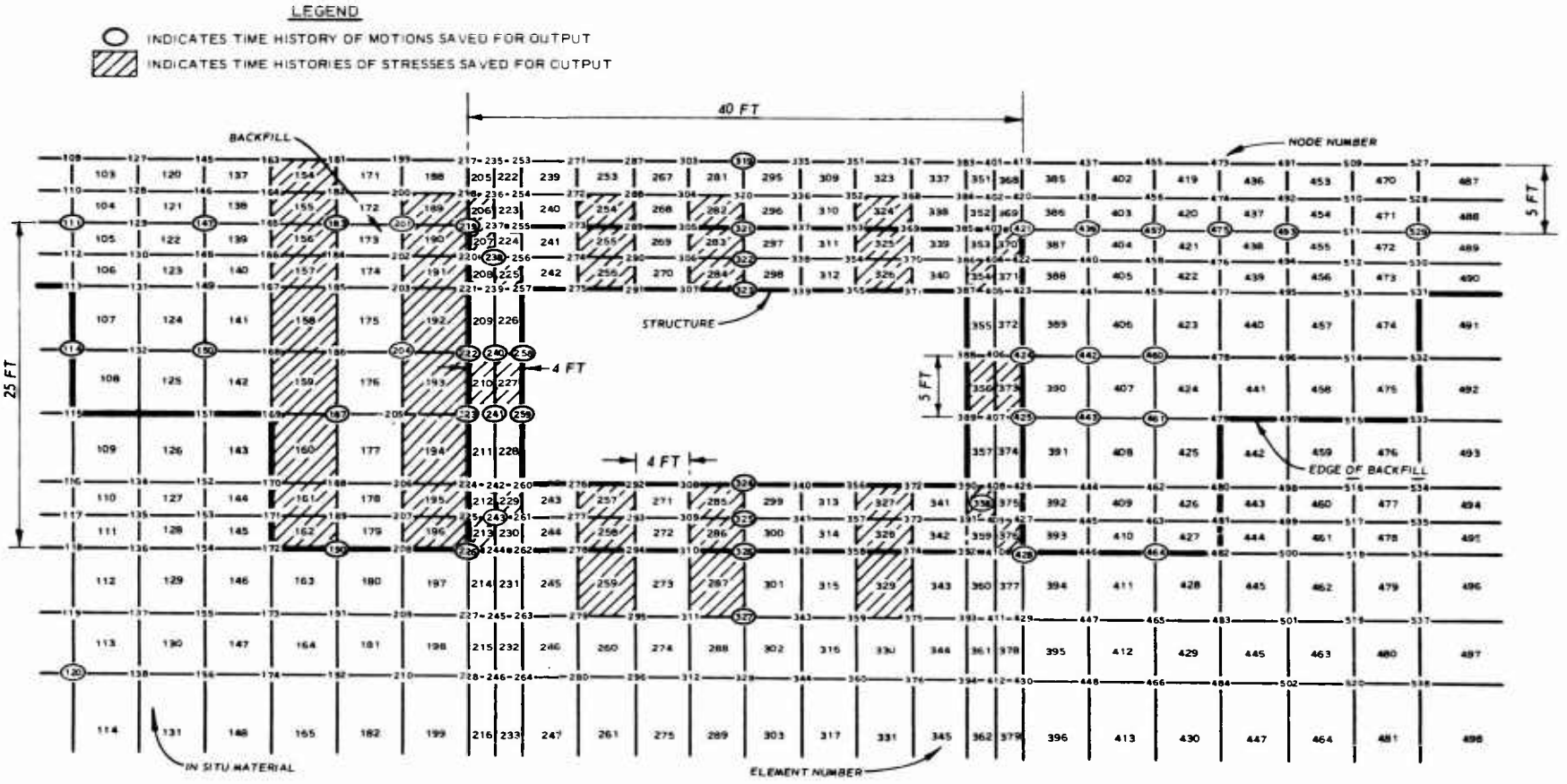

Figure 4. Detailed layout of the finite element grid in the vicinity of the structure

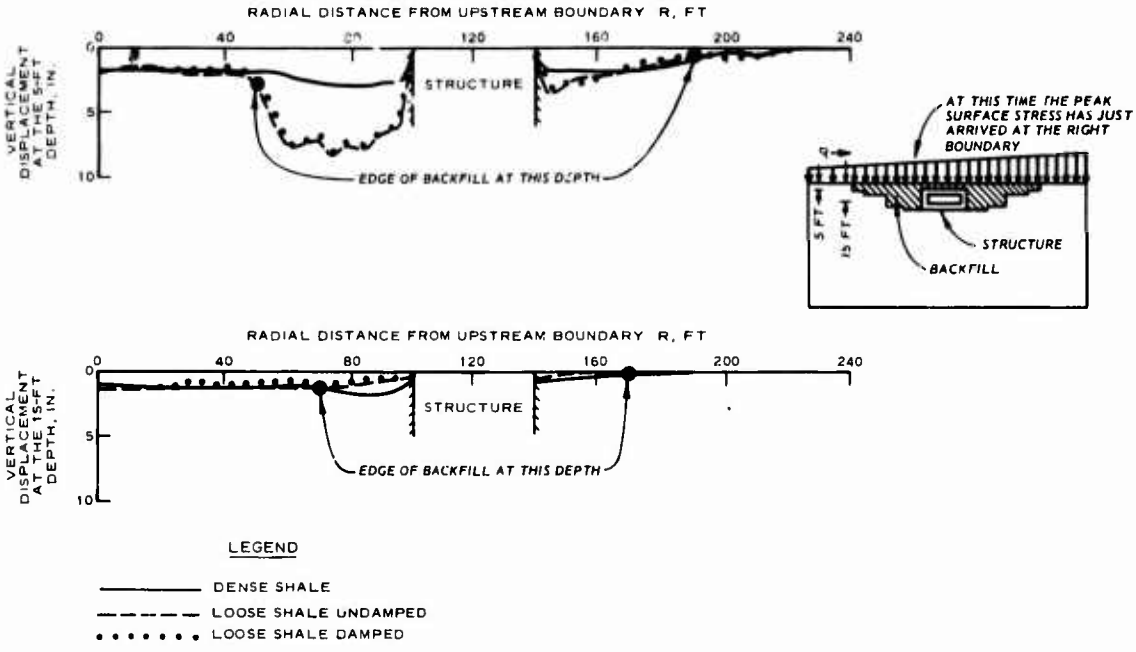

Figure 5. Instantaneous pattern of vertical displacements along two lines through the backfill zone at 105 msec after the start of the problem

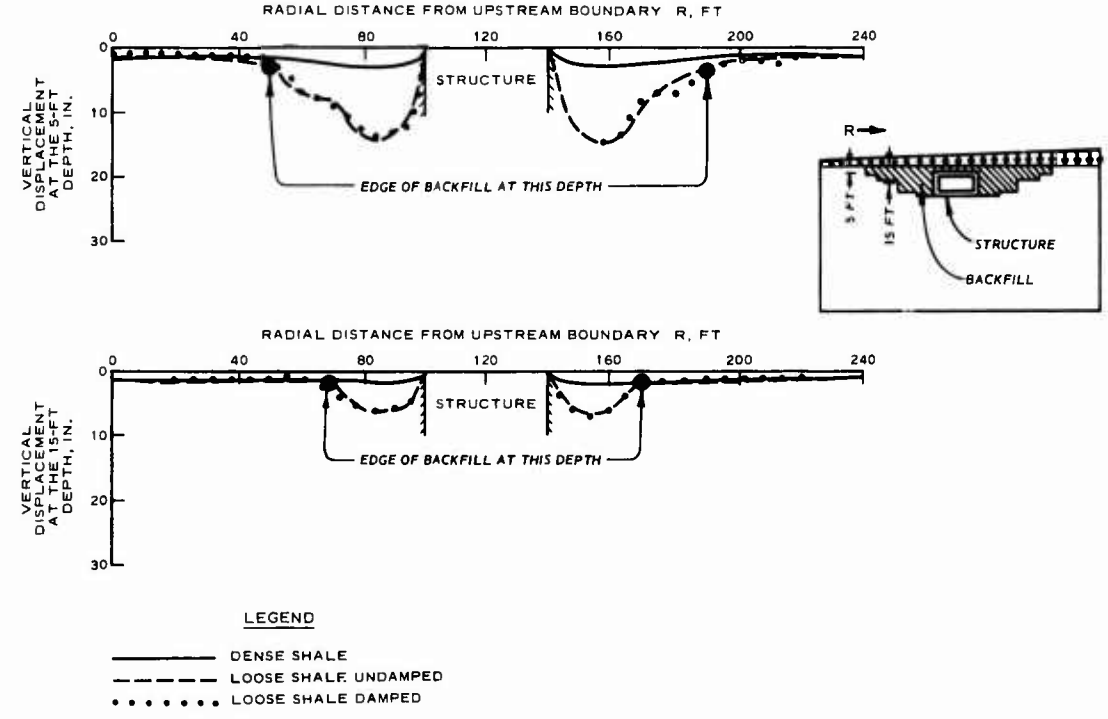

Figure 6. Instantaneous pattern of vertical displacements along two lines through the shale backfill zone at 285 msec after the start of the problem

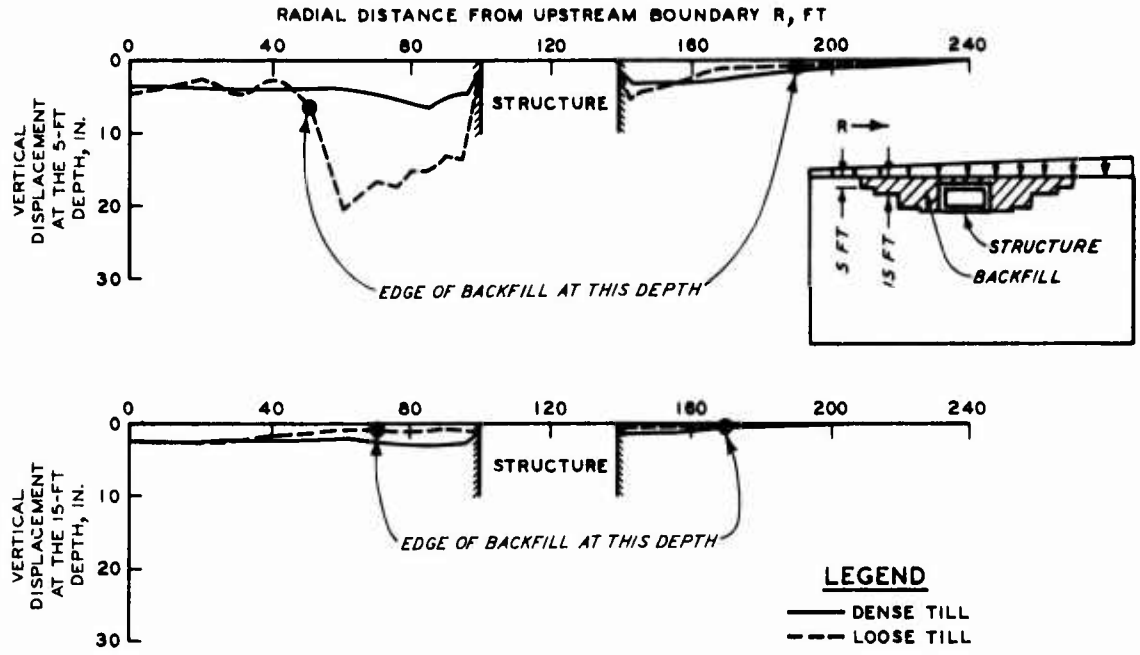

Figure 7. Instantaneous pattern of vertical displacements along two lines through the till backfill zone at 105 msec after the start of the problem

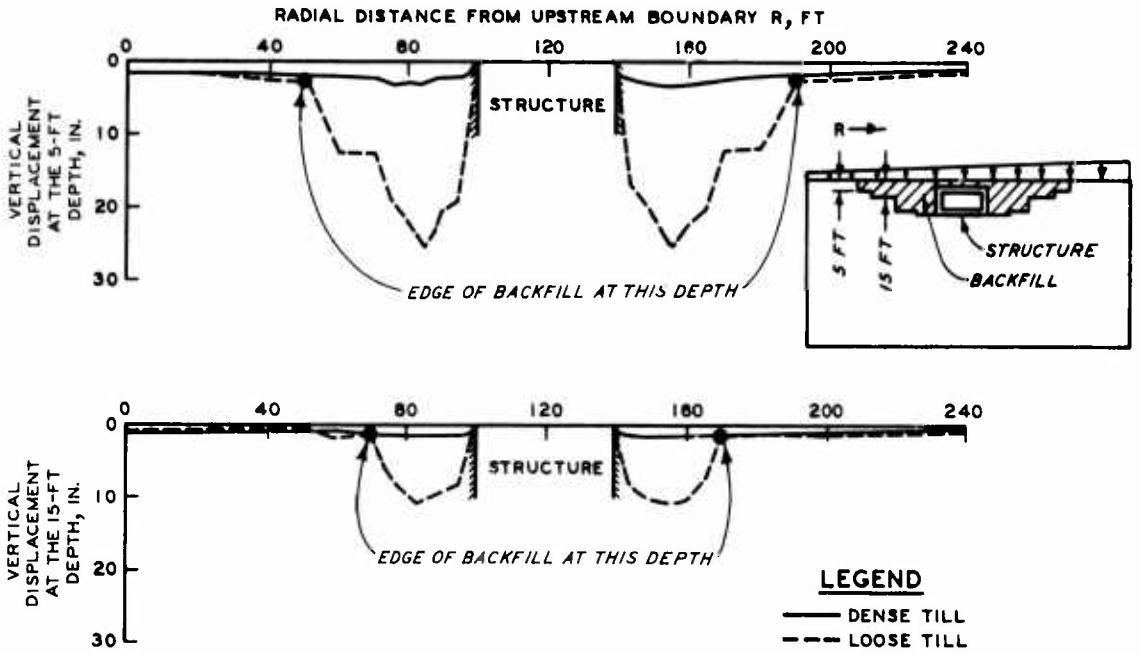

Figure 8. Instantaneous pattern of vertical displacements along two lines through the till backfill zone at 285 msec after the start of the problem

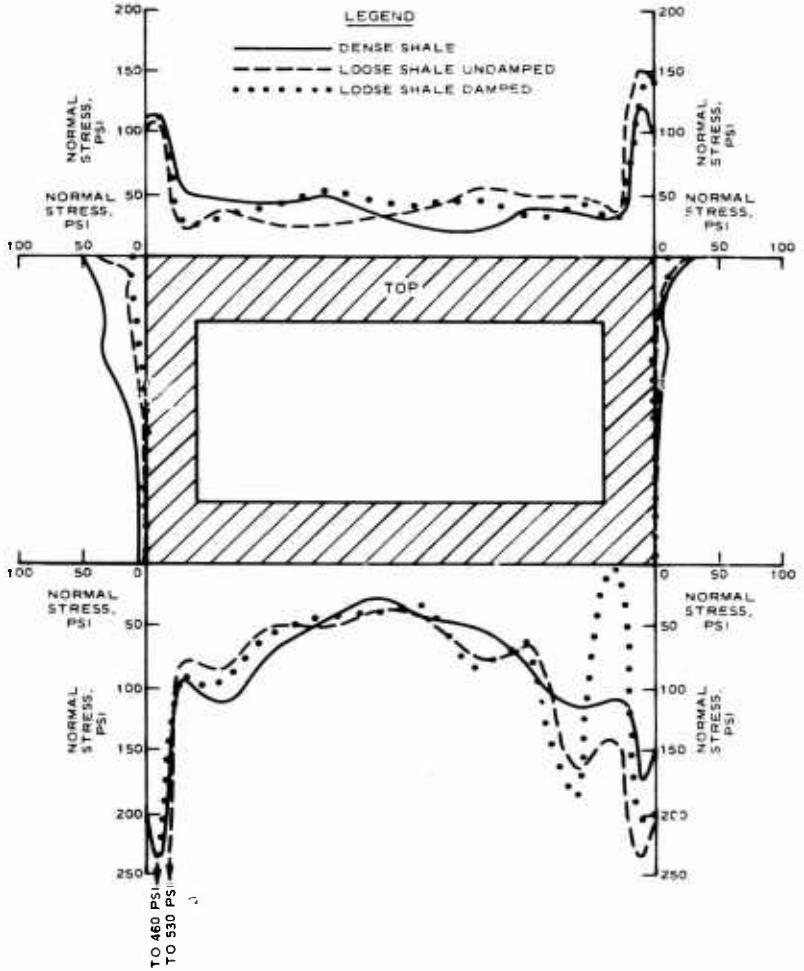

Figure 9. Instantaneous distribution of normal stresses on exterior surfaces of the structure surrounded by shale backfill at 105 msec

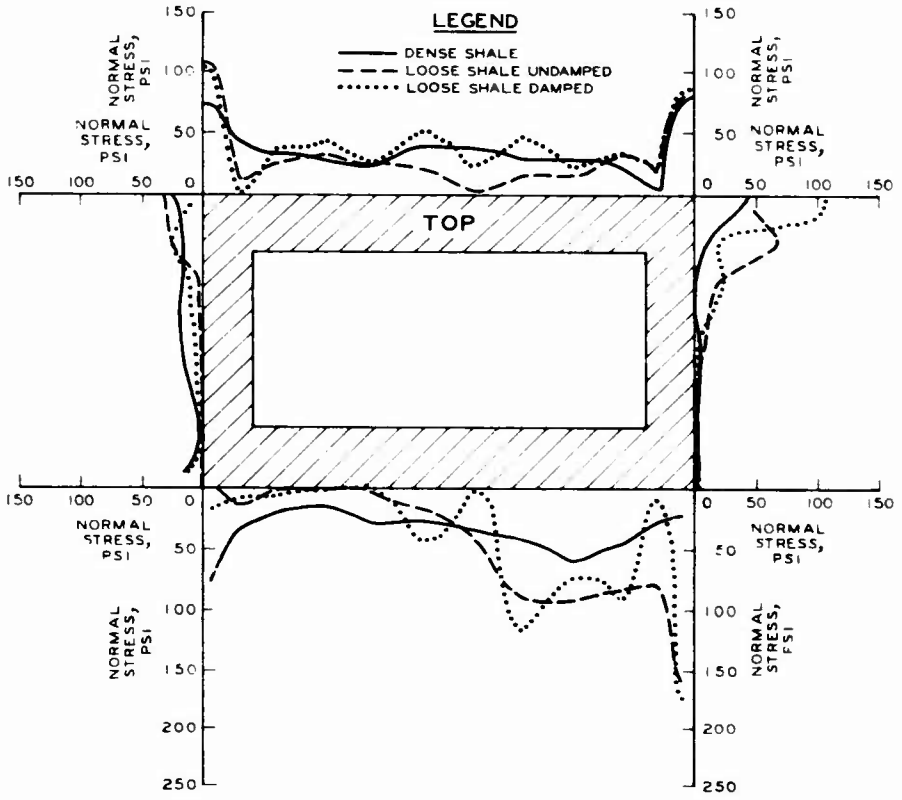

Figure 10. Instantaneous distribution of normal stresses on the exterior surfaces of the structure surrounded by shale backfill at 235 msec

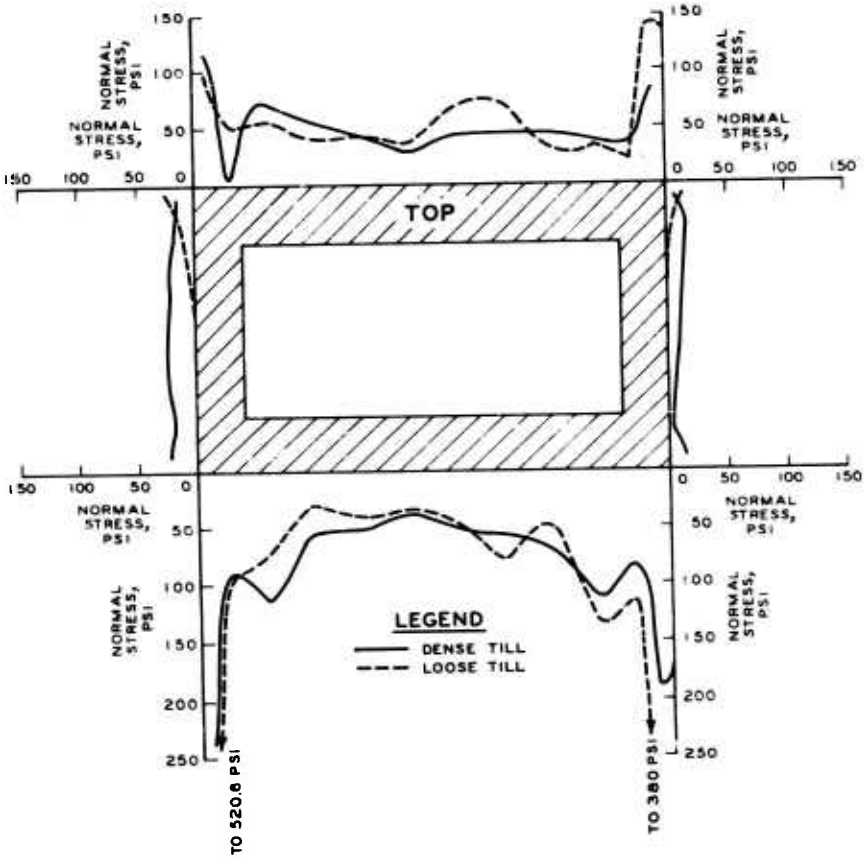

Figure 11. Instantaneous distribution of normal stresses on the exterior surfaces of the structure surrounded by till backfill at 115 msec

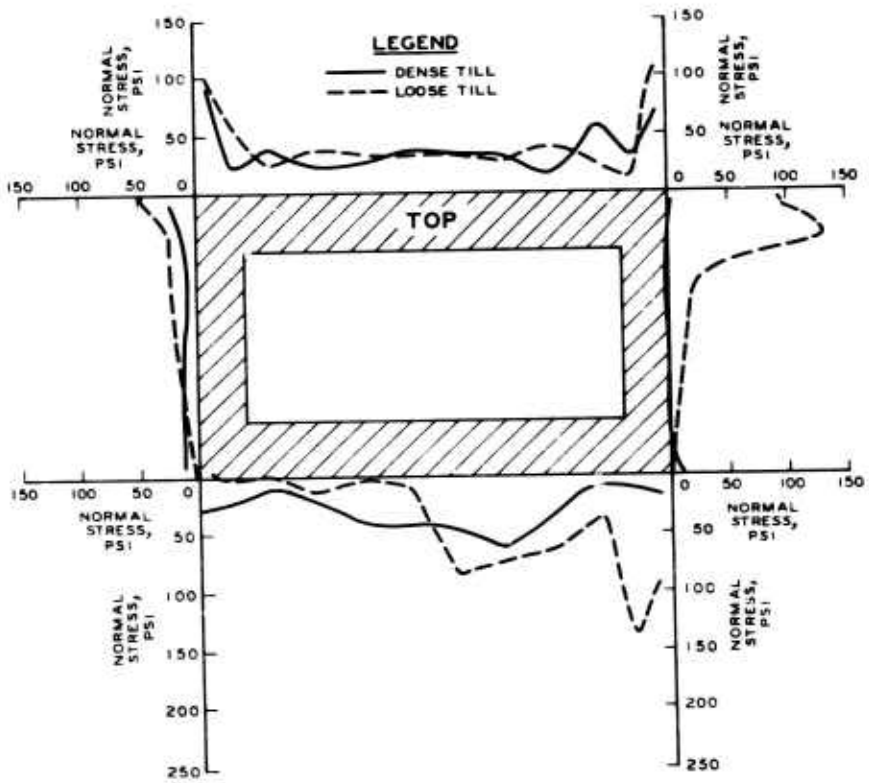

Figure 12. Instantaneous distribution of normal stresses on the exterior surfaces of the structure surrounded by till backfill at 230 msec

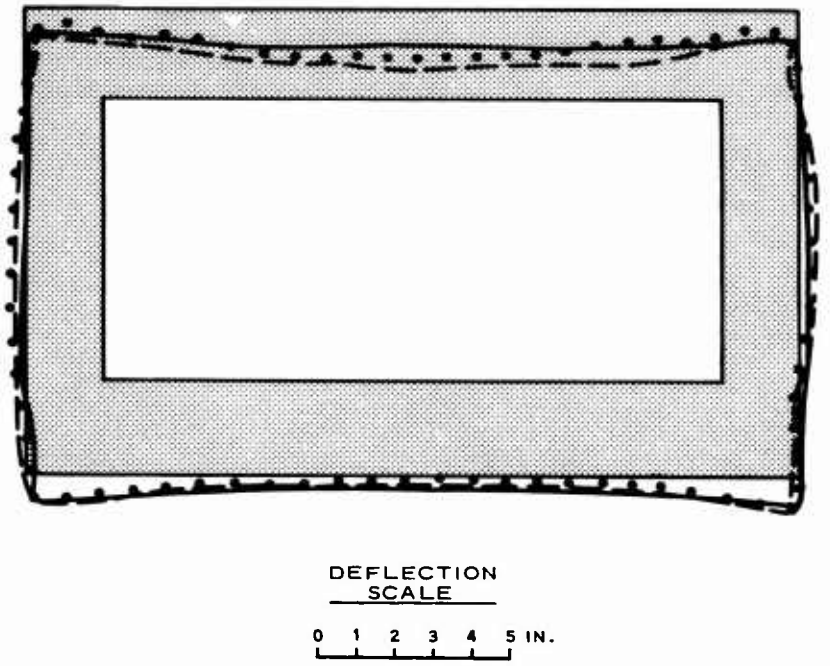

Figure 13. Instantaneous pattern of deflection along the structure's exterior surfaces at 105 msec; shale backfill

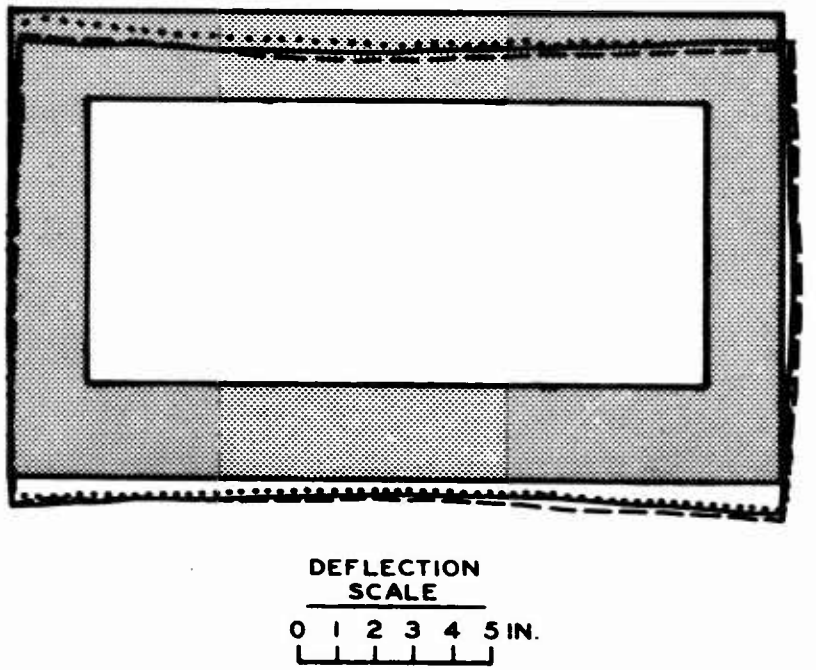

Figure 14. Instantaneous pattern of deflection along the structure's exterior surfaces at 235 msec; shale backfill

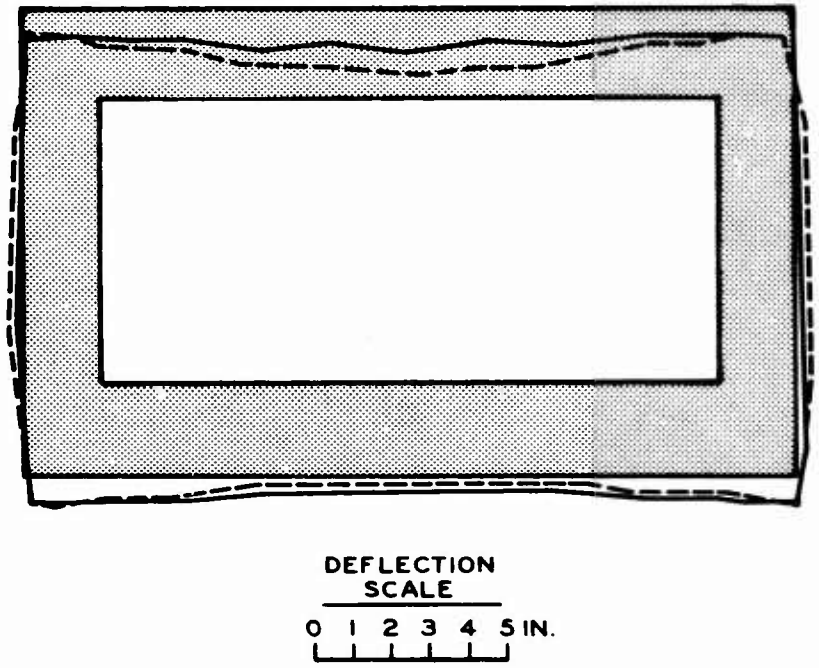

Figure 15. Instantaneous pattern of deflection along the structure's exterior surfaces at 115 msec; till backfill

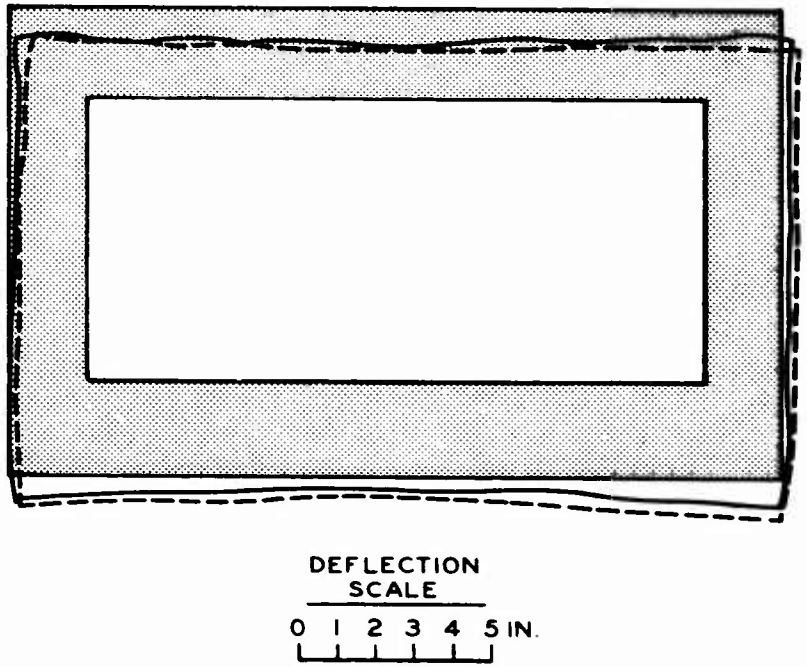

Figure 16. Instantaneous pattern of deflection along the structure's exterior surfaces at 230 msec; till backfill

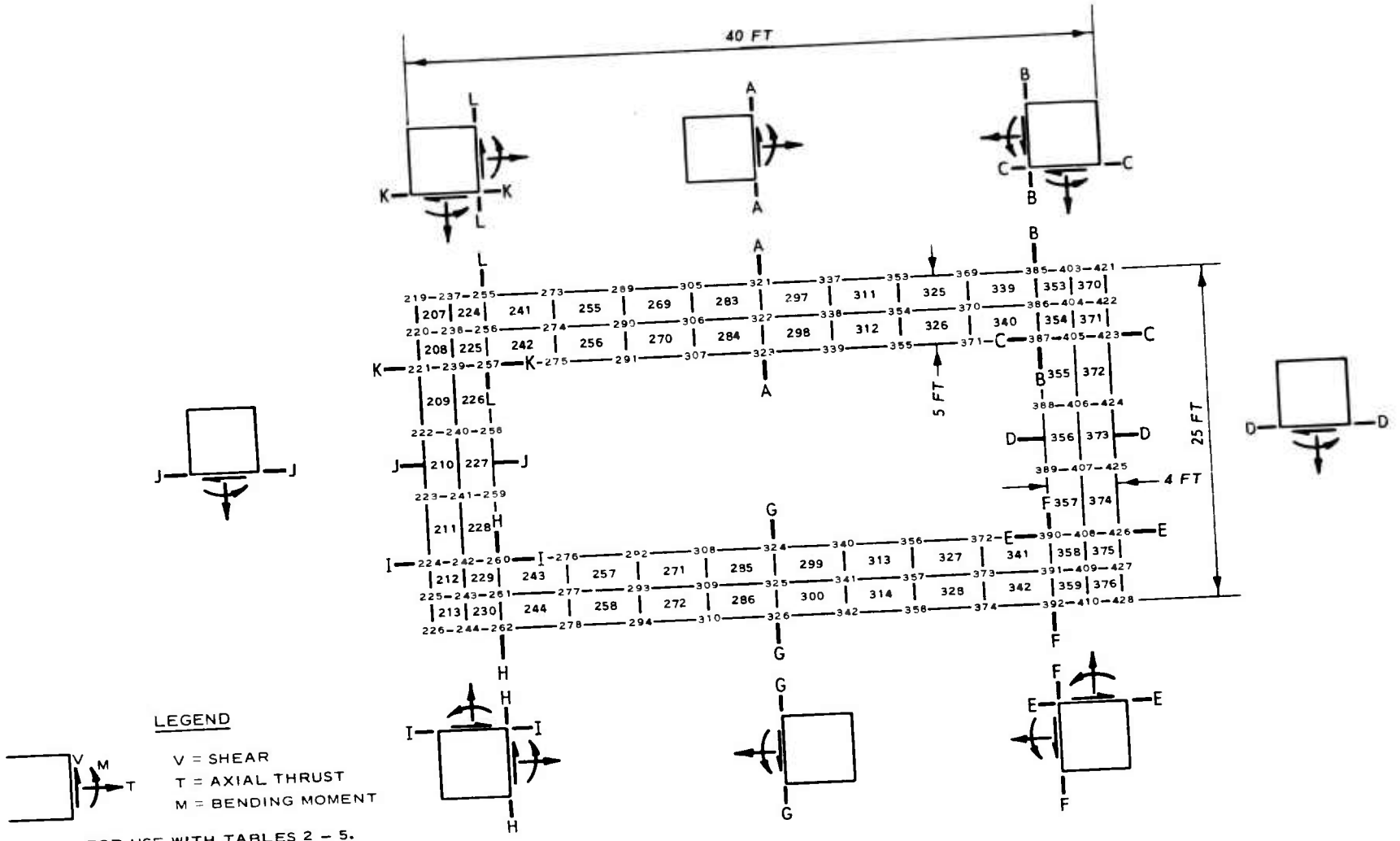

Figure 17. Structure sections for which shear, thrust, and bending moment are shown in Tables 2, 3, 4, and 5

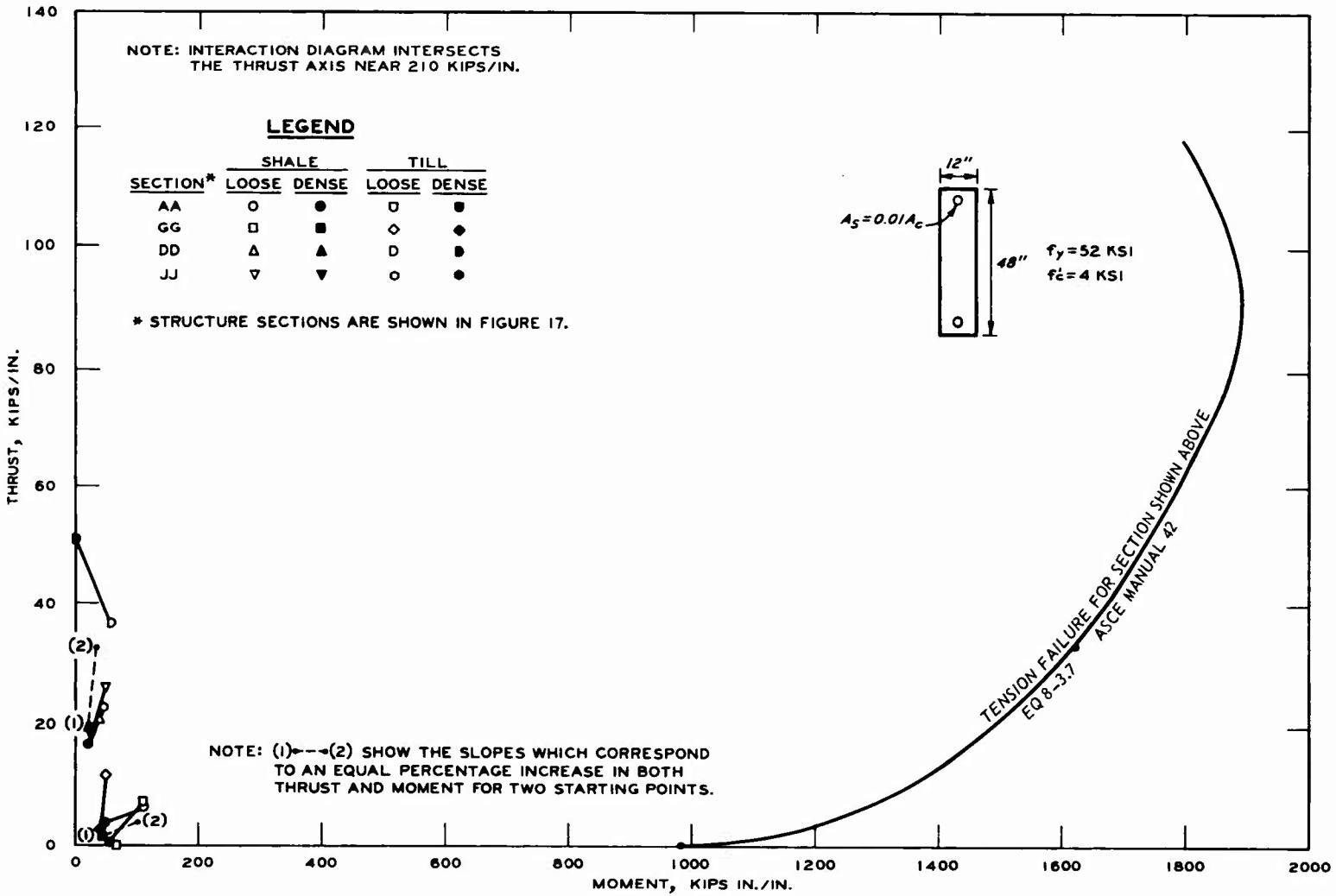

Figure 18. Moment-thrust interaction diagram for rectangular beam-column and data for selected sections at 105 msec

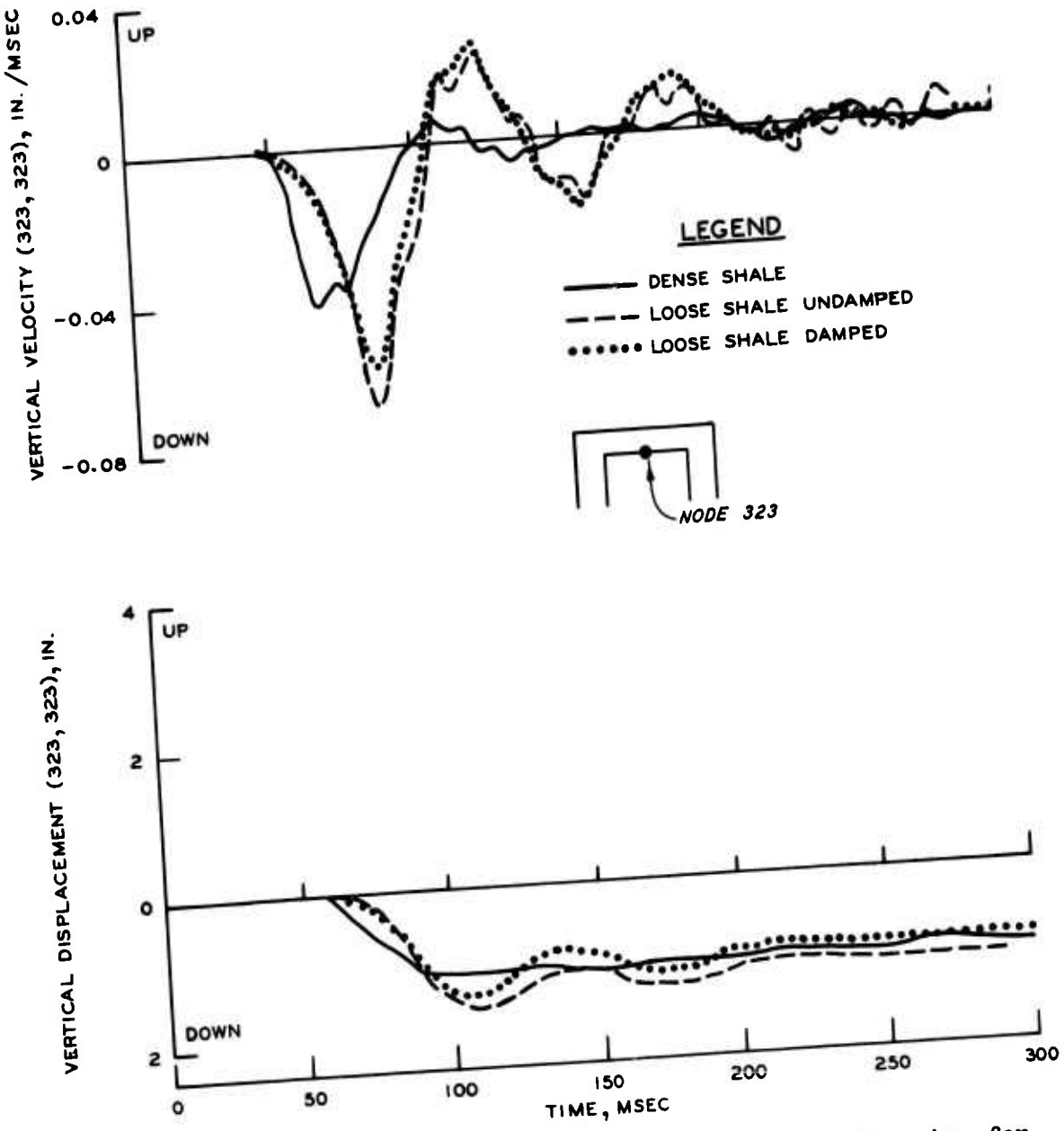

Figure 19. Vertical velocity and displacement time histories for the center of the structure roof, shale backfill

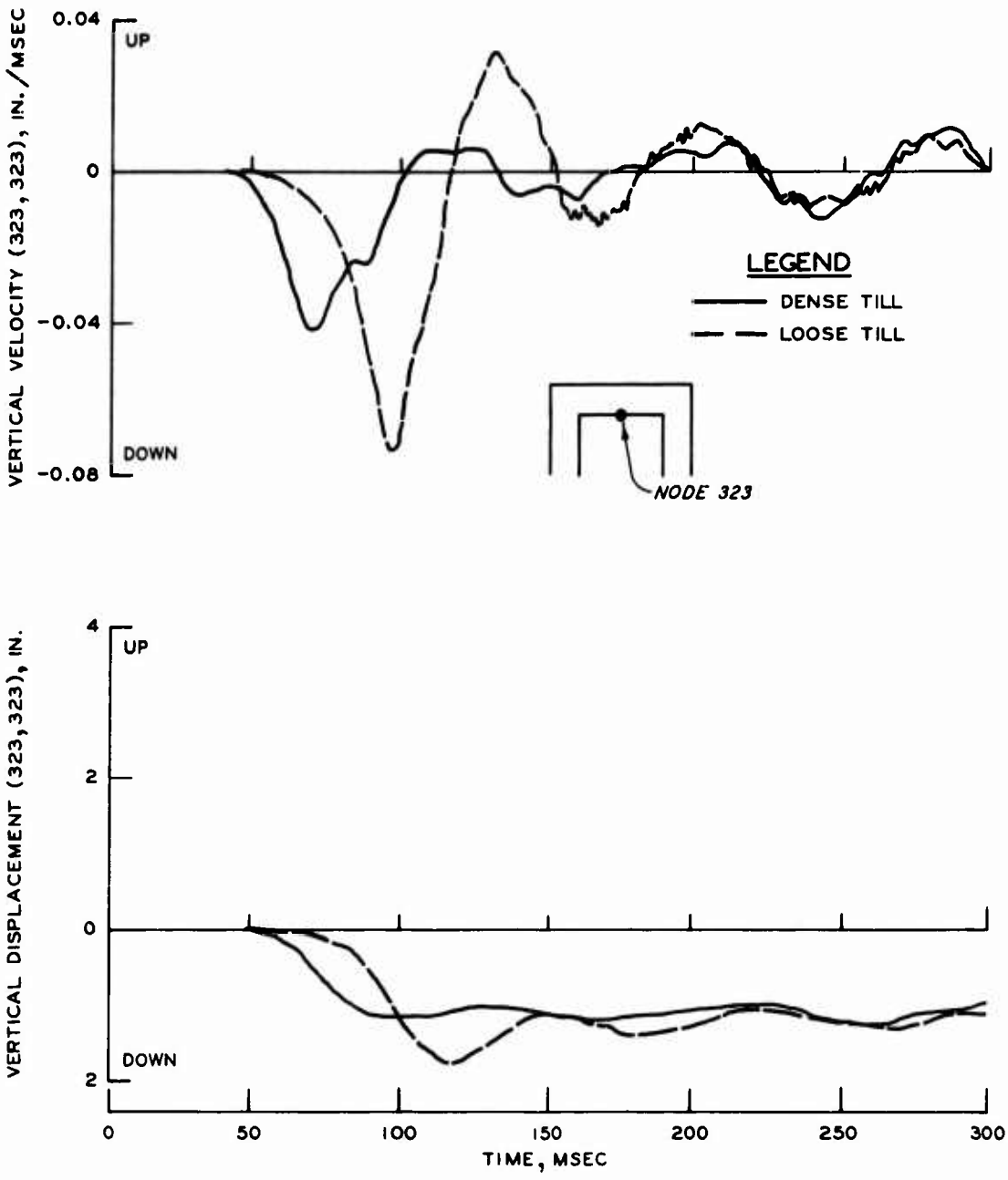

Figure 20. Vertical velocity and displacement time histories for the center of the structure roof; till backfill

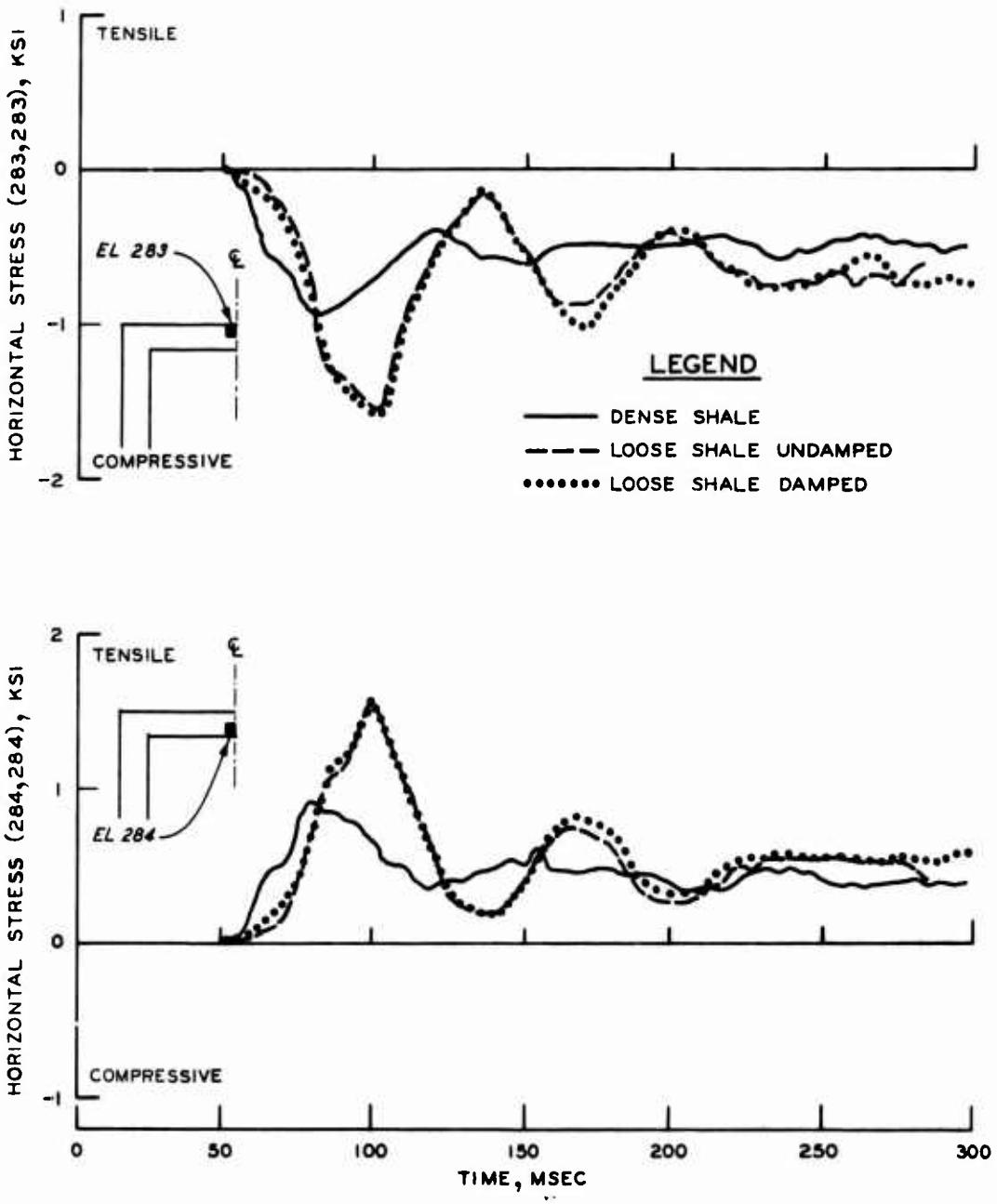

Figure 21. Horizontal stress time histories for points in the roof midway from the neutral axis to the top (el 283) and bottom (el 284) fiber; shale backfill

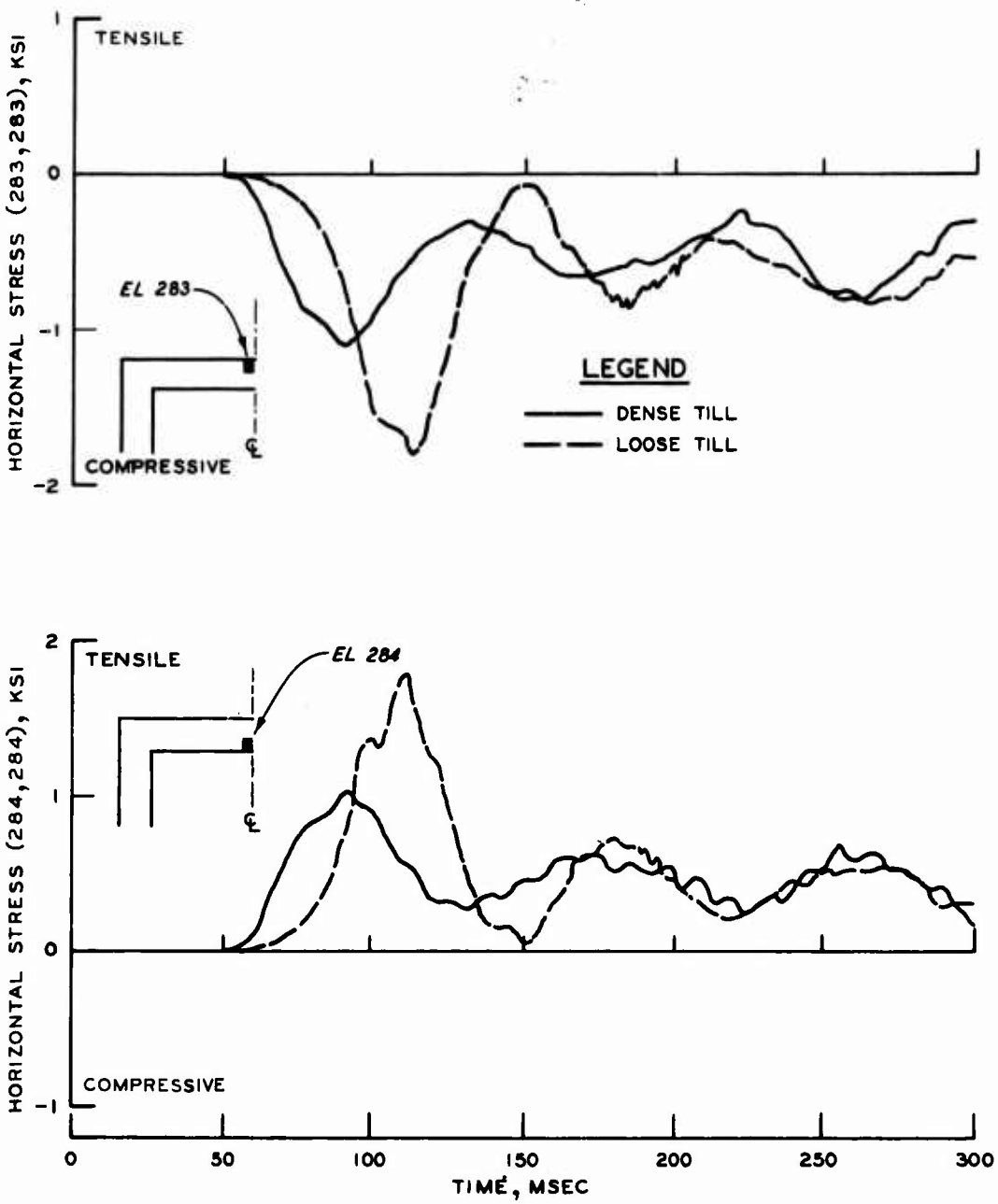

Figure 22. Horizontal stress time histories for points in the roof midway from the neutral axis to the top (el 283) and bottom (el 284) fiber; till backfill

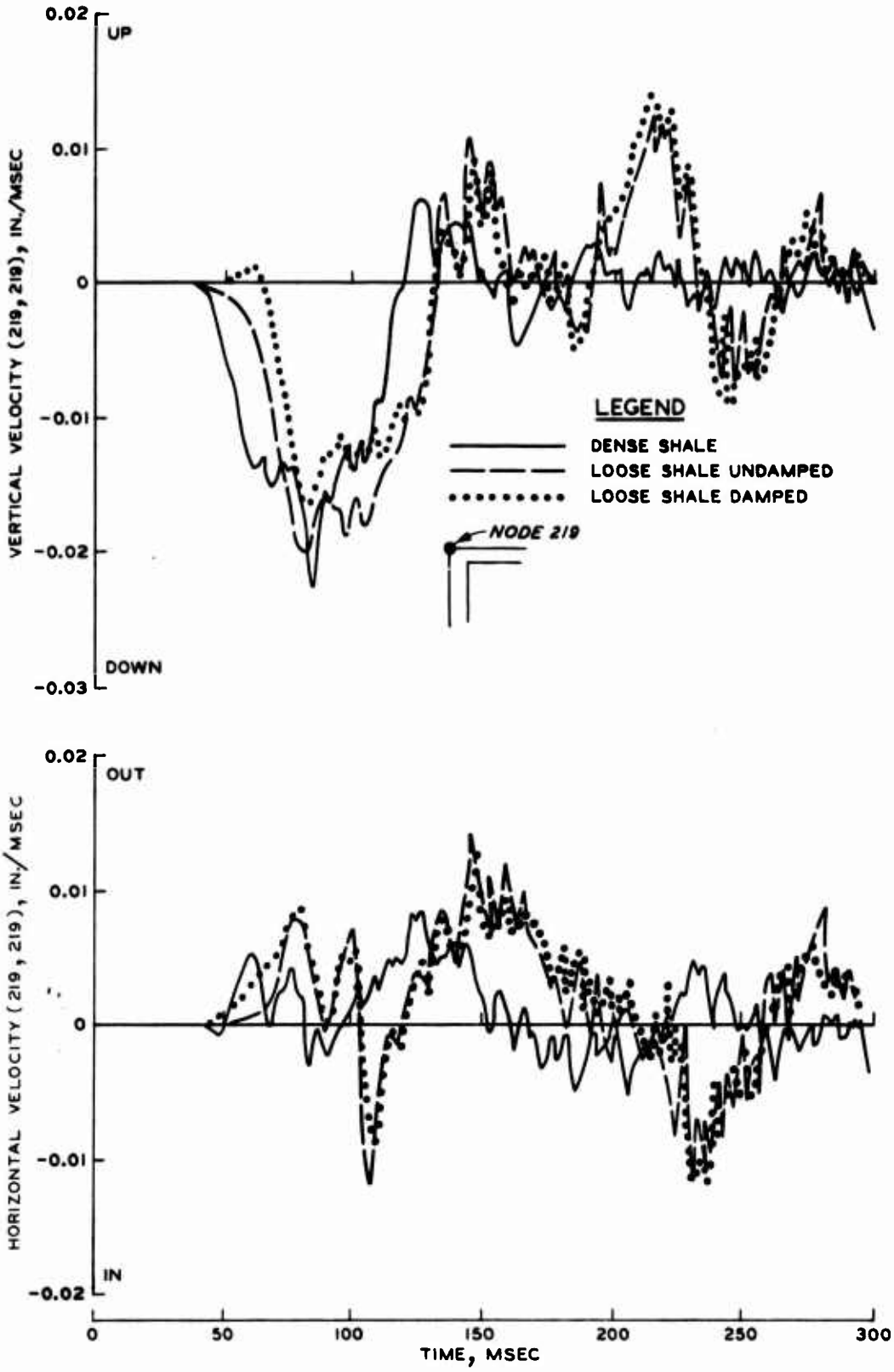

Figure 23. Velocity versus time for a point on the blastward sidewall; shale backfill

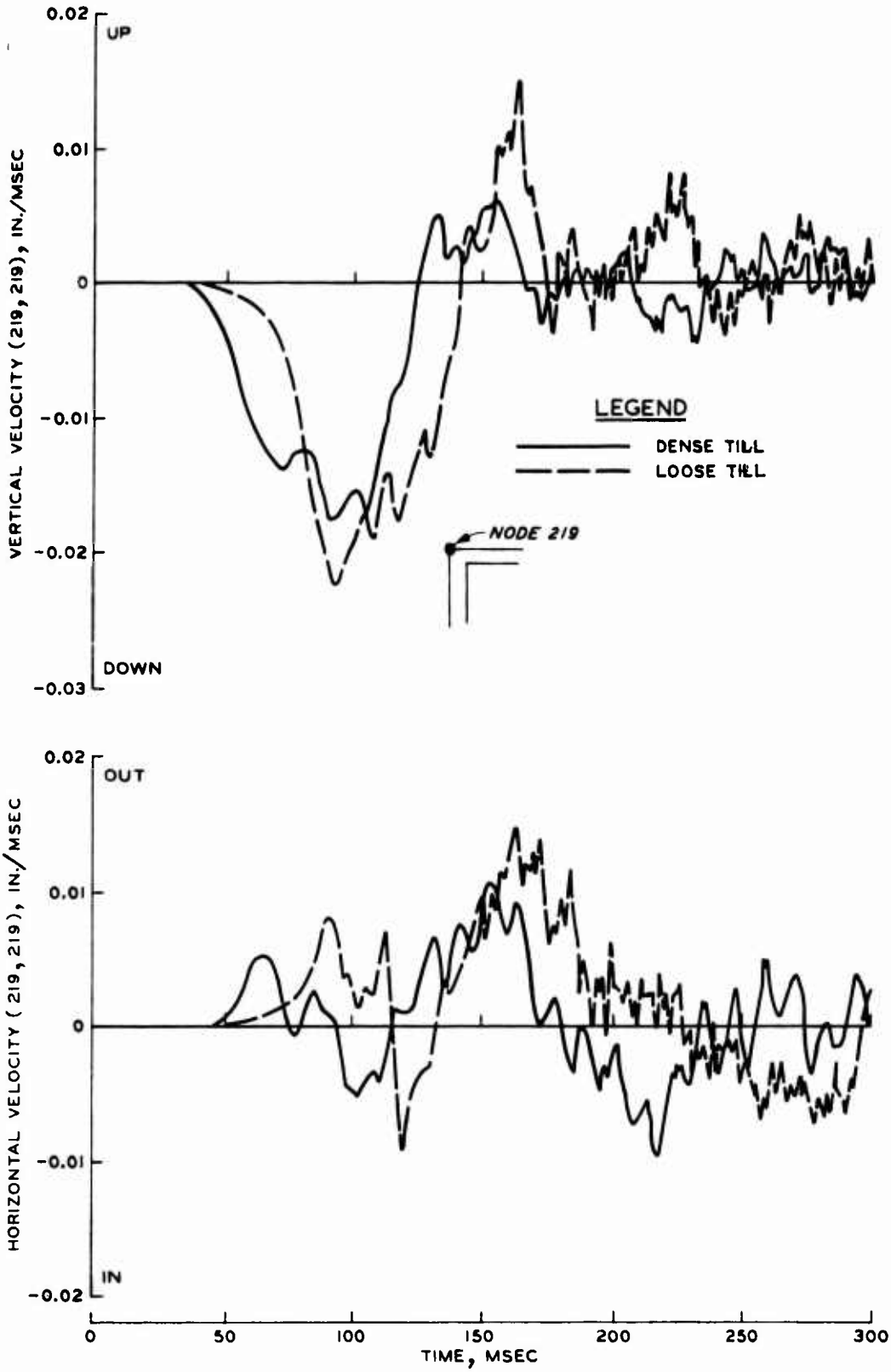

Figure 24. Velocity versus time for a point on the blastward sidewall; till backfill

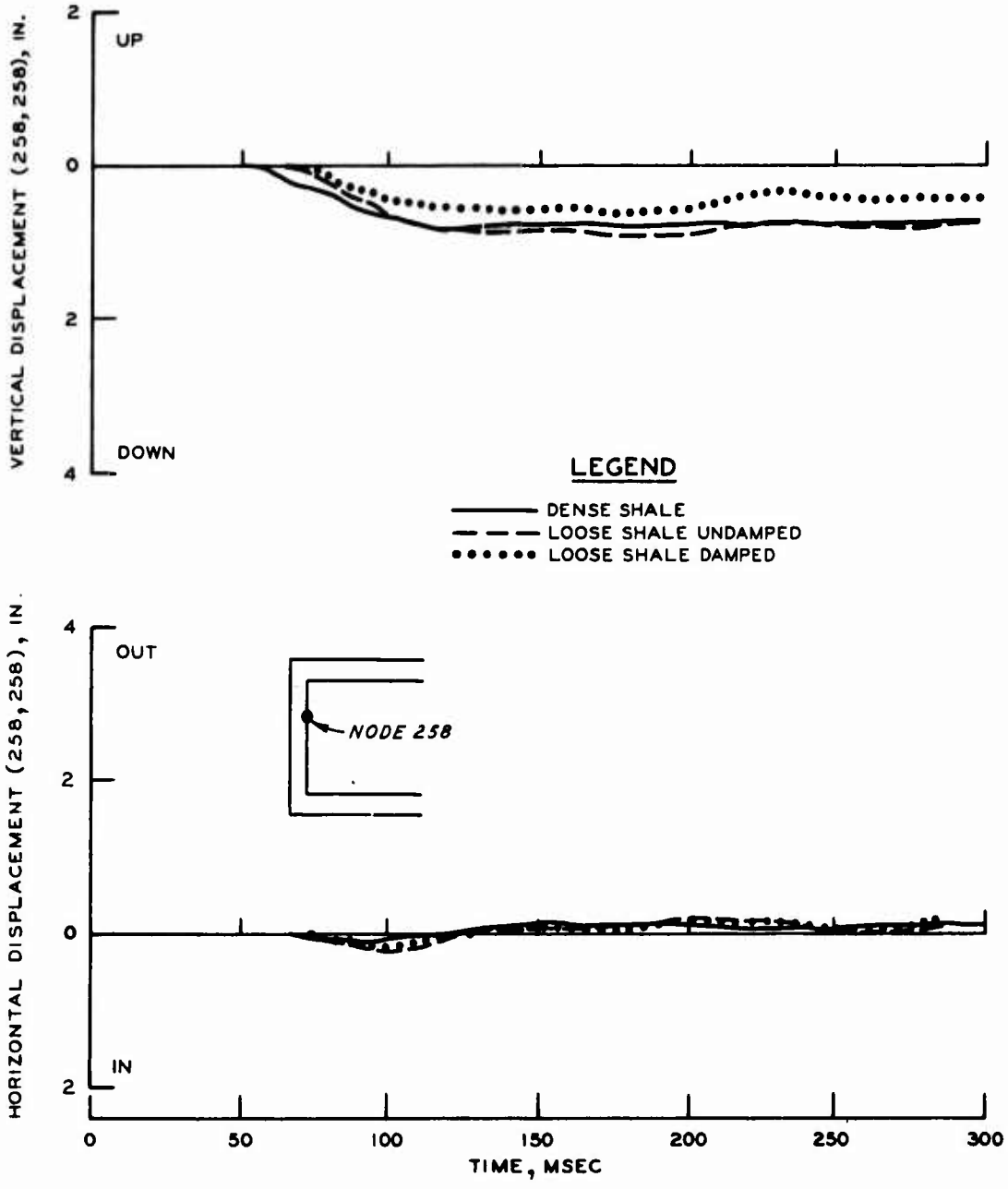

Figure 25. Displacement versus time histories for a point near the midheight of the blastward sidewall; shale backfill

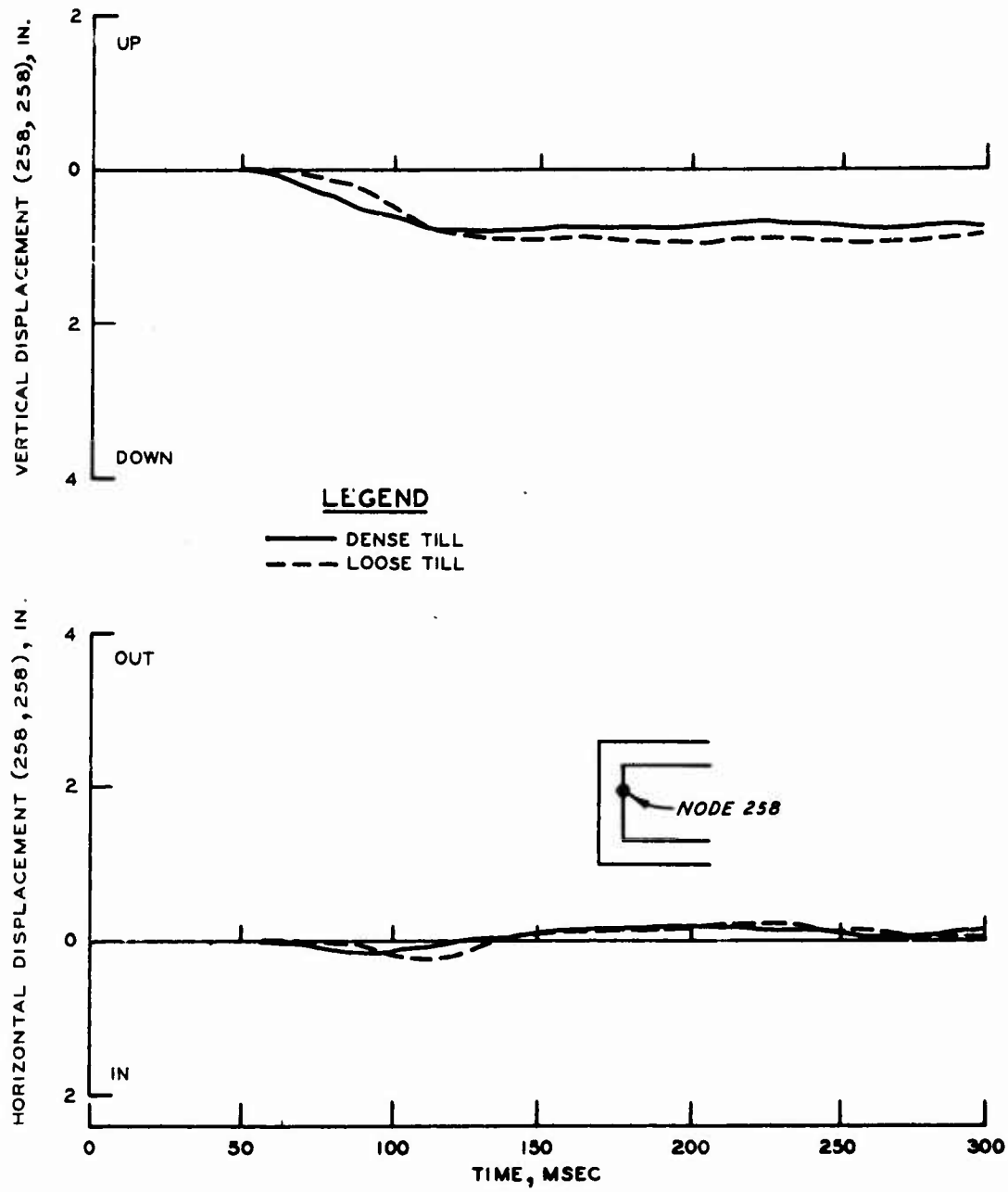

Figure 26. Displacement versus time histories for a point near the midheight of the blastward sidewall; till backfill

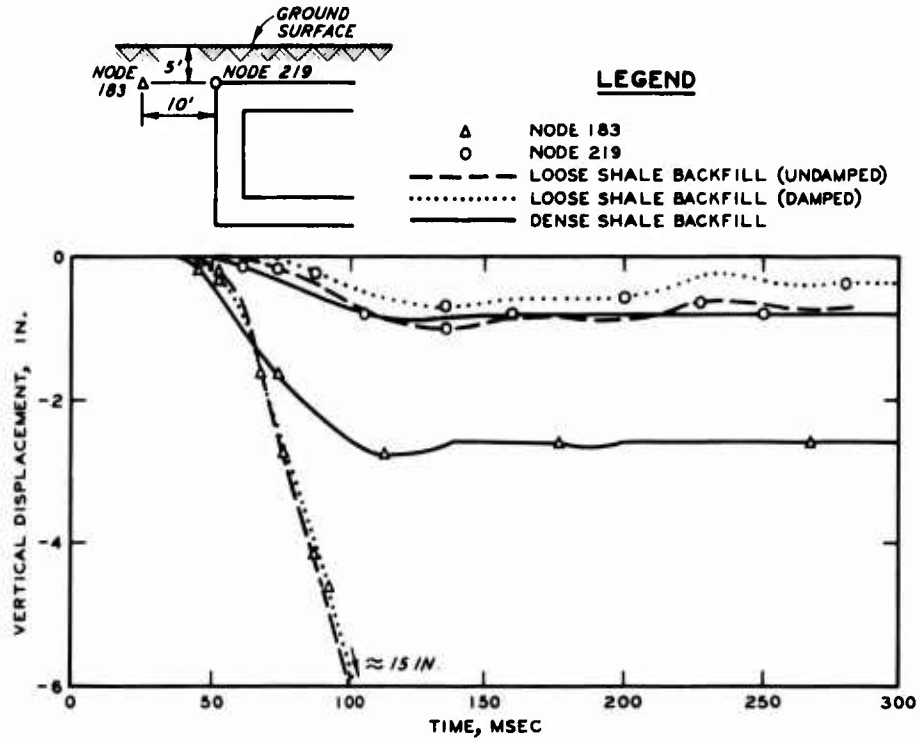

Figure 27. Comparison of the vertical deflection for a point on the structure at a depth of 5 ft below the ground surface with that for a point in the adjacent backfill for the shale backfill cases

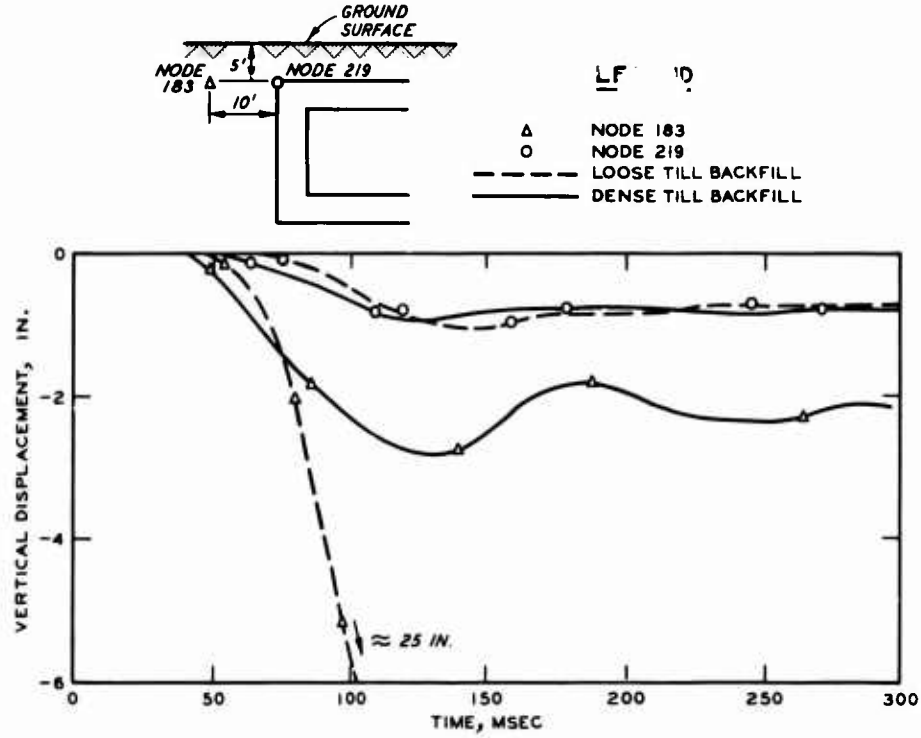

Figure 28. Comparison of the vertical deflection for a point on the structure at a depth of 5 ft below the ground surface with that for a point in the adjacent till backfill

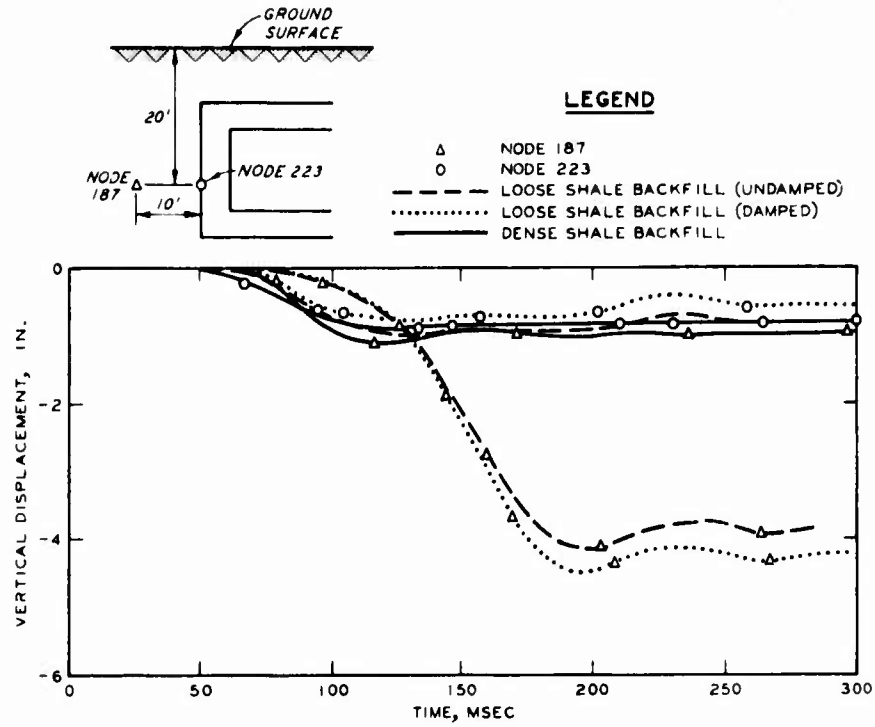

Figure 29. Comparison of the vertical displacement for a point on the structure at a depth of 20 ft below the ground surface with that for a point in the adjacent shale backfill

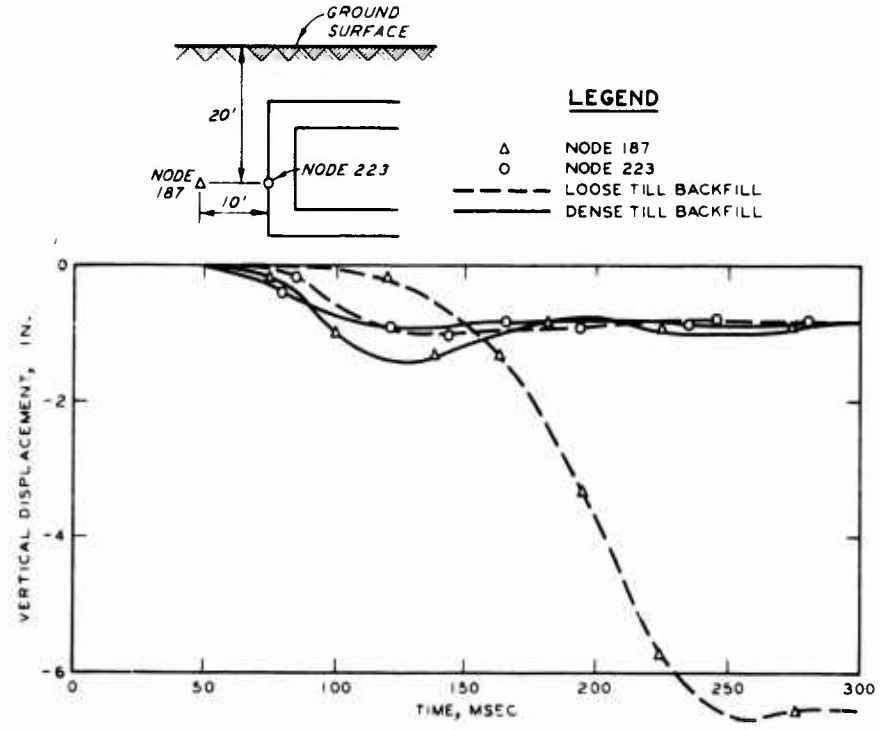

Figure 30. Comparison of the vertical displacement for a point on the structure 20 ft below the ground surface with that for a point in the adjacent till backfill

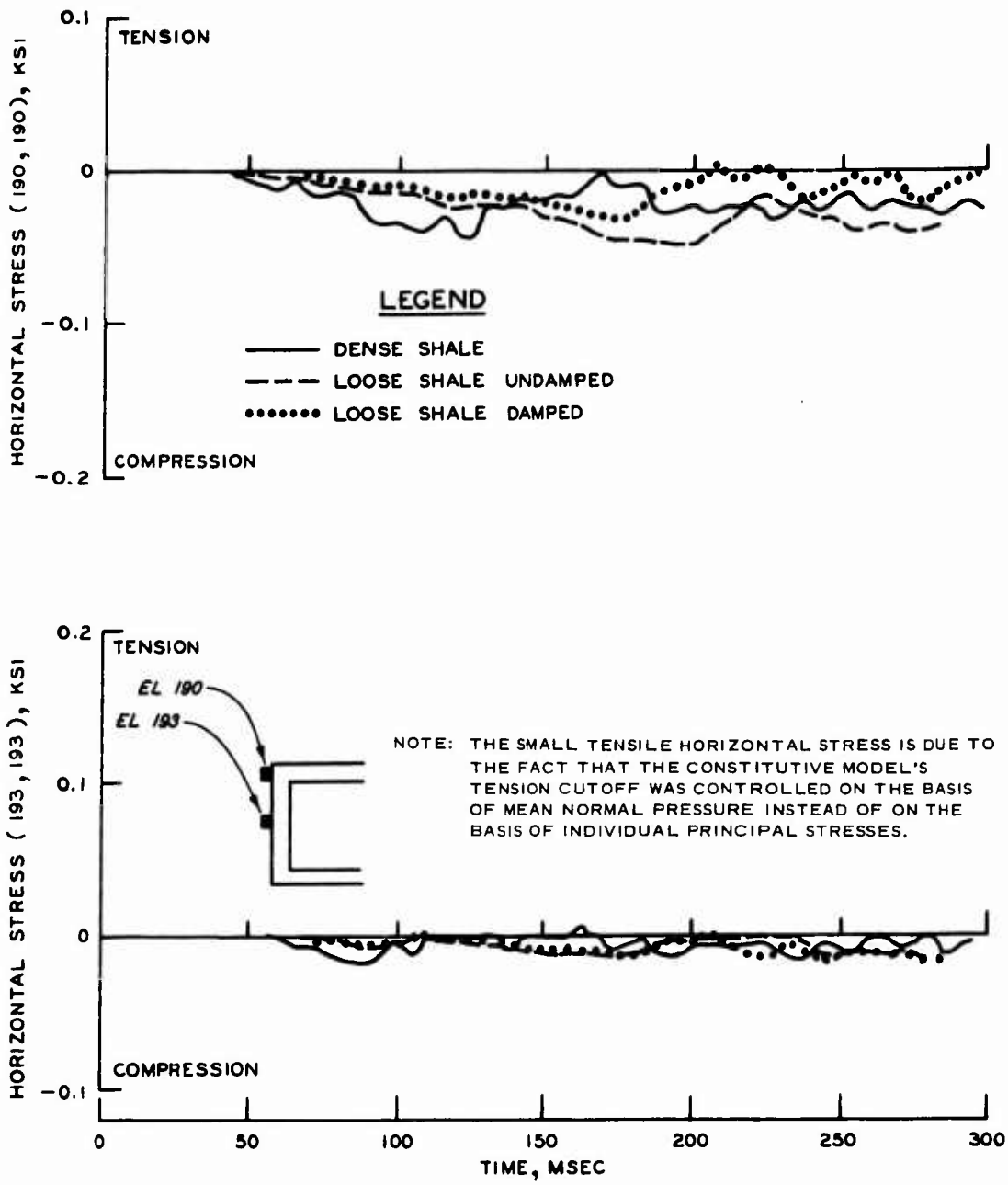

Figure 31. Comparison of horizontal stress time histories at points near the upstream sidewall of the structure; shale backfill

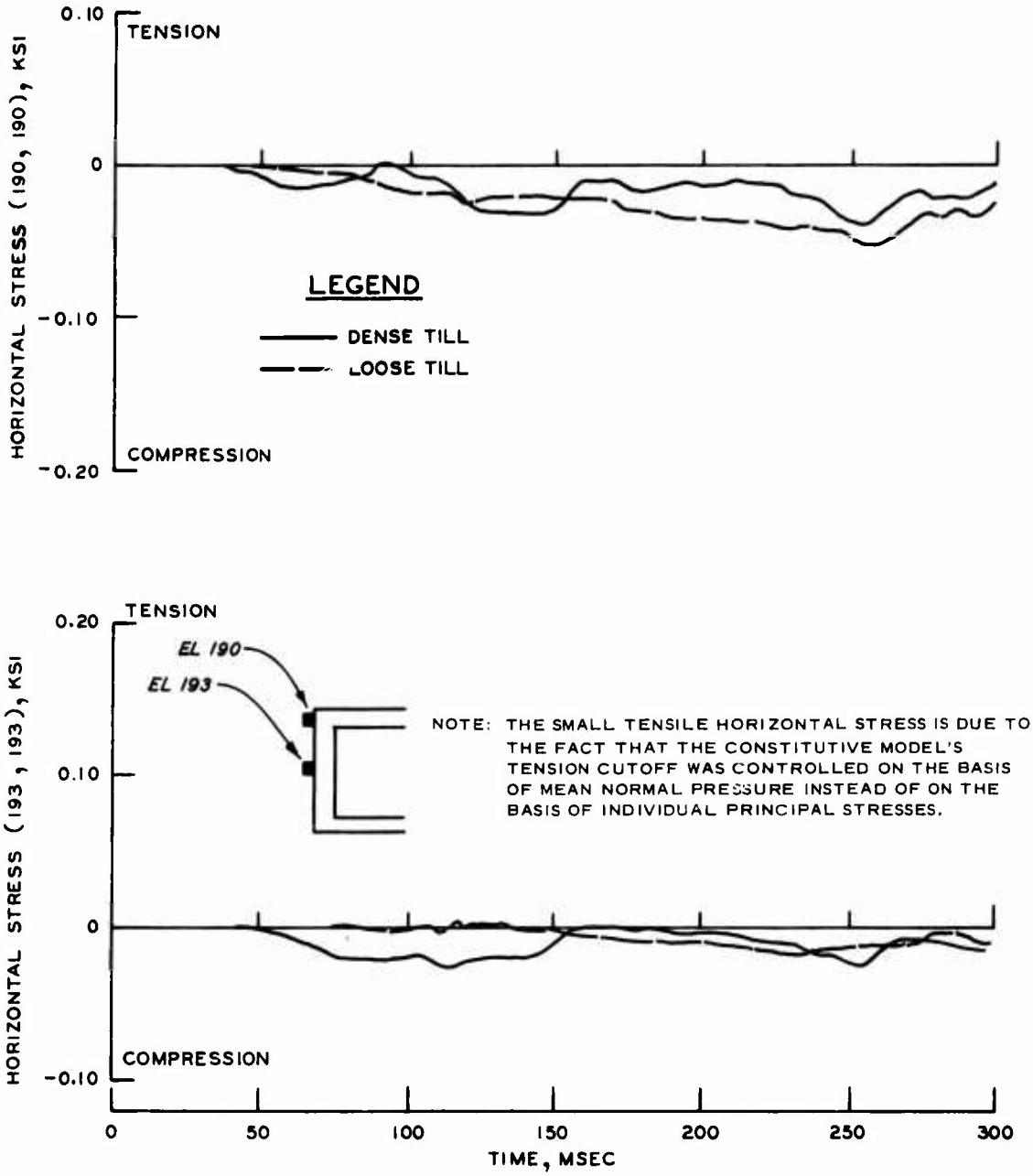

Figure 32. Comparison of horizontal stress time histories at points near the upstream sidewall of the structure; till backfill

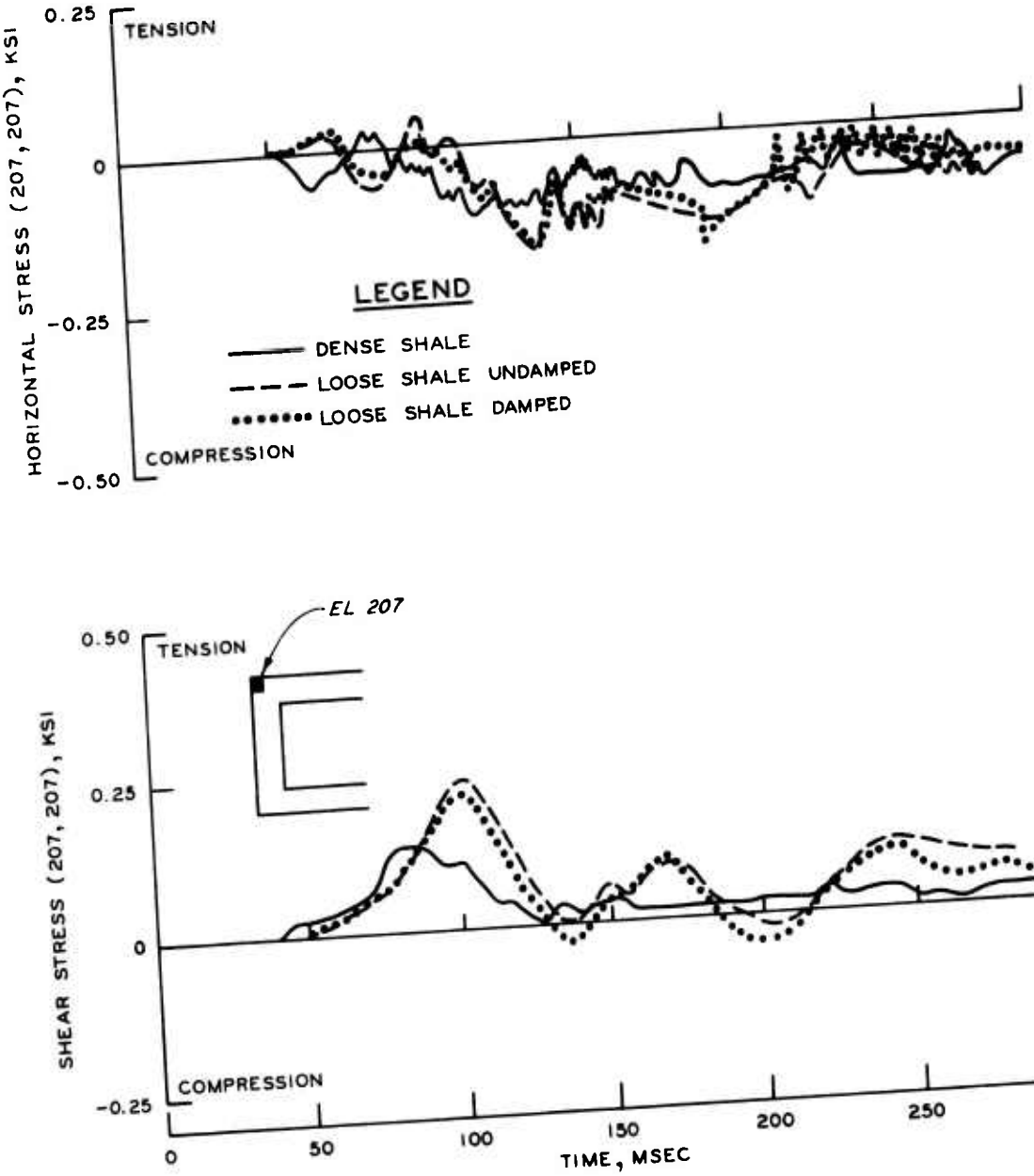

Figure 33. Horizontal and shear stress time histories for element 207; shale backfill

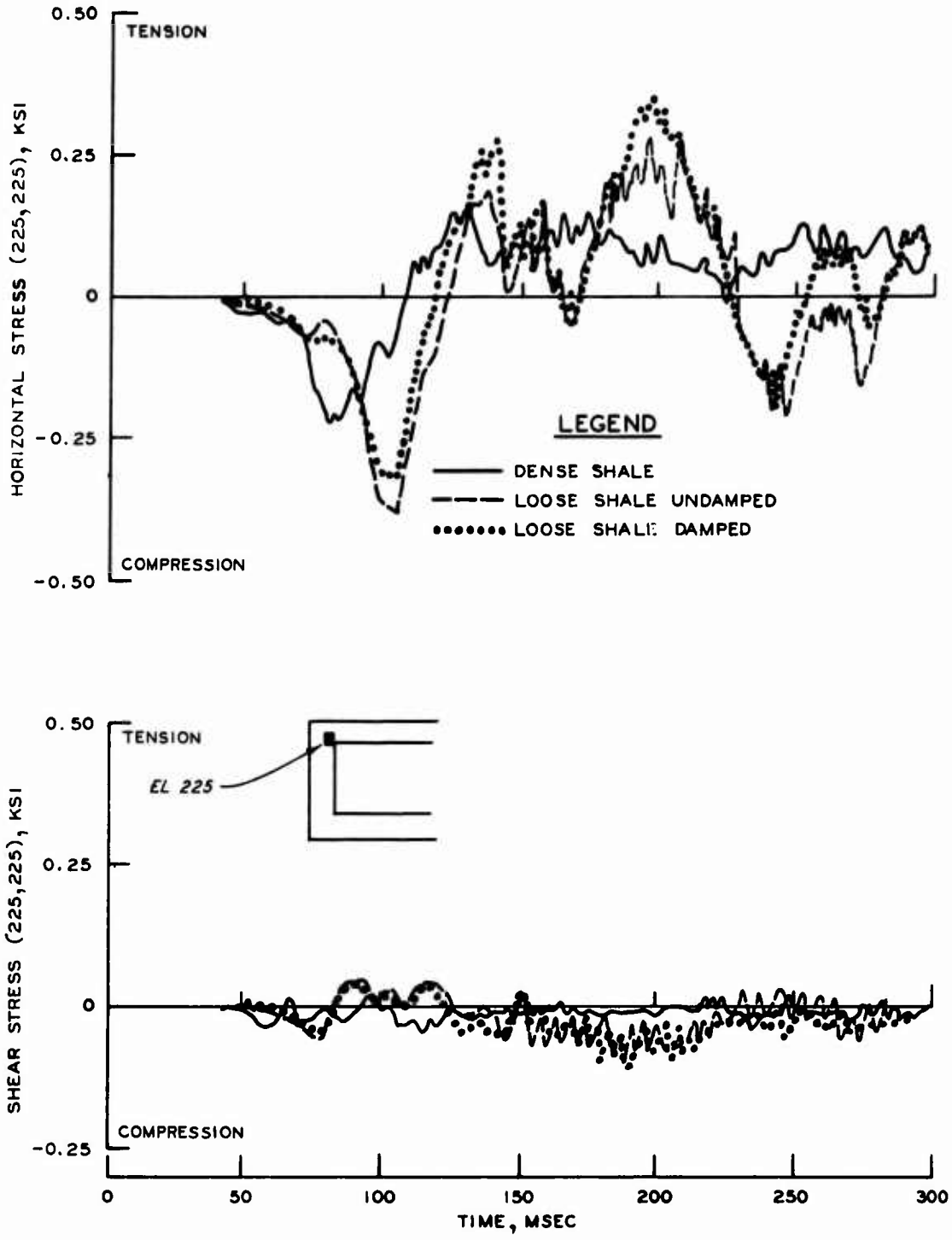

Figure 34. Horizontal and shear stress time histories for element 225; shale backfill

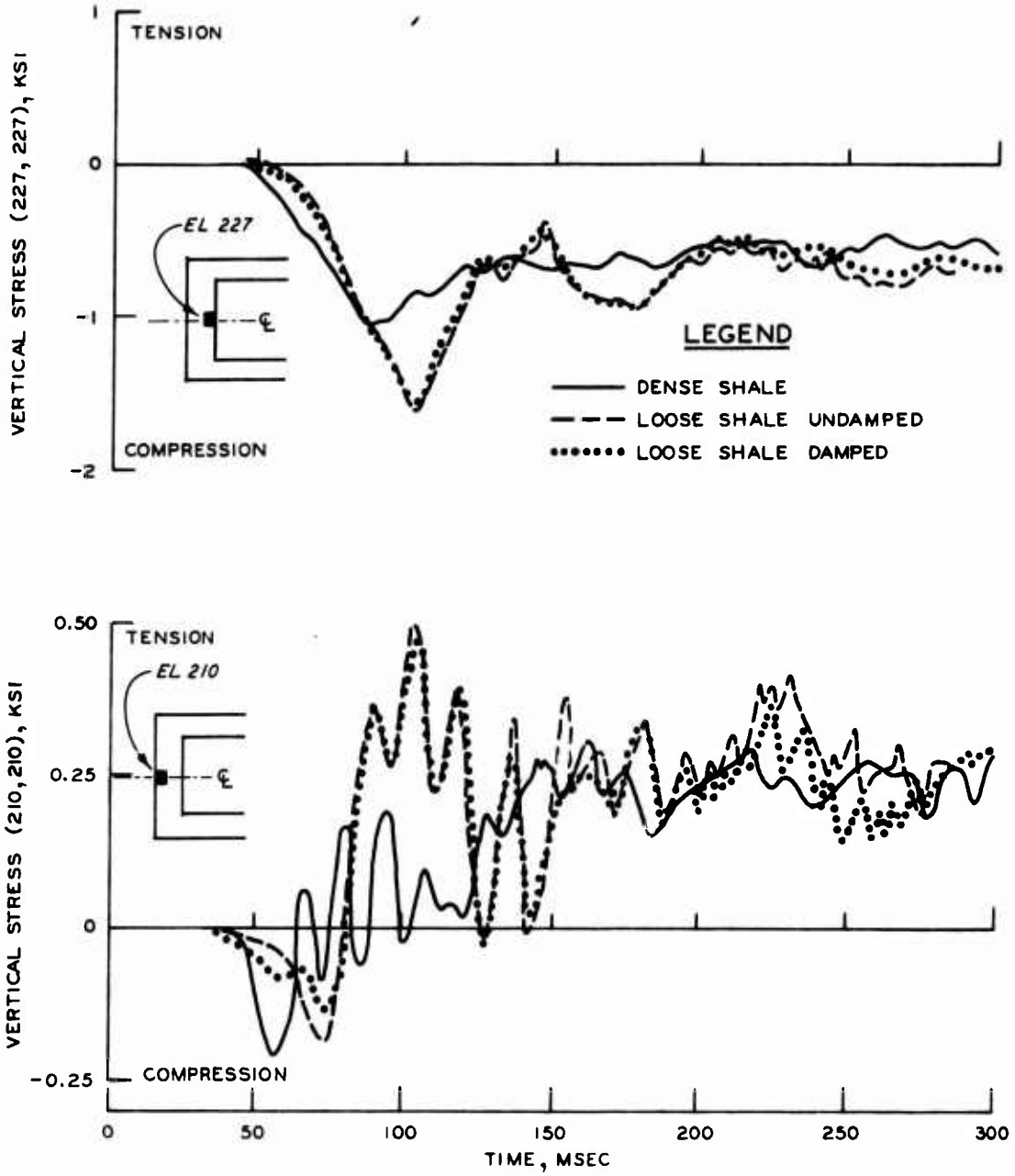

Figure 35. Vertical stress time histories at the midheight of the blastward sidewall; shale backfill

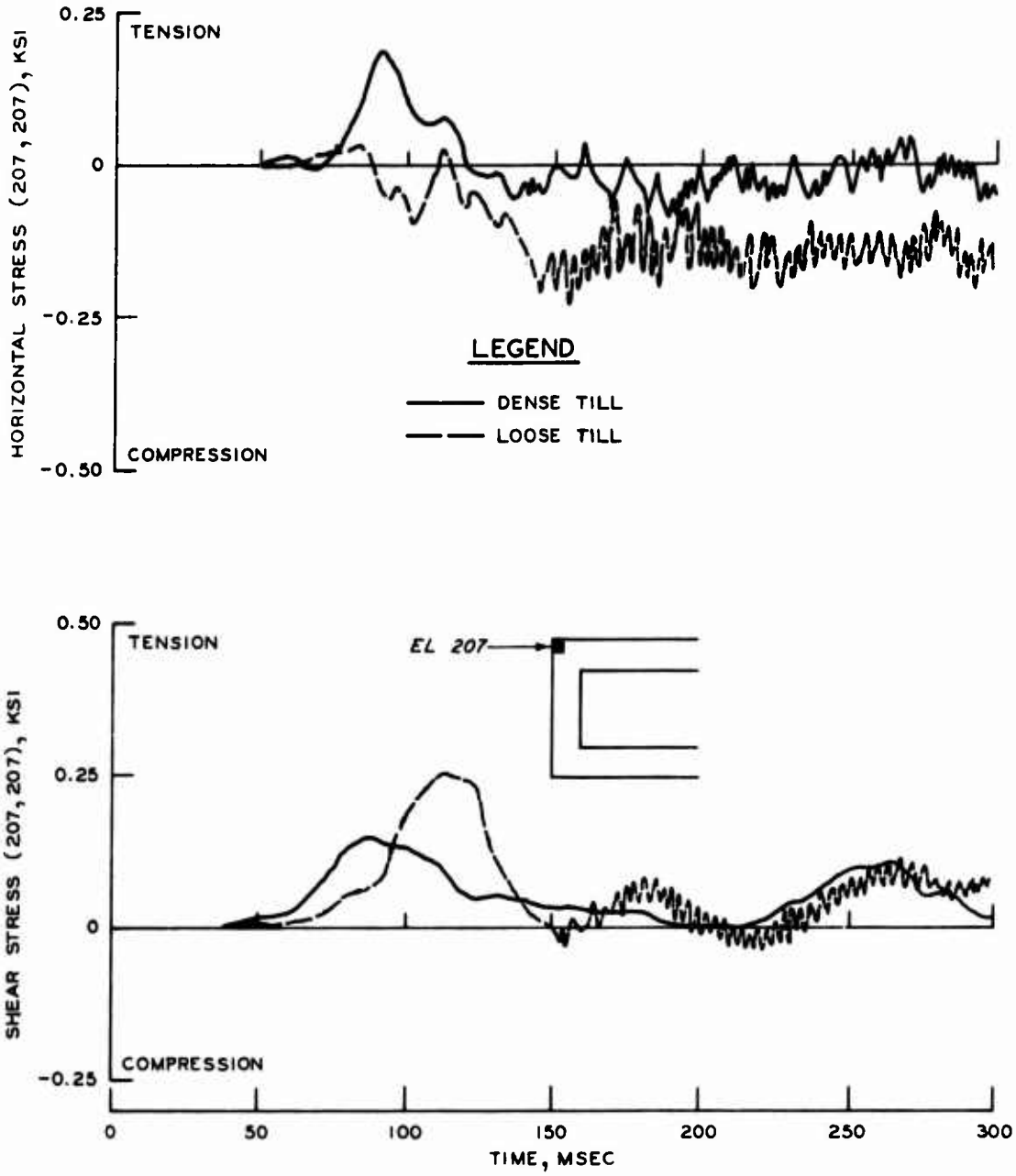

Figure 36. Horizontal and shear stress time histories for element 207; till backfill

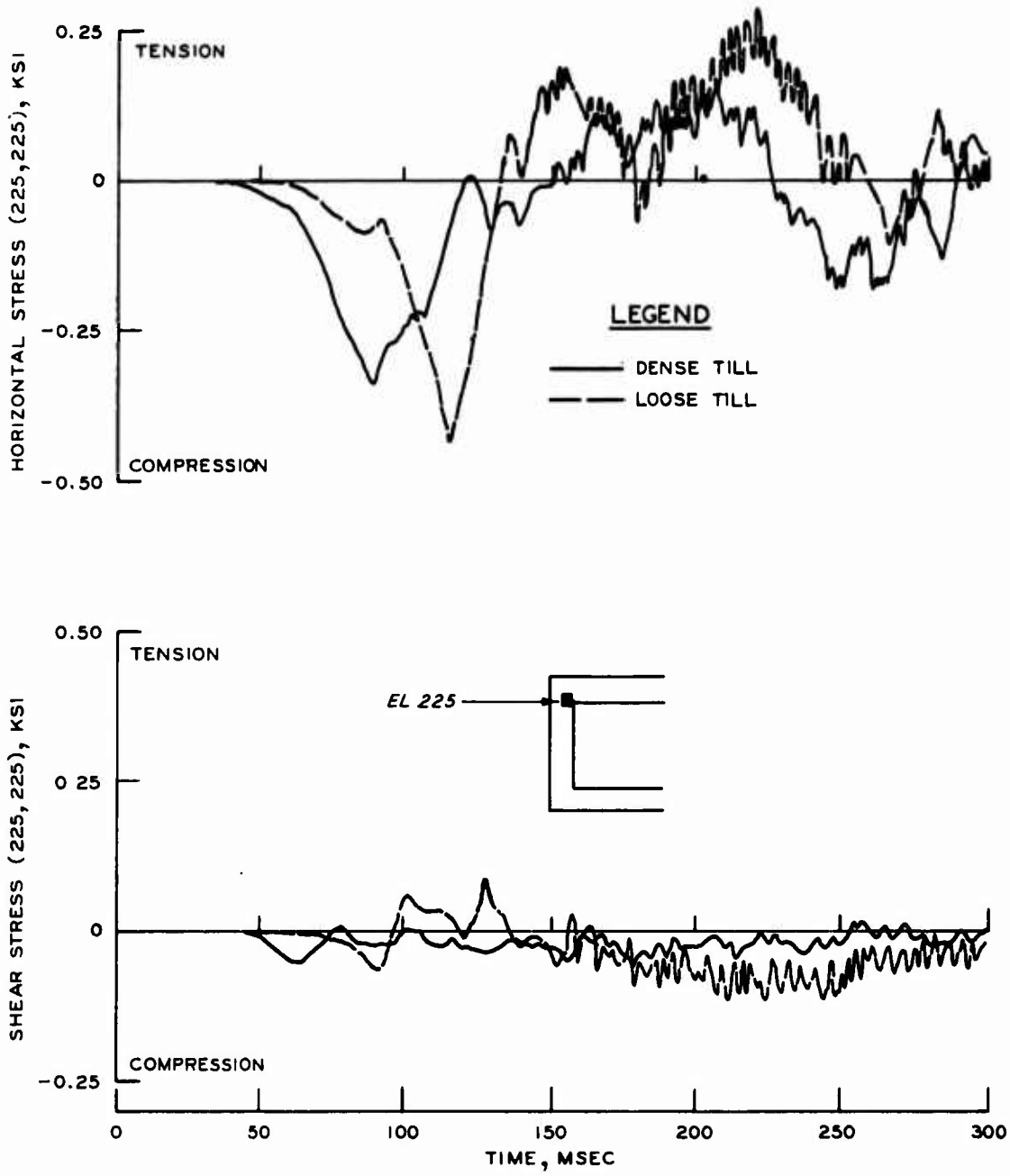

Figure 37. Horizontal and shear stress time histories for element 225; till backfill

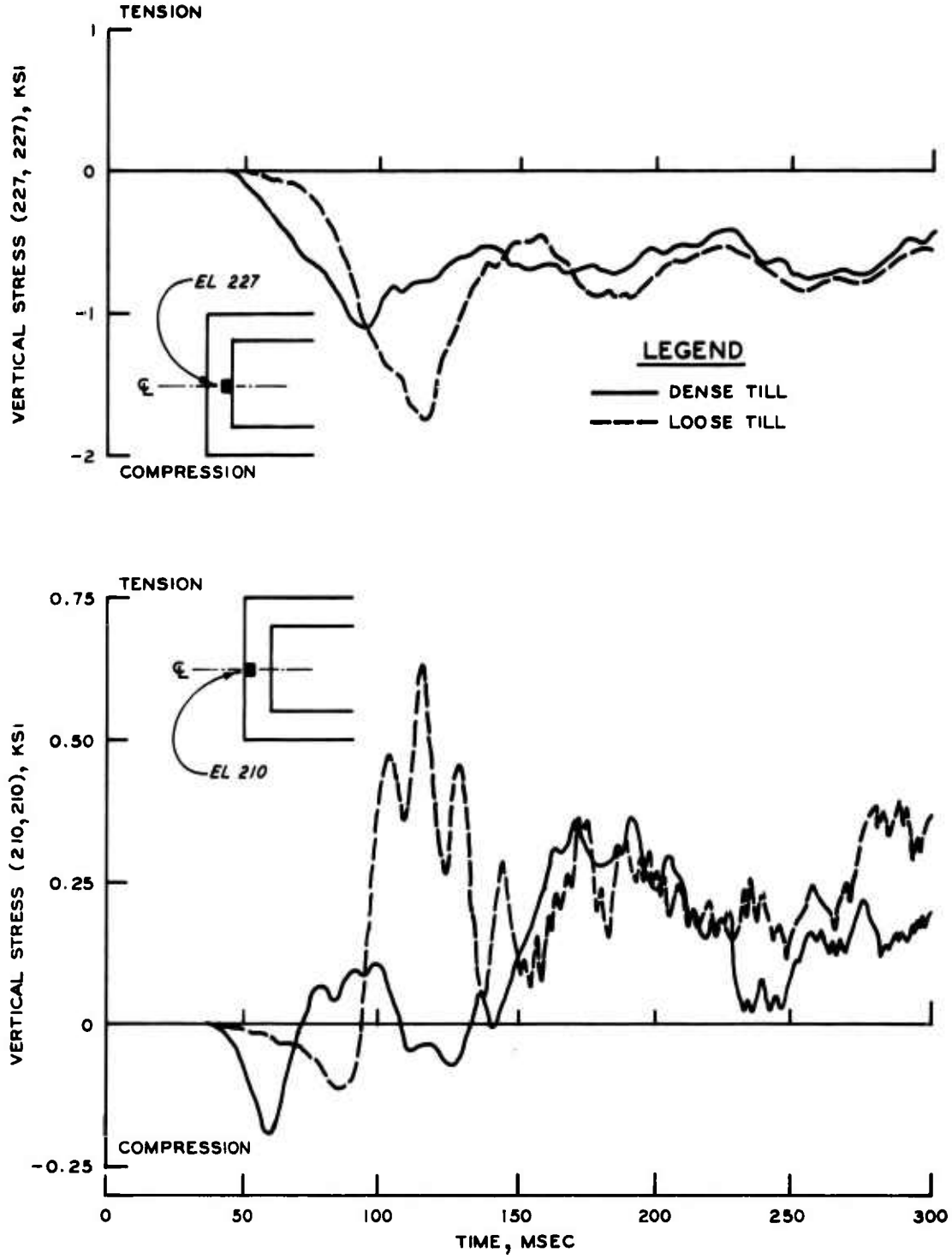

Figure 38. Vertical stress time histories at the midheight of the blastward sidewall; till backfill

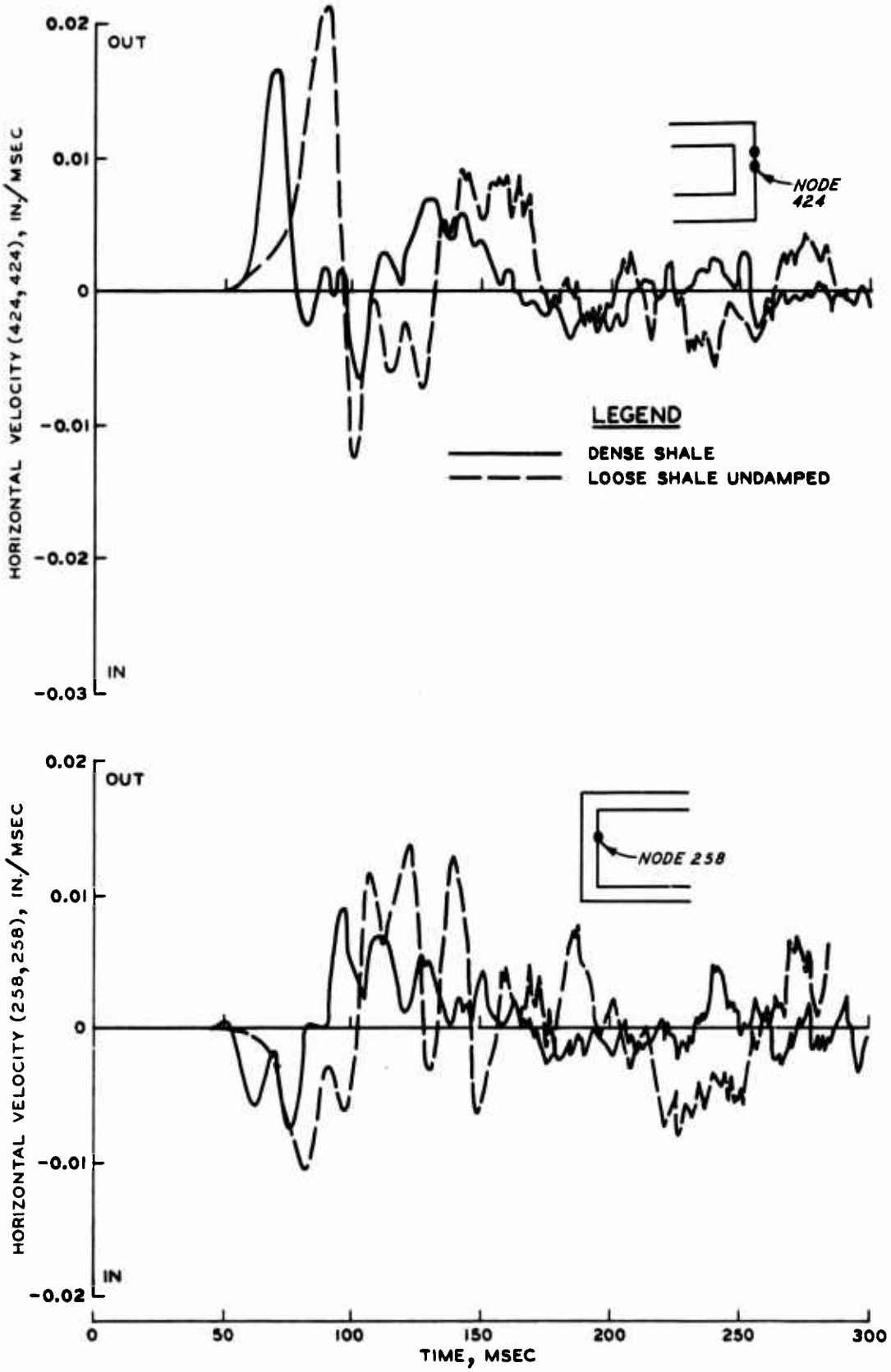

Figure 39. Horizontal velocity time histories for selected points in the structure sidewalls; shale backfill

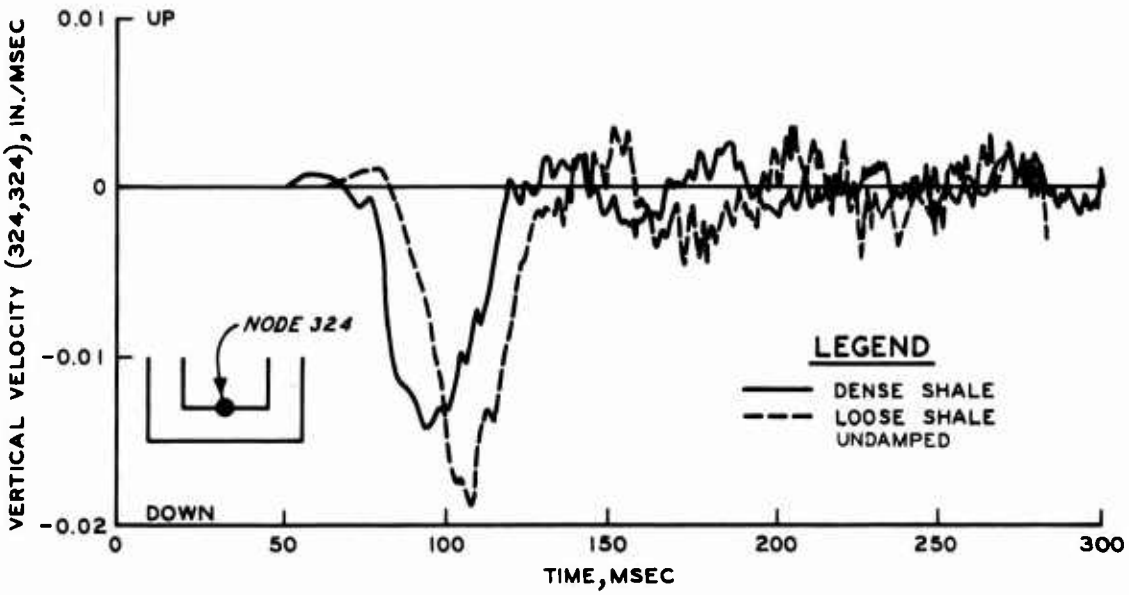

Figure 40. Vertical velocity time histories for the centerline of the floor of the structure; shale backfill

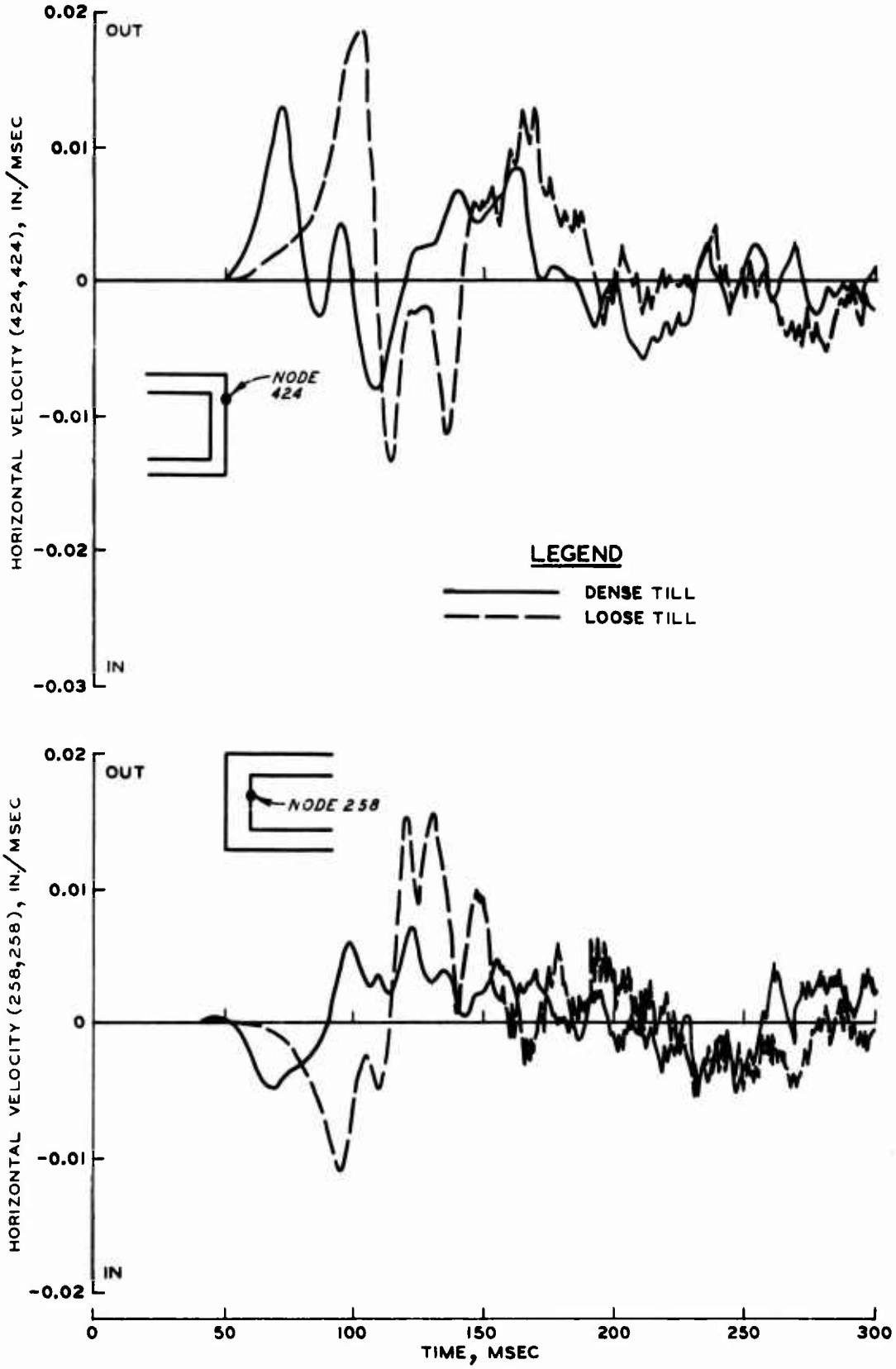

Figure 41. Horizontal velocity time histories for selected points in the structure sidewalls; till backfill

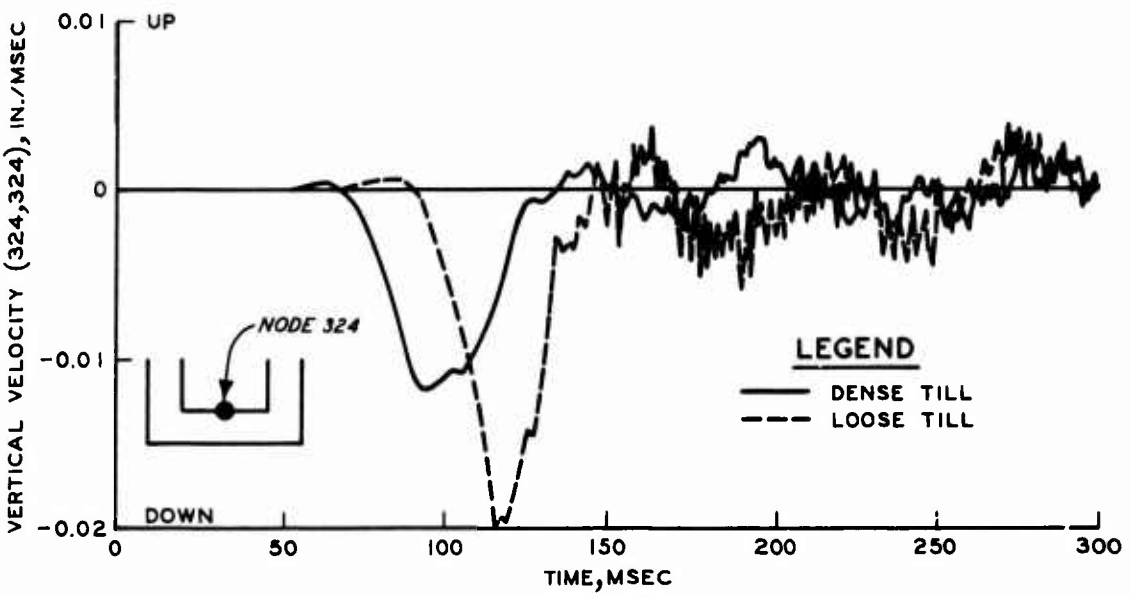

Figure 42. Vertical velocity time histories for the centerline of the floor of the structure; till backfill

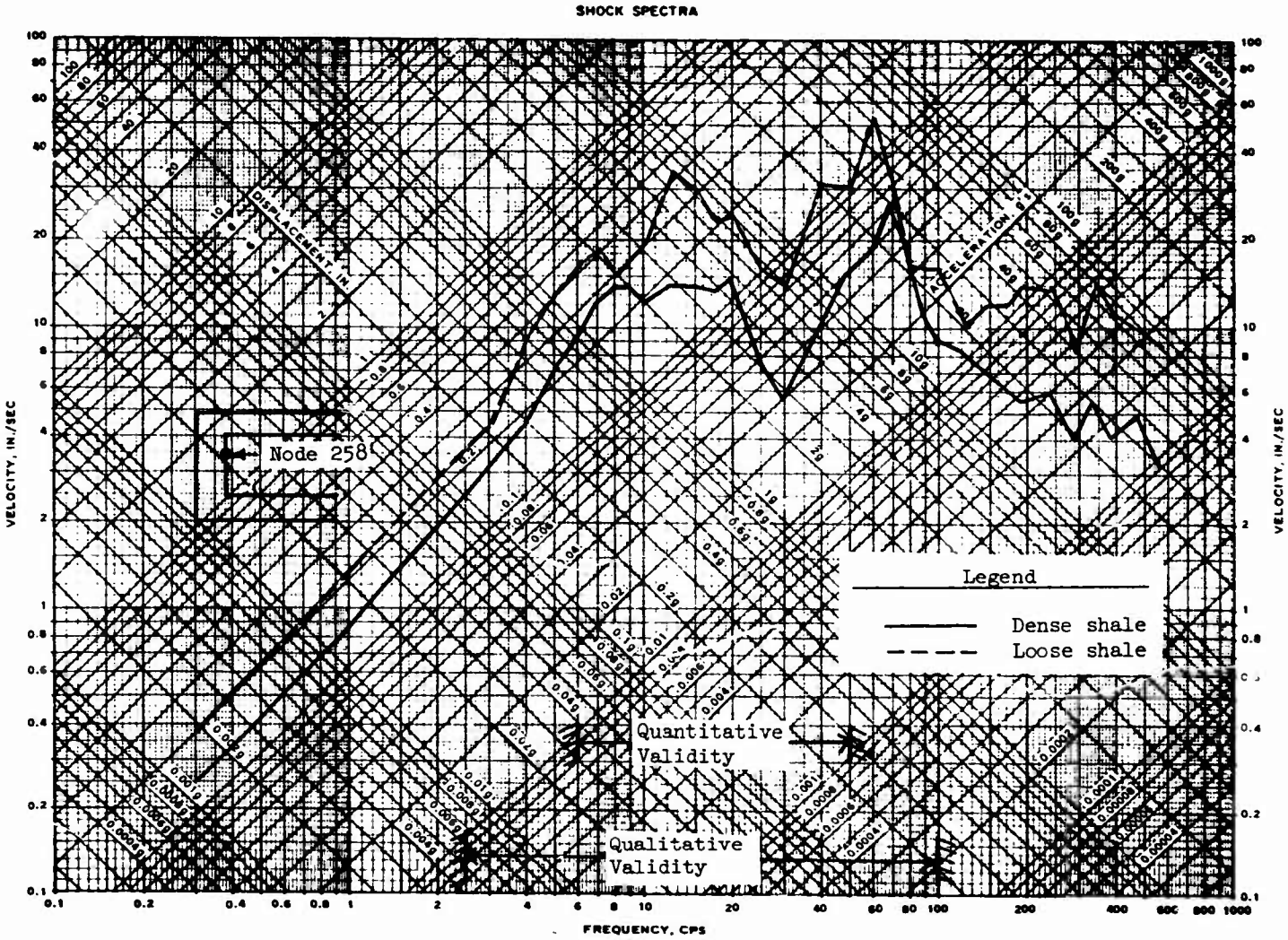

Figure 43. Horizontal shock spectra for a point (node 258) on the inside of the left sidewall of the structure; shale backfill

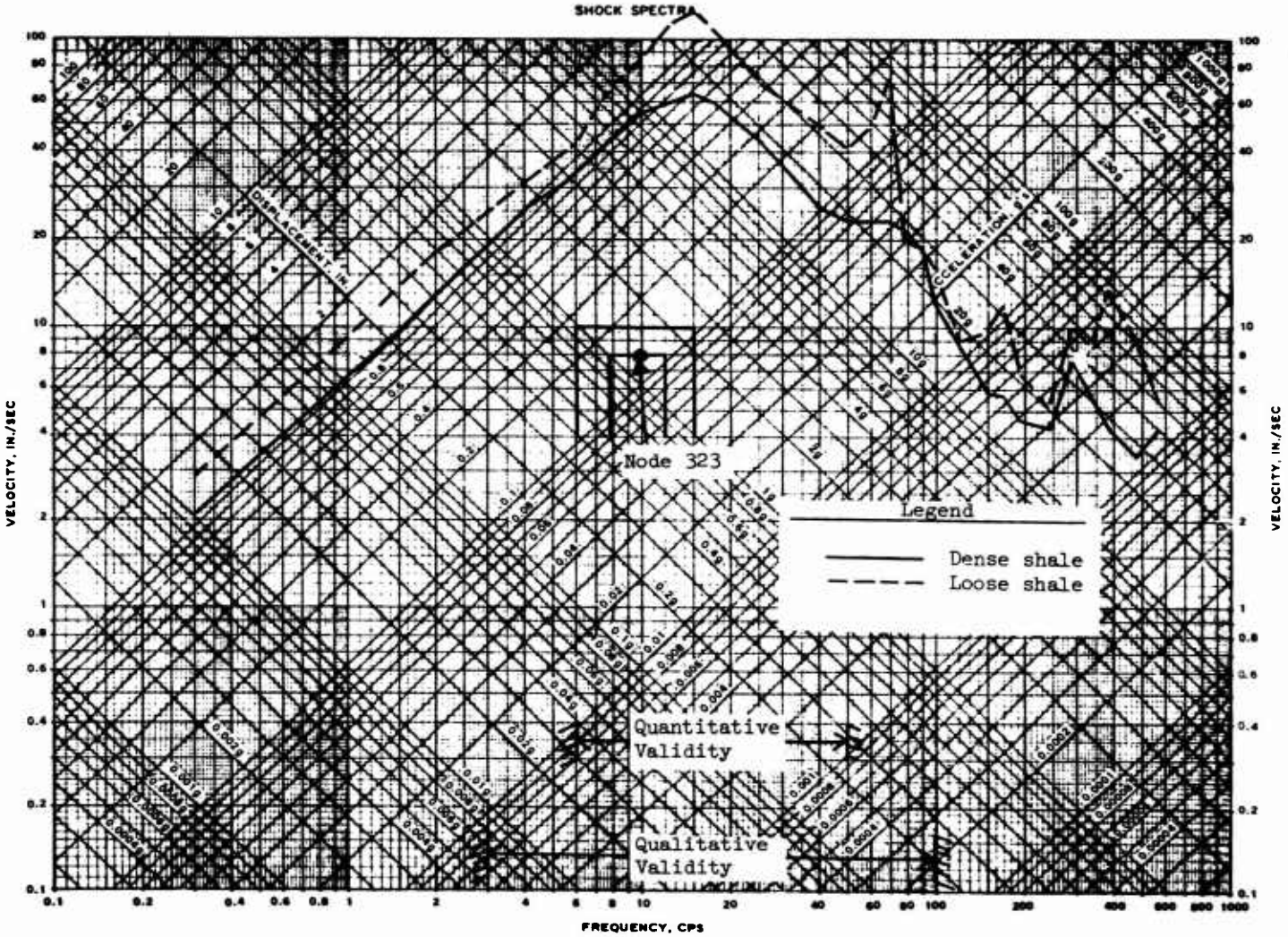

Figure 44. Vertical shock spectra for a point (node 323) on the inside of the roof of the structure; shale backfill

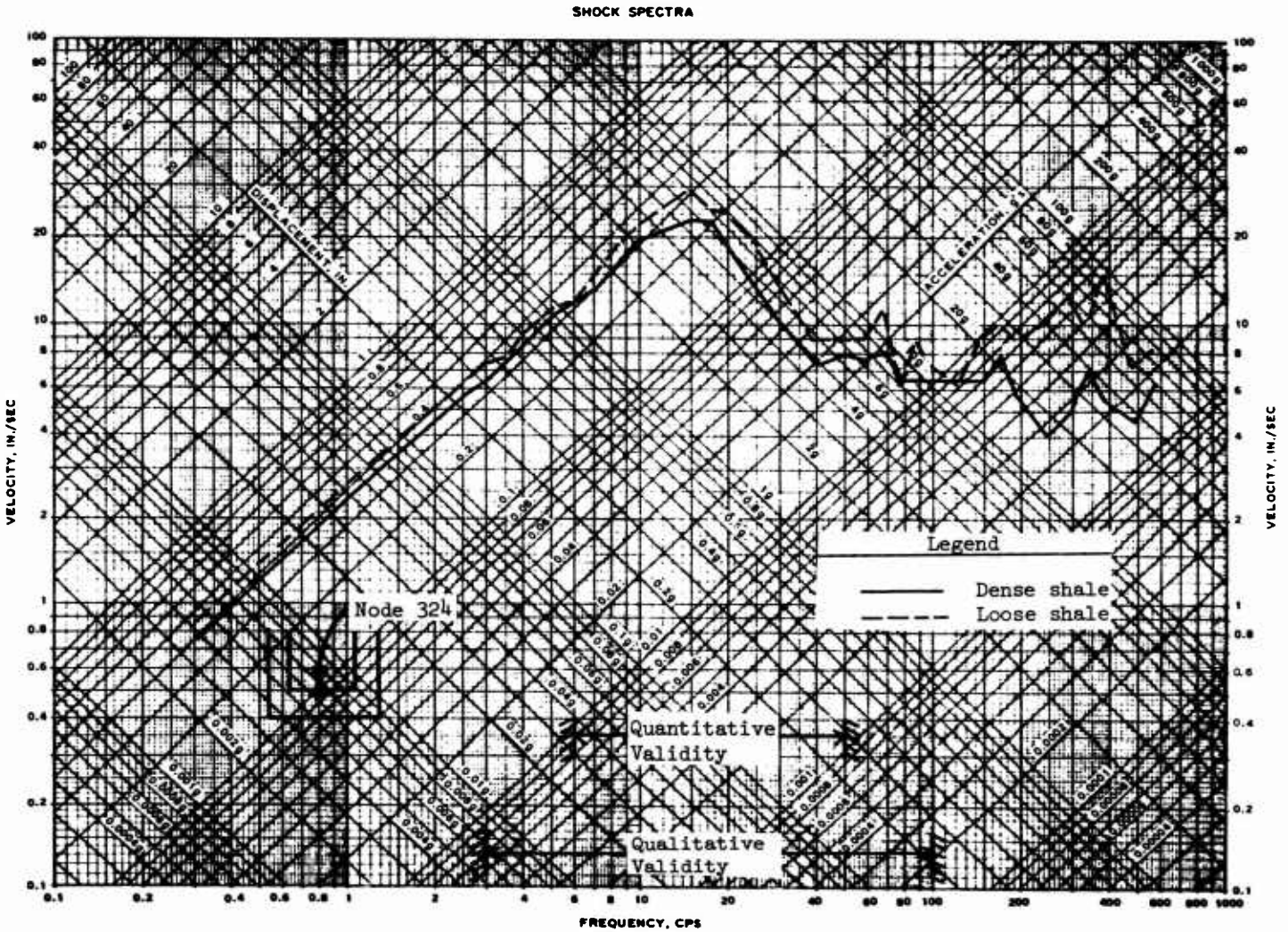

Figure 45. Vertical shock spectra for a point (node 324) on the floor of the structure; shale backfill

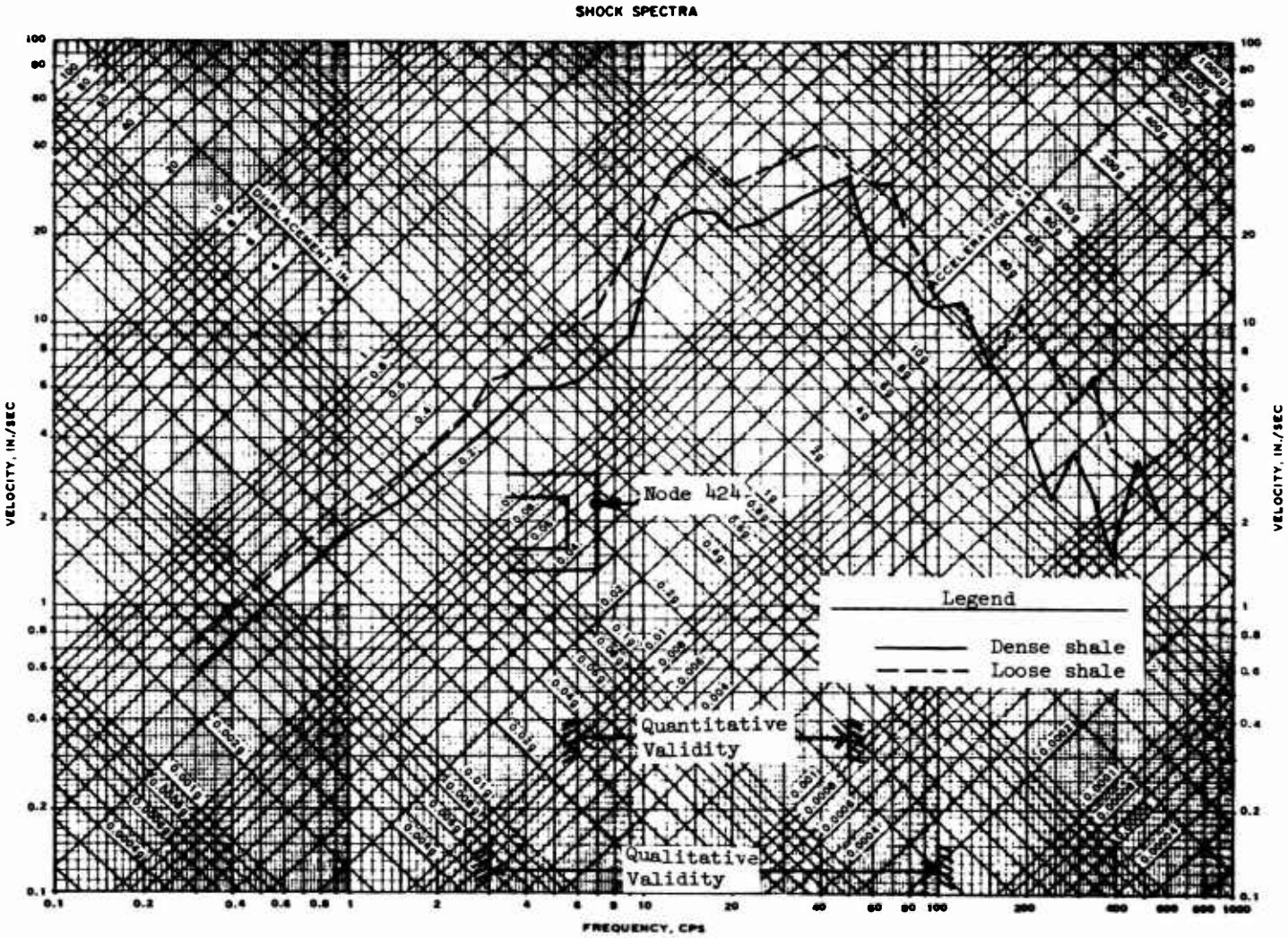

Figure 46. Horizontal shock spectra for a point (node 424) on the outside of the right sidewall of the structure; shale backfill

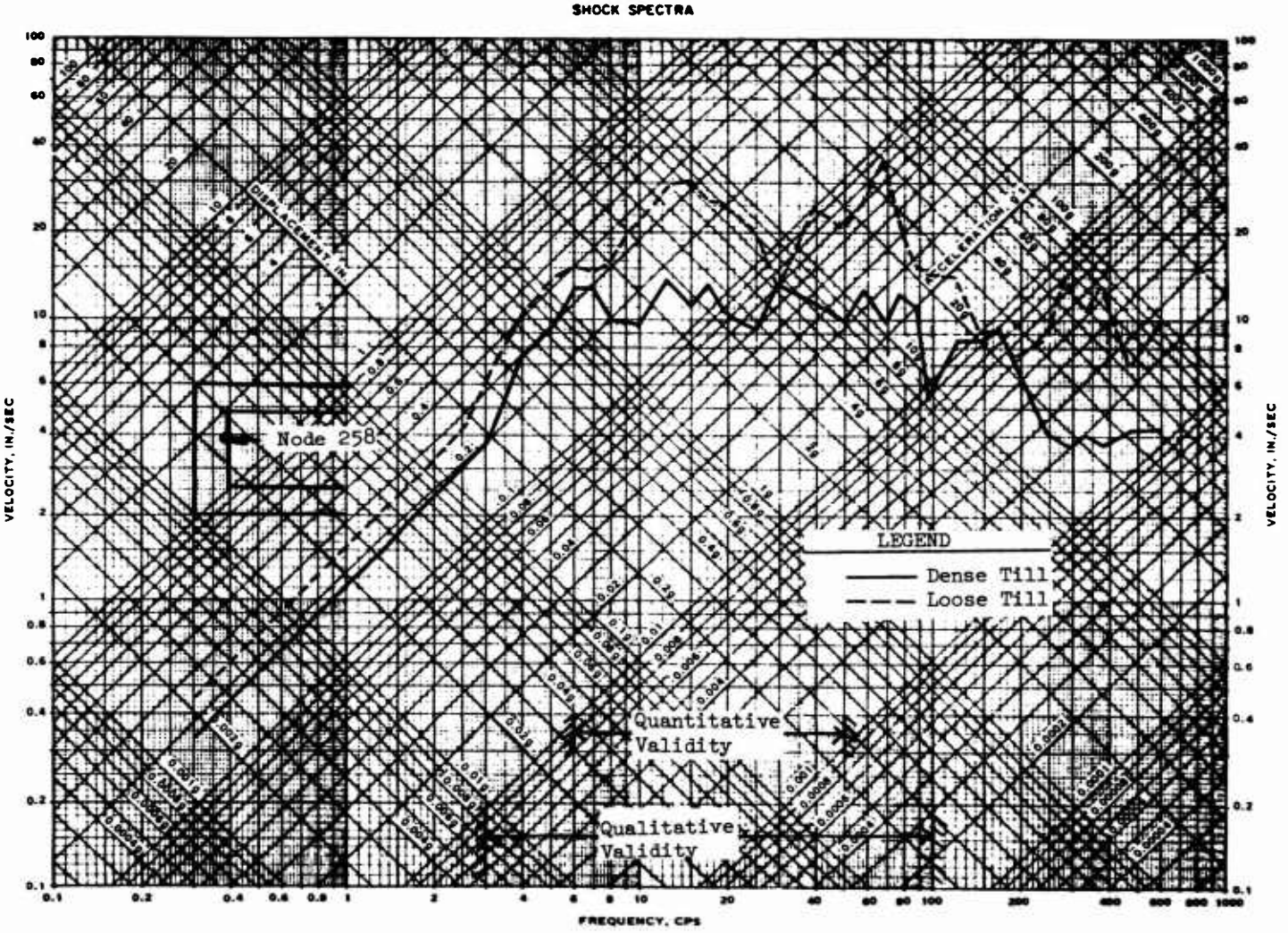

Figure 47. Horizontal shock spectra for a point (node 258) on the inside of the left sidewall of the structure; till backfill

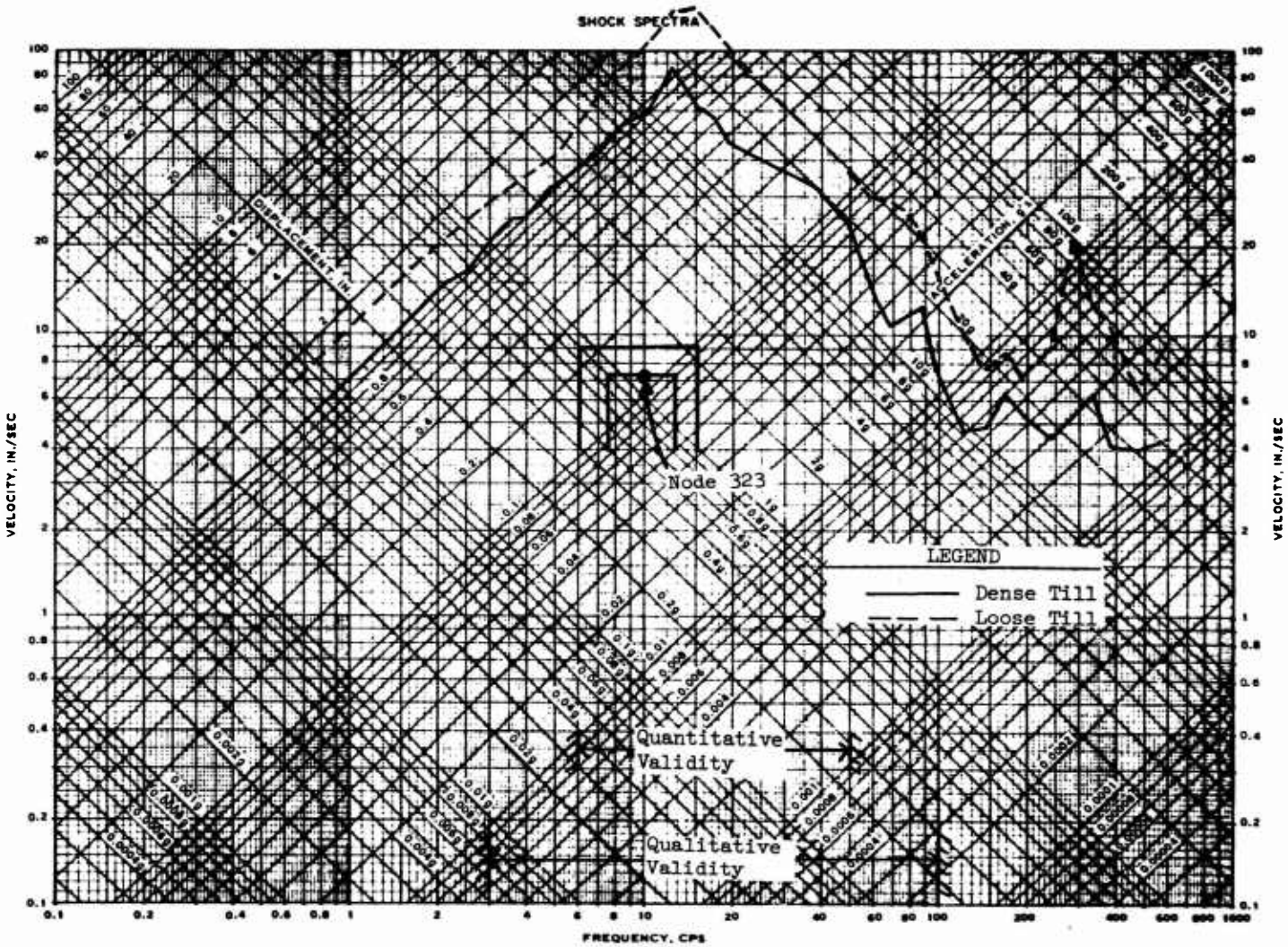

Figure 48. Vertical shock spectra for a point (node 323) on the inside of the roof of the structure; till backfill

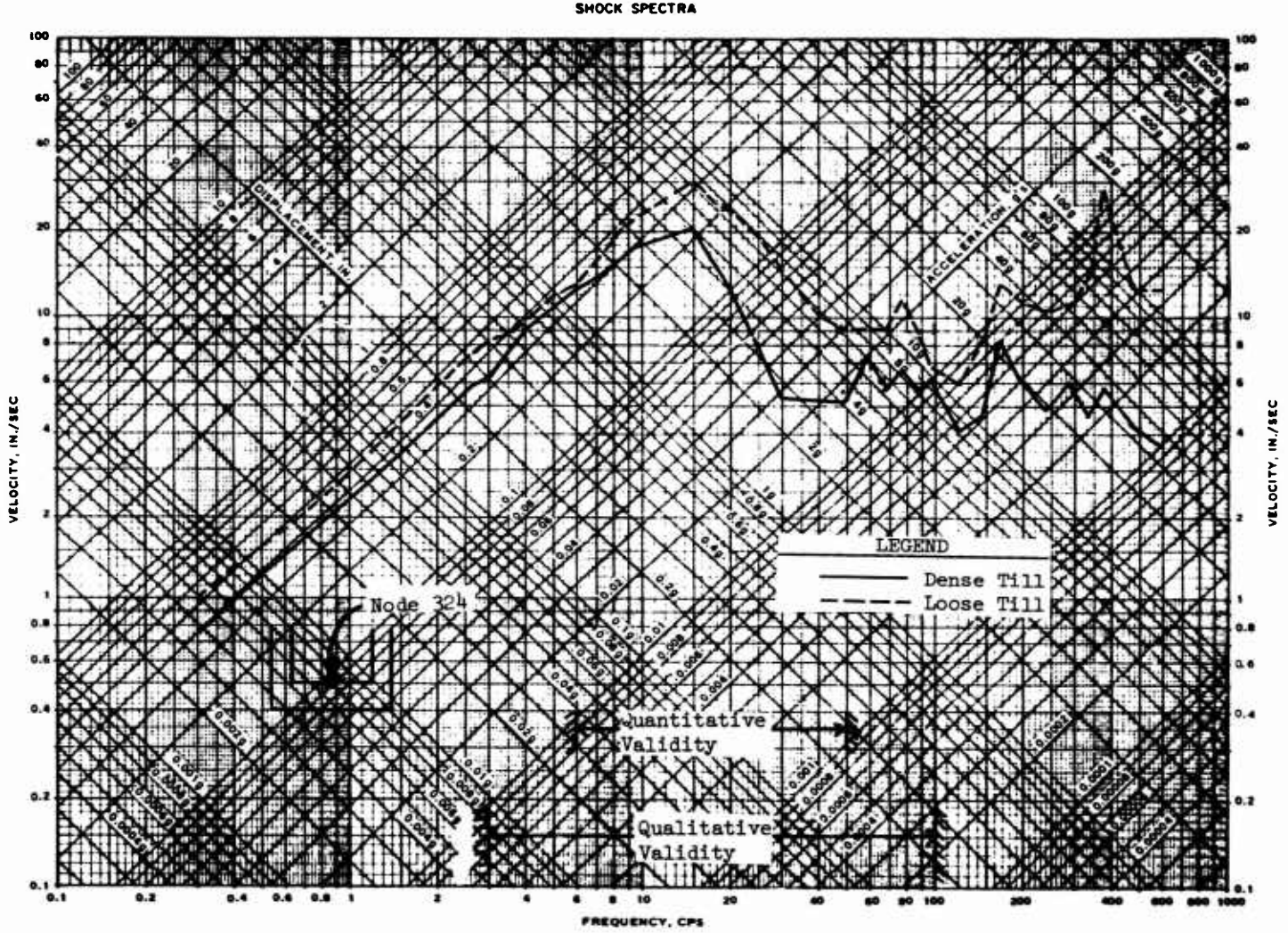

Figure 49. Vertical shock spectra for a point (node 324) on the floor of the structure; till backfill

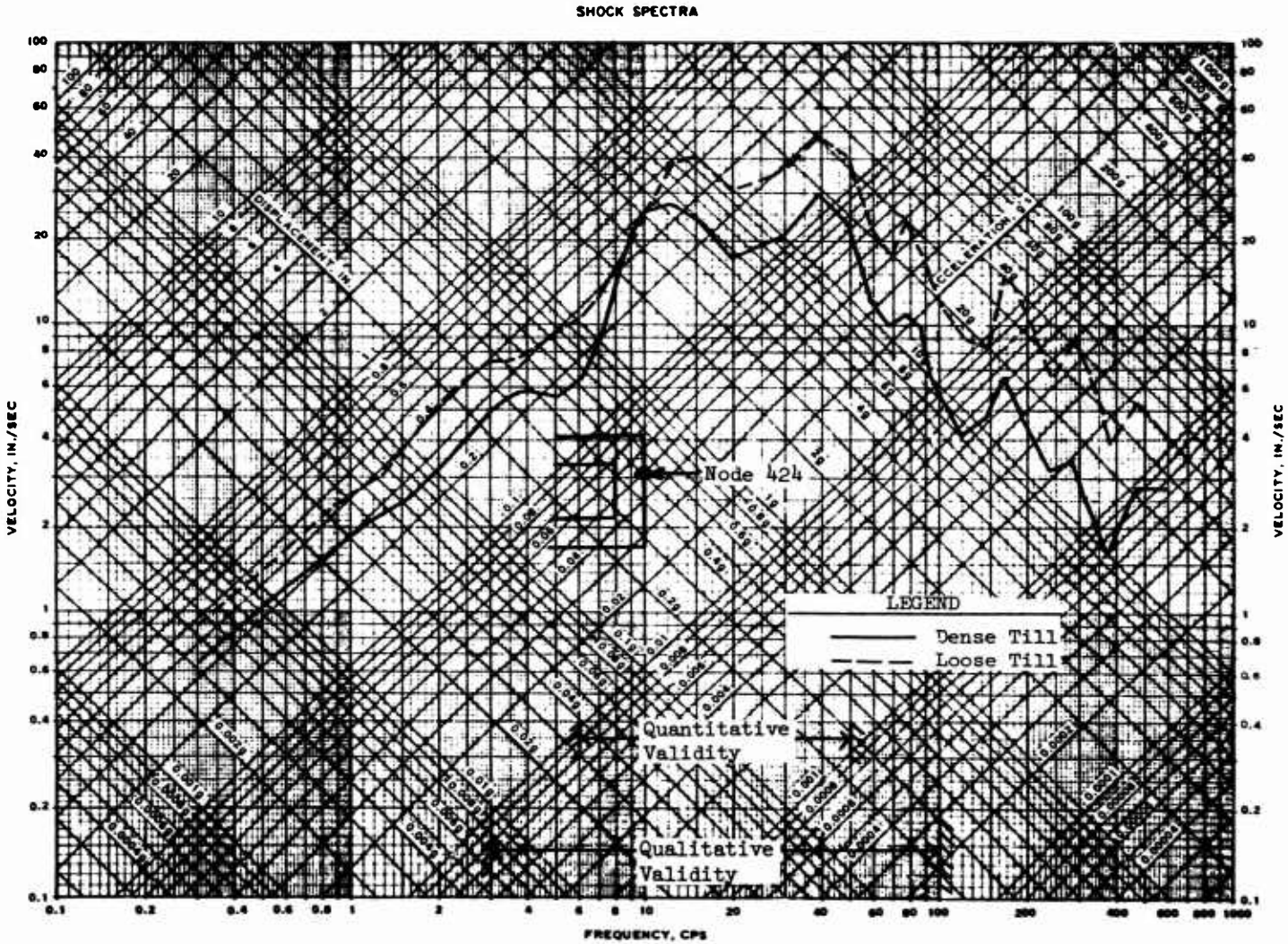

Figure 50. Horizontal shock spectra for a point (node 424) on the outside of the right sidewall of the structure; till backfill

Table 1

Maximum Rotation of the Chord Formed by the Two Bottom Outside Corners of the Structure

Shale Backfill Calculations

Type	Loose (Undamped) radians	Loose (Undamped) Time msec	Loose (Damped) radians	Loose (Damped) Time msec	Dense radians	Dense Time msec
Counterclockwise maximum	0.0006	90	0.0005	90	0.0005	70
Return to zero	0.0000	105	0.0000	100	0.0000	150
Clockwise maximum	0.0005	235	0.0010	235	0.0000	150-300

Till Backfill Calculations

Type	Loose radians	Loose Time msec	Dense radians	Dense Time msec
Counterclockwise maximum	0.0006	100	0.0004	75
Return to zero	0.0000	115	0.0000	150
Clockwise maximum	0.0005	230	0.0000	150-300

Table 2

Shear, Thrust, and Bending Moment for Selected Sections Through the Structure at a Time of 105 msec After the Start of the Shale Calculations

	Bending Moment in.-lb/in.			Axial Thrust lb/in.			Shear lb/in.		
Section*	Loose (UD)**	Loose (D)†	Dense	Loose (UD)	Lcose (D)	Dense	Loose (UD)	Loose (D)	Dense
AA	1,336,560	1,336,560	535,200	-7,440	-5,370	-4,060	-1920	-1700	-280
BB	198,360	133,560	93,480	1,610	2,060	-1,260	-6170	-5160	-650
CC	-462,480	-412,560	-186,480	-14,340	-12,690	-12,690	-8110	-7120	-2670
DD	-480,360	-526,440	-271,560	-20,700	-23,140	-19,790	1740	1250	-1200
EE	232,320	294,480	232,560	-16,640	-17,850	-15,350	3150	1620	2030
FF	156,680	132,000	-40,320	4,790	1,470	-600	50	2090	470
GG	753,600	846,600	590,920	270	3,620	1,640	-1280	-320	-770
HH	25,560	18,000	106,800	3,490	5,780	1,200	-1500	-1430	-1500
II	-49,080	-68,640	-156,480	-25,450	-21,830	-16,700	-4510	-4430	-3840
JJ	597,600	577,320	264,480	-26,330	-25,430	-19,610	-3030	-2390	1200
KK	484,080	450,840	166,920	-17,120	-16,520	-11,320	6240	5500	3080
LL	-282,600	-244,800	-15,720	-4,890	-3,380	-1,960	4260	2620	1430

* See Figure 17 for the location of these sections.
** UD = undamped calculation.
† D = damped calculation.

Table 3

Shear, Thrust, and Bending Moment for Selected Sections Through the Structure at a Time of 210 msec After the Start of the Shale Calculations

Section*	Bending Moment in.-lb/in.			Axial Thrust lb/in.			Shear lb/in.		
	Loose (UD)**	Loose (D)†	Dense	Loose (UD)	Loose (D)	Dense	Loose (UD)	Loose (D)	Dense
AA	321,240	329,640	329,640	-5,610	-3,850	-1,990	-1470	790	230
BB	113,400	86,160	12,840	-2,650	-2,320	80	-2930	-3080	-1120
CC	100,080	-96,160	-56,040	-6,840	-7,610	-6,050	-4330	-4600	-2890
DD	-211,920	-195,960	-235,320	-15,660	-13,000	-10,140	-750	-330	-1310
EE	207,600	176,760	280,080	-14,250	-10,290	-5,300	2230	1930	1200
FF	-106,800	-100,800	-100,200	630	670	-750	580	-790	160
GG	695,520	779,640	-581,640	-3,780	-4,680	-3,340	460	330	210
HH	285,360	274,800	134,040	500	910	510	-5090	-6180	-2220
II	-334,920	-326,400	-207,720	-3,570	-2,890	-3,400	-5650	-5480	-3040
JJ	249,360	224,520	228,120	-7,660	-6,800	-7,090	3290	2800	980
KK	-17,760	-43,200	76,920	-4,240	-4,570	-5,770	-430	-1990	990
LL	225,120	253,080	74,880	-1,200	-910	-1,090	-1330	-2890	-90

* See Figure 17 for the location of these sections.
** UD = undamped calculation.
† D = damped calculation.

Table 4

Shear, Thrust, and Bending Moment for Selected Sections Through the Structure at a Time of 105 msec After the Start of the Till Calculations

Section	Bending Moment in.-lb/in.		Axial Thrust lb/in.		Shear lb/in.	
	Loose	Dense	Loose	Dense	Loose	Dense
AA	1,343,760	687,720	-8,160	840	-4760	-3040
BB	385,680	132,200	-2,870	1,930	-2740	-1570
CC	-810,360	-276,720	-27,270	-14,230	-6900	-4740
DD	-701,040	-12,120	-37,730	-51,460	7340	440
EE	-79,440	145,320	-30,950	-18,410	1530	2320
FF	274,320	58,800	7,580	1,540	-4380	-170
GG	573,120	530,400	12,120	2,710	2300	20
HH	-79,440	141,480	7,750	660	-2230	-630
II	-74,520	-154,680	-18,900	-13,390	-5080	-2890
JJ	532,440	246,000	-23,550	-18,220	-2530	-250
KK	506,400	228,360	-16,070	-10,870	7660	4440
LL	-214,560	-204,840	-760	590	5490	2470

Table 5

Shear, Thrust, and Bending Moment for Selected Sections Through the Structure at a Time of 210 msec After the Start of the Till Calculations

Section	Bending Moment in.-lb/in.		Axial Thrust lb/in.		Shear lb/in.	
	Loose	Dense	Loose	Dense	Loose	Dense
AA	333,000	388,560	-3,880	1740	1630	140
BB	94,560	113,880	-2,830	1120	-3880	-2180
CC	-153,120	-150,360	-6,950	-5580	-3370	-3060
DD	-238,560	-238,200	-11,890	-8640	700	540
EE	150,000	143,160	-9,720	-5140	2560	840
FF	-23,280	-56,880	1,610	100	990	-1130
GG	819,480	513,960	-6,520	-1250	700	410
HH	365,160	135,960	-1,390	1490	-6180	-2900
II	-400,800	-224,400	-3,990	-3470	-5610	-3830
JJ	238,560	227,880	-9,630	-6520	4090	-1680
KK	-17,760	57,960	-8,010	-4800	90	1320
LL	212,640	72,360	-1,790	3470	-2050	-960

APPENDIX A: CAP MODEL FITS FOR BACKFILL MATERIALS

1. The material model incorporated into DUFE and used for these calculations is identical to the one described in a WES letter to HQDA (see footnote on page 5 of main text). The cap model fits and the material properties for free-field layers 1-4 (Figure 1 of main text) are also presented in the above-mentioned letter. The material properties for the backfill materials used in this study (i.e., dry loose and dense till and dry loose and dense shale backfill) are presented in Reference 1. Cap model fits of the type presented in the WES letter were also made for these backfill materials.

2. Figures A1 and A2 compare the cap model fits with the recommended (UX) stress-strain curves for the dry dense and loose shale materials, respectively. Figures A3 and A4 present the same comparisons for the dry dense and loose till materials, respectively. As shown in these figures, very good fits were obtained to the recommended UX stress-strain relations. Since the maximum input overpressure was 50 psi, more attention was directed toward modeling the lower pressure portions of the UX curves. For example, in Figure A1, the unloading from 80 psi was modeled more closely than the unloading from 160 psi.

3. Cap model fits to the yield surface and stress paths are compared with the recommended material properties for the dense and loose shale backfill in Figures A5 and A6, respectively. Figures A7 and A8 show similar comparisons for the dense and loose till backfill materials. The fits are considered very good.

4. The material constants which define these model fits and which are actually used as calculational input are shown in Tables A1 and A2 for the till and shale backfill, respectively.

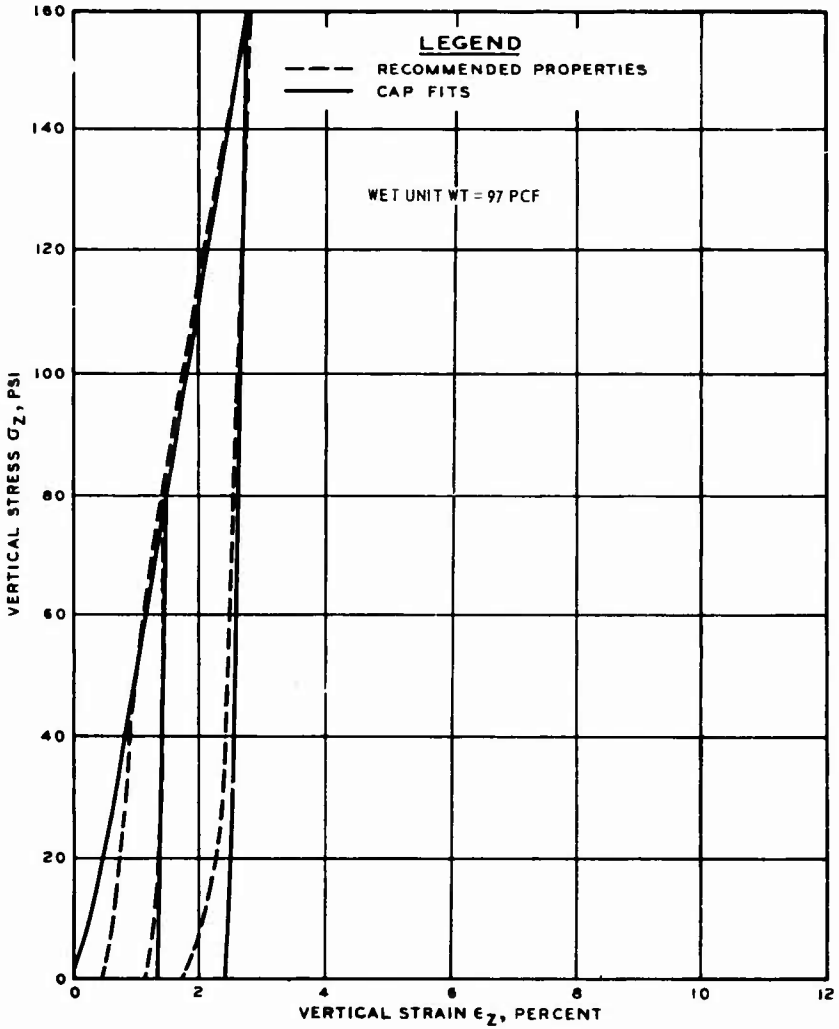

Figure A1. Comparison of model fit with recommended UX stress-strain curve for dense shale

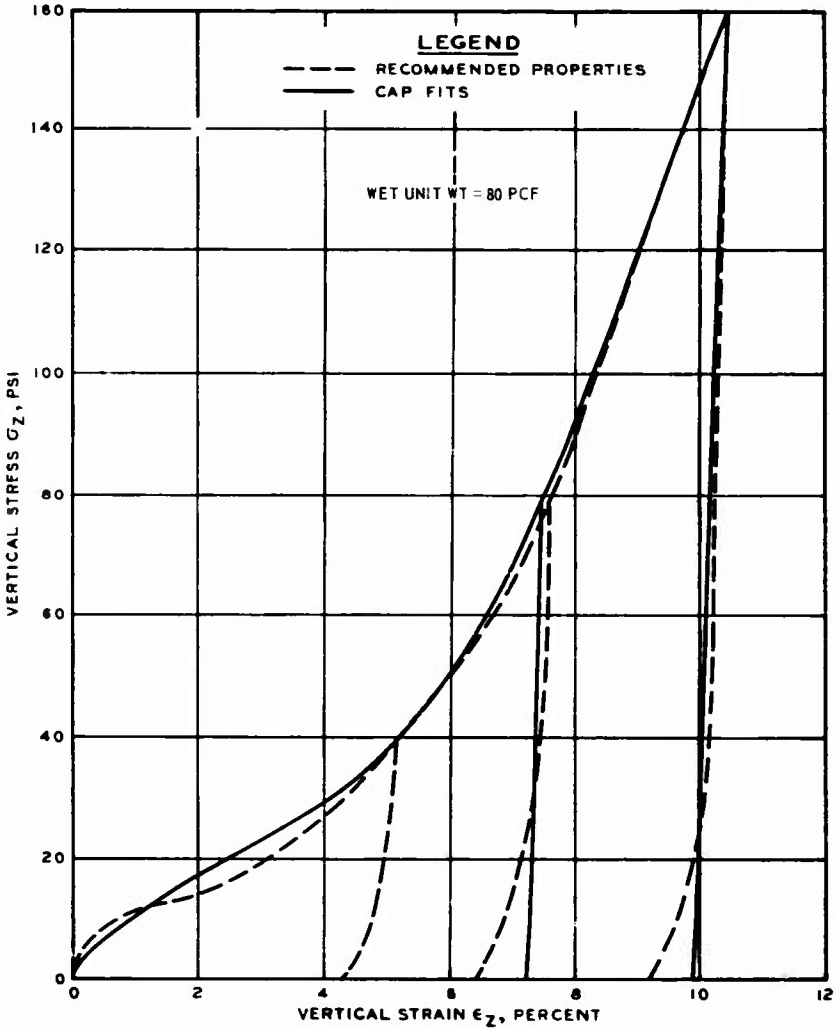

Figure A2. Comparison of model fit with recommended UX stress-strain curve for loose shale

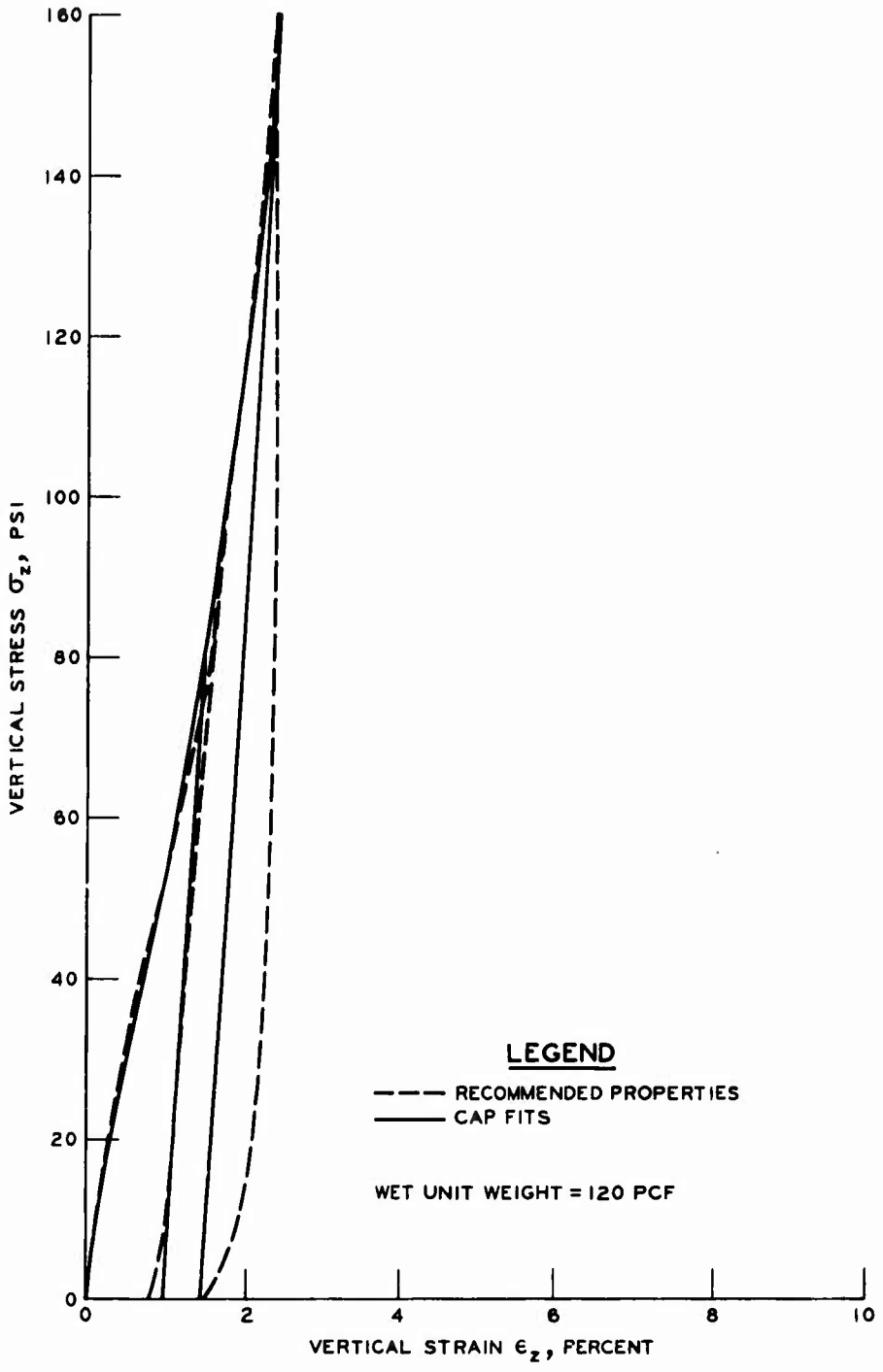

Figure A3. Comparison of model fit with recommended UX stress-strain curve for dense till

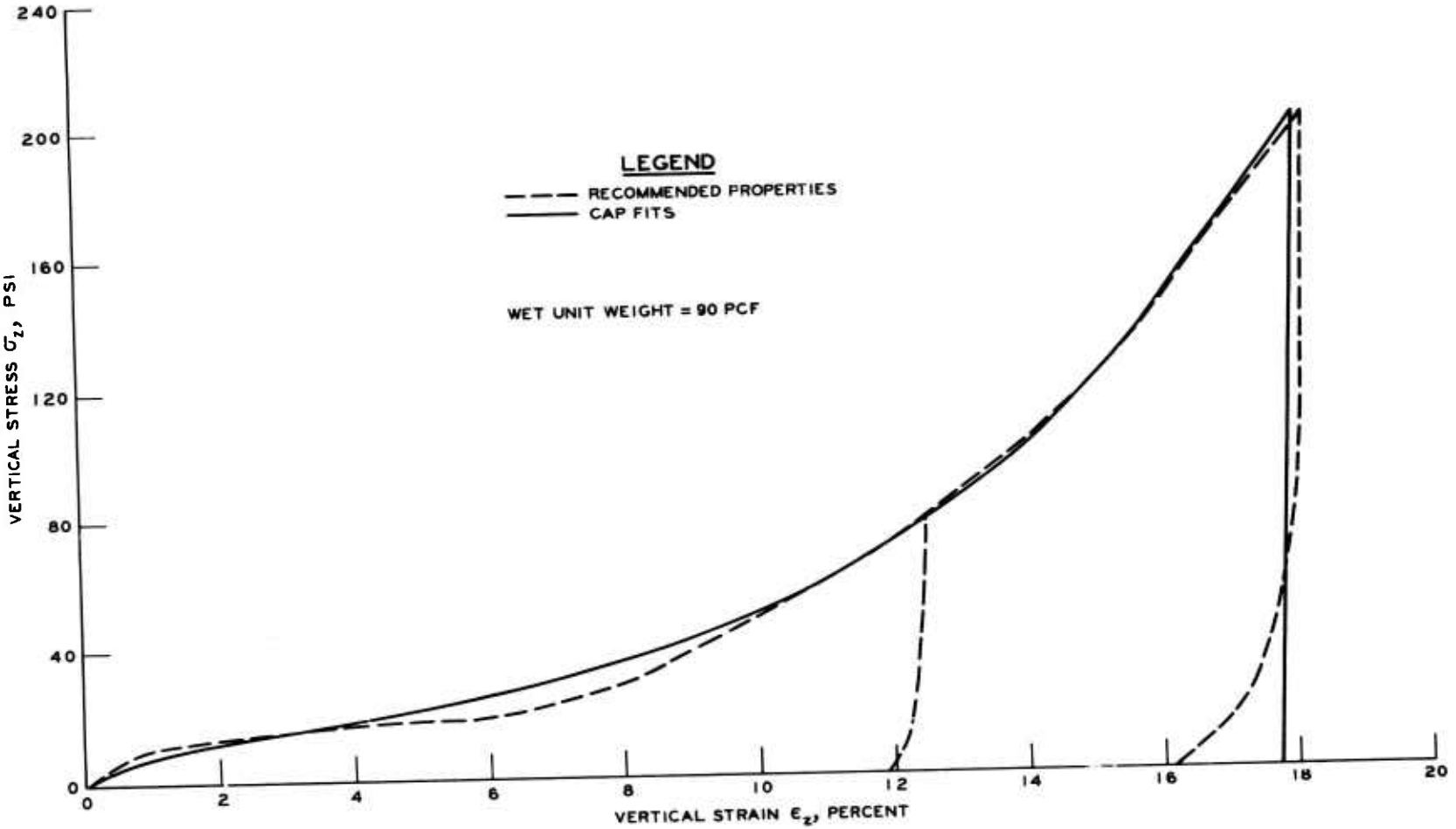

Figure A4. Comparison of model fit with recommended UX stress-strain curve for loose till

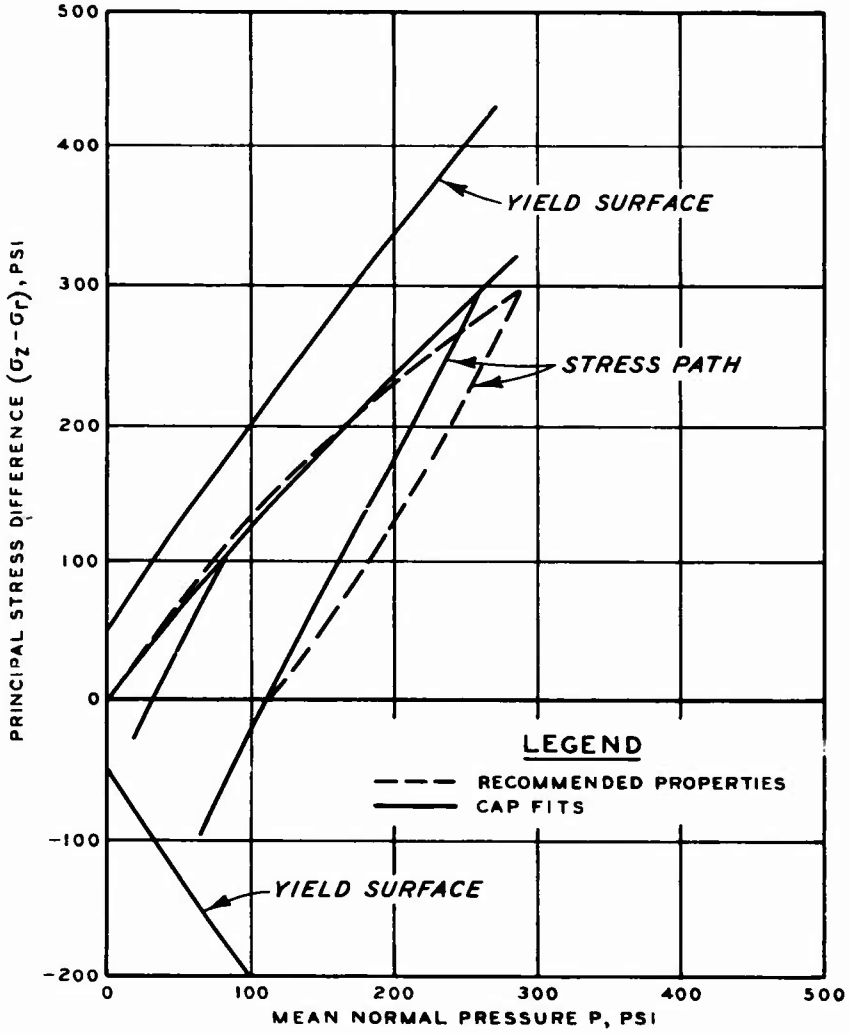

Figure A5. Comparison of model fit with recommended yield surface and UX stress path for dense shale

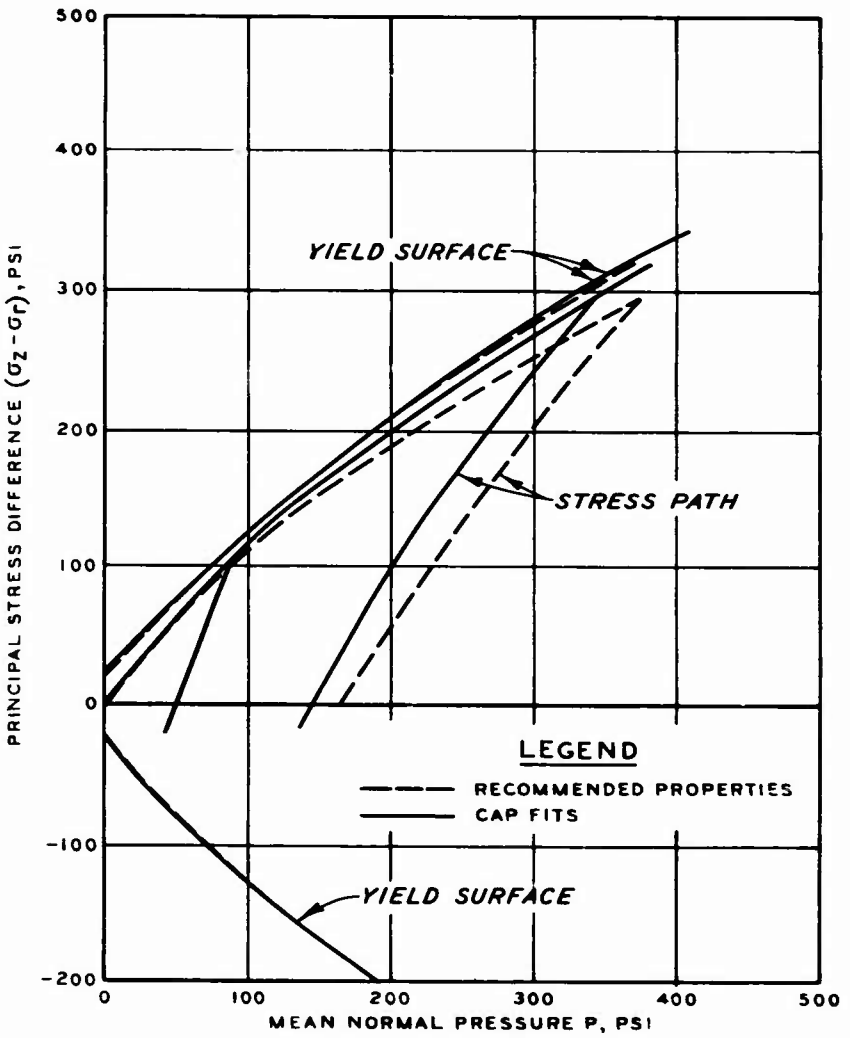

Figure A6. Comparison of model fit with recommended yield surface and UX stress path for loose shale

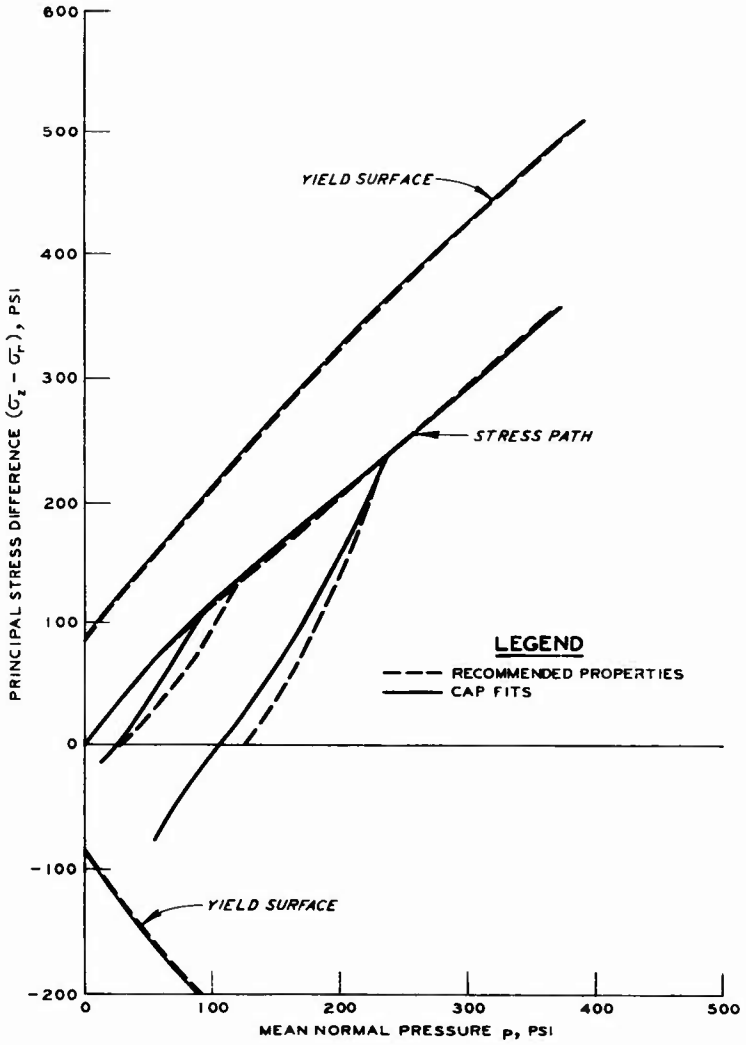

Figure A7. Comparison of model fit with recommended yield surface and UX stress path for dense till

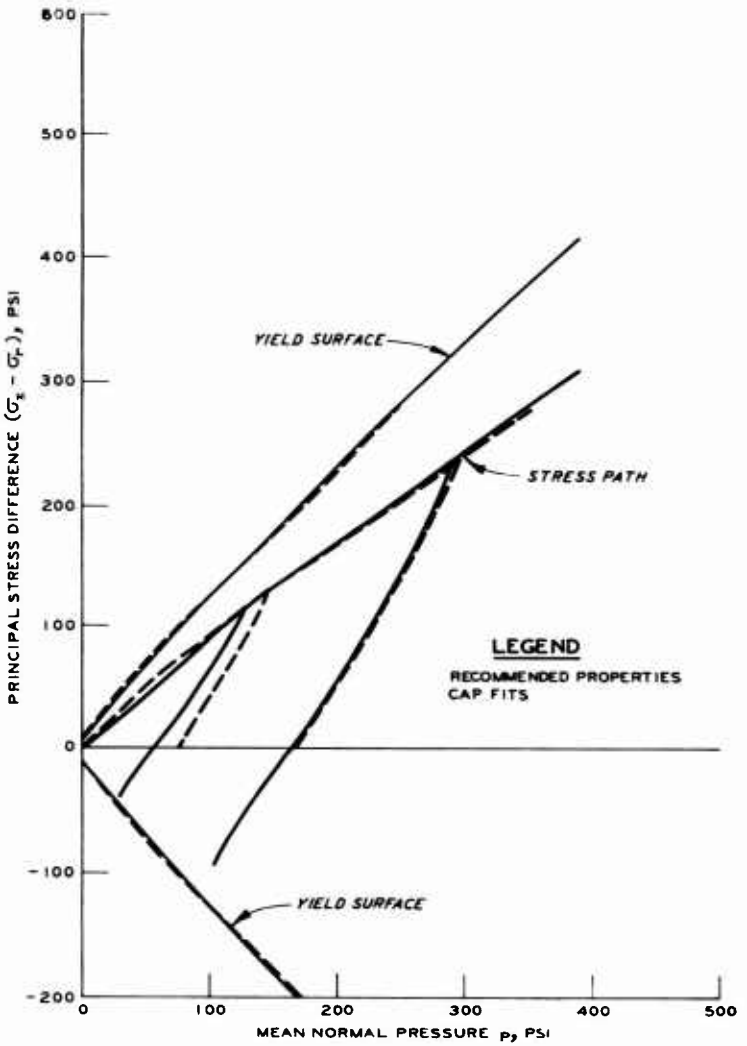

Figure A8. Comparison of model fit with recommended yield surface and UX stress path for loose till

Table A1

Material Constants for Cap Fits for

Dry Type I (Till) Materials

Term*	Units	Constants for Dry Dense Till	Constants for Dry Loose Till
A	ksi	0.7436	0.8718
B	ksi^{-1}	0.37	0.27
C	ksi	0.6928	0.86603
R_0		8.0	2.0
R_1		-0.5	1.0
R_2	ksi^{-1}	10.0	15.0
W		0.0125	0.15
D	ksi^{-1}	9.0	9.0
α		1.0	0.8
D_1	ksi^{-1}	14.0	9.1
D_2	ksi^{-2}	20.0	500.0
W_1	ksi^{-2}	0.0021	0.15
D_F	ksi^{-1}	0.5	0.1
K_{max}	ksi	8.0	25.0
K_1		0.0	0.0
DK_1	ksi^{-1}	0.0	0.0
DK_2	ksi^{-2}	0.0	0.0
G_{max}	ksi	10.25	32.0
G_R		0.5	0.5
G_1	ksi^{-1}	10.00	10.0

* See Reference 4 for definition of these terms.

Table A2

Material Constants for Cap Fits for

Dry Type II (Shale) Materials

Term*	Units	Constants for Dry Dense Shale	Constants for Dry Loose Shale
A	ksi	1.045	0.37124
B	ksi^{-1}	0.3	0.6
C	ksi	1.016	0.35796
R_0		2.1	0.875
R_1		0.75	3.0
R_2	ksi^{-1}	9.0	11.0
W		0.097	0.152
D	ksi^{-1}	0.8	3.0
α		0.0	1.0
D_1	ksi^{-1}	0.0	12.0
D_2	ksi^{-2}	0.0	600.0
W_1	ksi^{-2}	4.0	11.0
D_F	ksi^{-1}	40.0	20.0
K_{max}	ksi	22.0	30.0
K_1		0.0	0.7
DK_1	ksi^{-1}	0.0	0.0
DK_2	ksi^{-2}	0.0	1.0
G_{max}	ksi	22.0	13.0
G_R		0.0	0.0
G_1	ksi^{-1}	0.0	0.0

* See Reference 4 for definition of these terms.

APPENDIX B: PROBLEMS ENCOUNTERED WITH LOOSE BACKFILL CALCULATIONS

1. No problems were encountered in conducting the dense till and shale calculations. However, when the loose shale calculation was performed using the same grid spacing as was used for the dense shale calculation, large oscillations resulted in some of the stress and acceleration time history output. This was traced to the combination of the exaggerated "S" shaped nature of the UX stress-strain curve (see Figure 2 of the main text of this report) and the coarse grid in the backfill and the low loading moduli inherent in parts of the "S" shaped curve. The possibilities for overcoming this problem are to reduce the grid spacing or to introduce artificial viscosity. Although the best way to solve the problem is to reduce the grid size, this alternative was determined to be too costly in terms of money and computer time for the present investigation. Therefore, the artificial viscosity route was pursued.

2. Various methods of achieving damping by introducing artificial viscosity and various percentages of damping were used in 1D wave propagation calculations for the loose shale material. The artificial viscosity used with this program was operated by adding increments of stress to the existing σ_{ij}. The stress increments were computed as follows:

$$\dot{\sigma}_{ij} = \frac{C_2 \dot{\epsilon}_{kk}}{3} + C_2 \dot{e}_{ij} \text{ for } i = j \tag{B1}$$

$$\dot{\sigma}_{ij} = 0 \text{ for } i \neq j \tag{B2}$$

where

$\dot{\sigma}_{ij}$ = components of the total stress increment tensor due to damping

C_2 = damping coefficient

$\dot{\epsilon}_{kk}$ = sum of the incremental normal strains = incremental change in volumetric strain

$\dot{e}_{ij}$ = components of the deviatoric strain increment tensor

i = index*

j = index

For the plane strain problem solved the new radial σ_{rr}, vertical σ_{zz}, and tangential $\sigma_{\theta\theta}$ stresses after adding the increment of stresses calculated by Equation B1 become:

$$\sigma_{rr\ new} = \sigma_{rr\ old} + \dot{\sigma}_{rr} \tag{B3}$$

$$\sigma_{zz\ new} = \sigma_{zz\ old} + \dot{\sigma}_{zz} \tag{B4}$$

$$\sigma_{\theta\theta\ new} = \sigma_{\theta\theta\ old} + \dot{\sigma}_{\theta\theta} \tag{B5}$$

These new stress components are used to compute a new internal force vector for the next time step and, thus, an artificial viscosity effect is introduced. The final value of C_2 used with the loose shale calculations was 10,000 psi.

3. The basic problem encountered with the use of artificial viscosity to damp out oscillations was that the material properties were, in effect, changed by the introduction of the additional terms to the equations of motion. The UX stress-strain curve for the loose shale backfill became less compressible and the stress path was altered so that, for the same value of mean normal pressure, a larger stress difference was obtained for the stress path for damped conditions than was obtained for undamped conditions. After a great many trials, an optimum amount of damping was determined which would alter the material properties the least possible amount and would also cut the stress oscillations to a tolerable level. An additional loose shale 2D calculation was then conducted which was identical to the undamped calculation except for the added artificial viscosity.

4. In Figure B1, the output vertical stress time histories at

---

* Indices take on the value of 1, 2, or 3. A repeated index is to be summed out over its range.

the 1.25-ft depth from 1D loose shale calculations with and without artificial viscosity are compared to a vertical stress time history for the same depth obtained by the method of characteristics (i.e., by assuming that the material had a linear stress-strain relation and that its constrained modulus was equal to the actual secant loading modulus to peak stress). As can be seen in Figure B1, in the stress time history for the undamped calculation, the maximum and minimum stresses were 80 and -3 psi, respectively, while the maximum and minimum stresses in the damped stress time history were 70 and 14 psi, respectively. It can also be seen that the oscillations appear to be decaying at a more rapid rate in the damped stress time history and is closer to the relation obtained by the method of characteristics.

5. The apparent variations in material properties caused by the artificial viscosity are depicted in Figures B2 and B3. In Figure B2 the cap fit to the UX vertical stress σ_z versus vertical strain ε_z curve is compared with the σ_z versus ε_z relations derived from output from the loose shale 1D wave propagation calculations with and without artificial viscosity. The σ_z versus ε_z relation from the undamped calculation was identical to the cap fit, but as can be seen, the loading σ_z versus ε_z relation from the damped calculation is less compressible than the σ_z versus ε_z fit.* The cap model fit to the loose shale stress path is compared with the output stress paths from the same calculations in Figure B3. The stress path from the undamped calculation is identical to the cap fit. However, the loading stress path from the damped calculation depicts larger stress differences than does the cap fit for the same values of mean normal pressure. The unloading stress paths are identical for all cases (see the footnote at the bottom of the page).

6. Comparison of the structure response in the damped and undamped loose shale 2D calculations showed only small differences between

---

* Artificial viscosity was only applied during loading and reloading phases; therefore, the unloading curves are identical in all cases. The same was true in the case of the large 2D calculation in loose shale.

the two sets of results as has been illustrated in many of the figures accompanying the main text. Therefore, only an undamped 2D calculation was conducted for the loose till case.

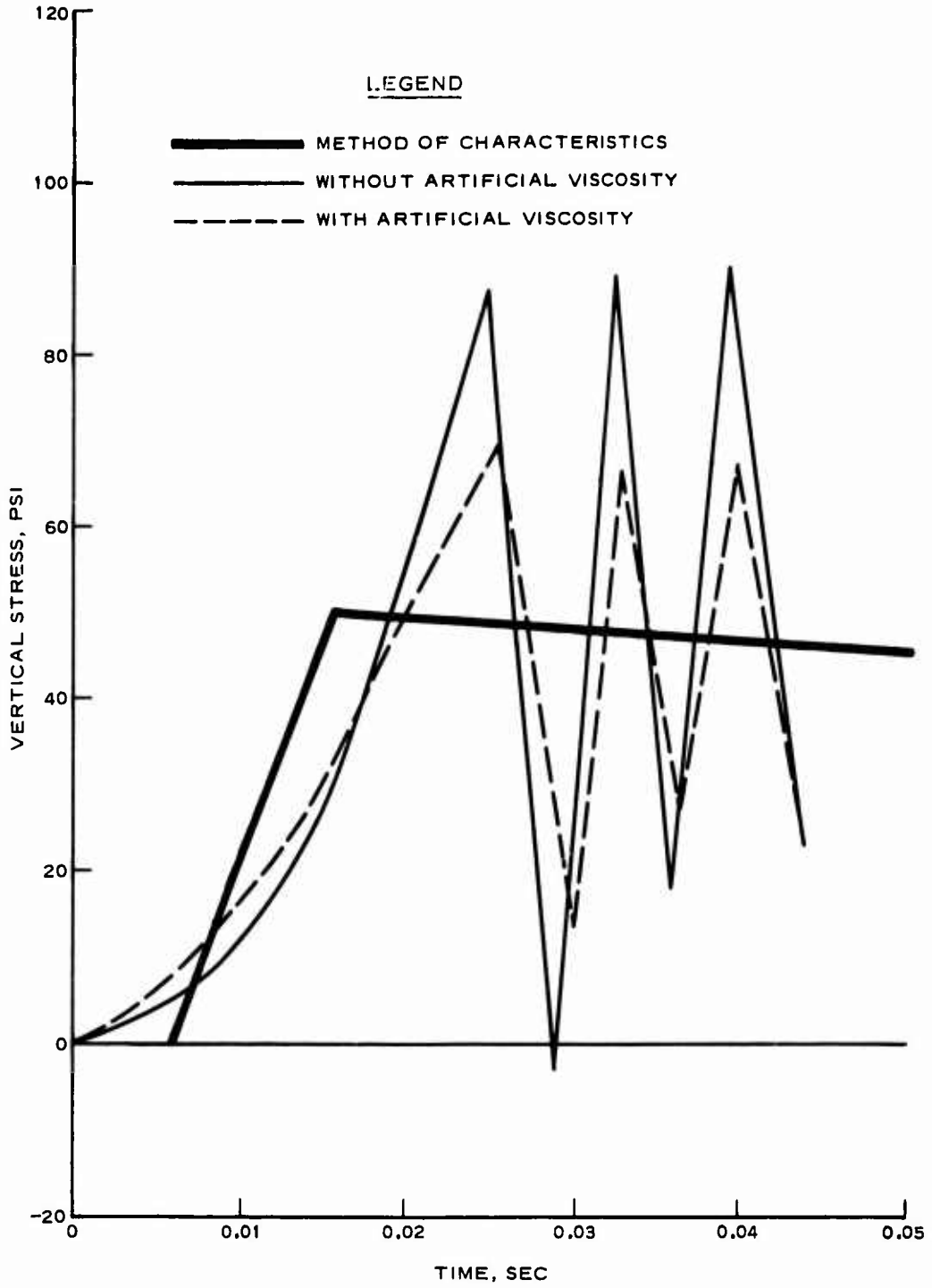

Figure B1. Comparison of calculated vertical stress time histories at the 1.25-ft depth from the loose shale 1D calculations (with and without artificial viscosity) with that calculated for this depth by the method of characteristics (assuming a linear stress-strain curve whose slope is the secant modulus to peak stress)

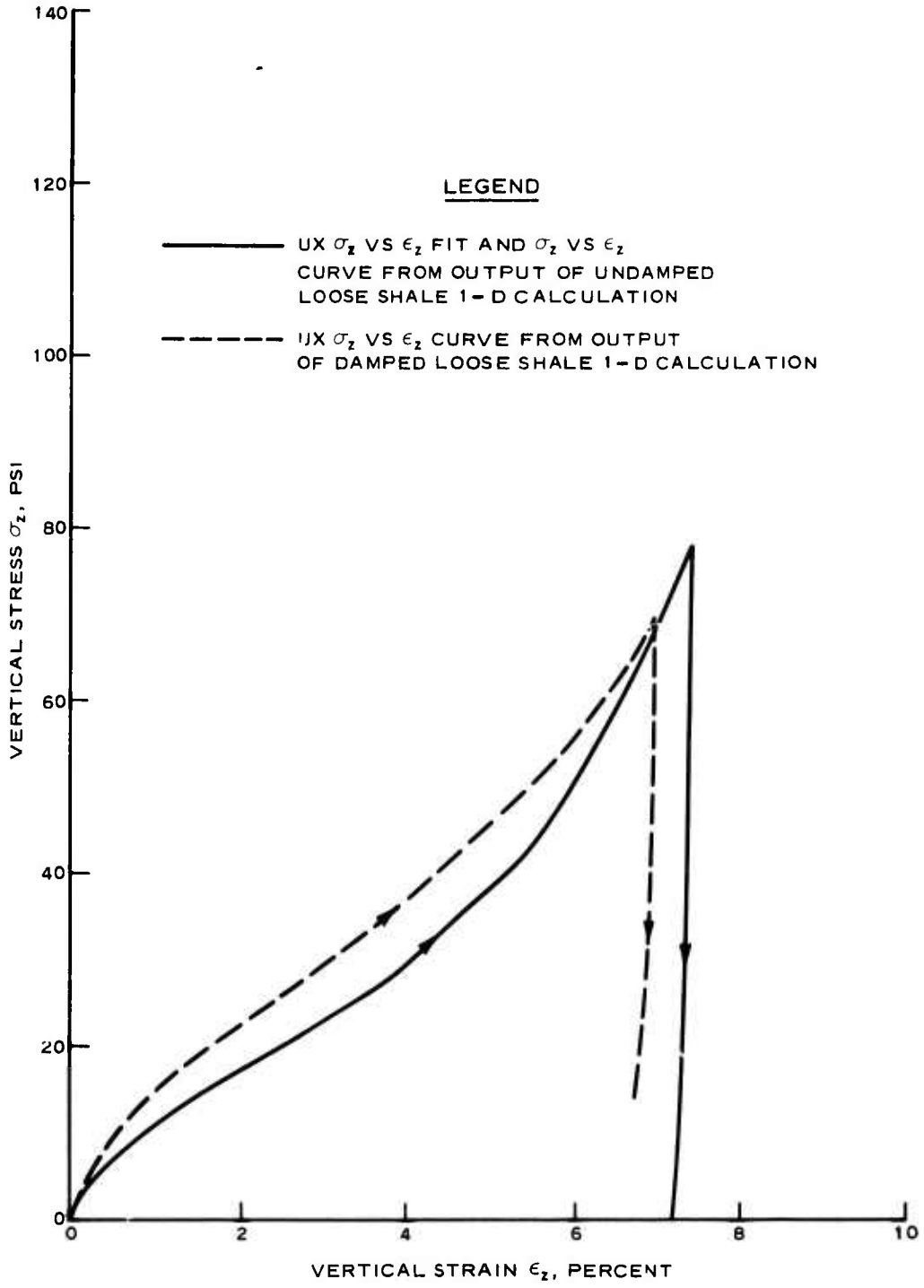

Figure B2. Comparison of UX stress-strain cap fit with UX stress-strain output from loose shale 1D calculations with and without artificial viscosity

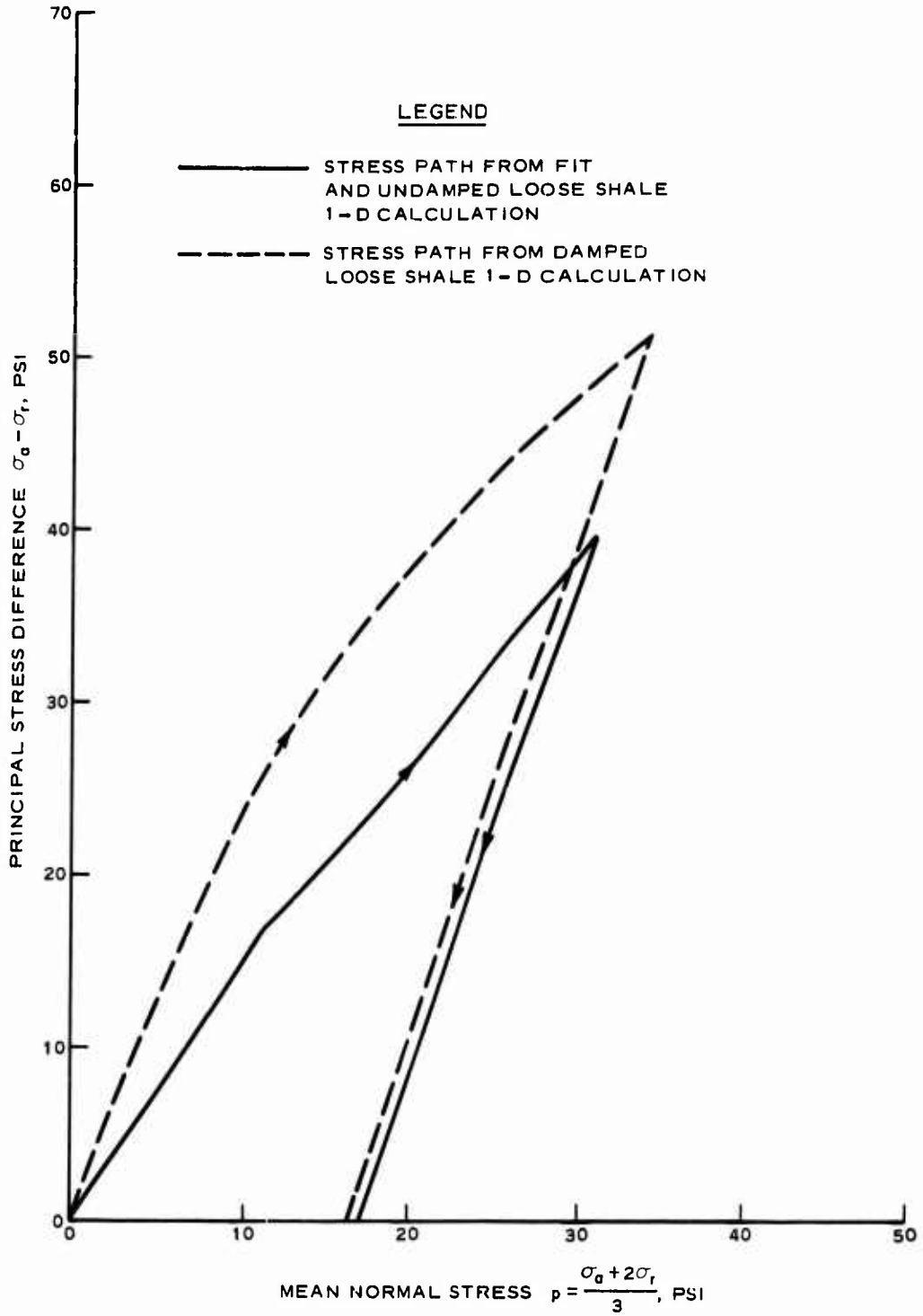

Figure B3. Comparison of UX stress-path cap fit with stress-path output from loose shale 1D calculations with and without artificial viscosity

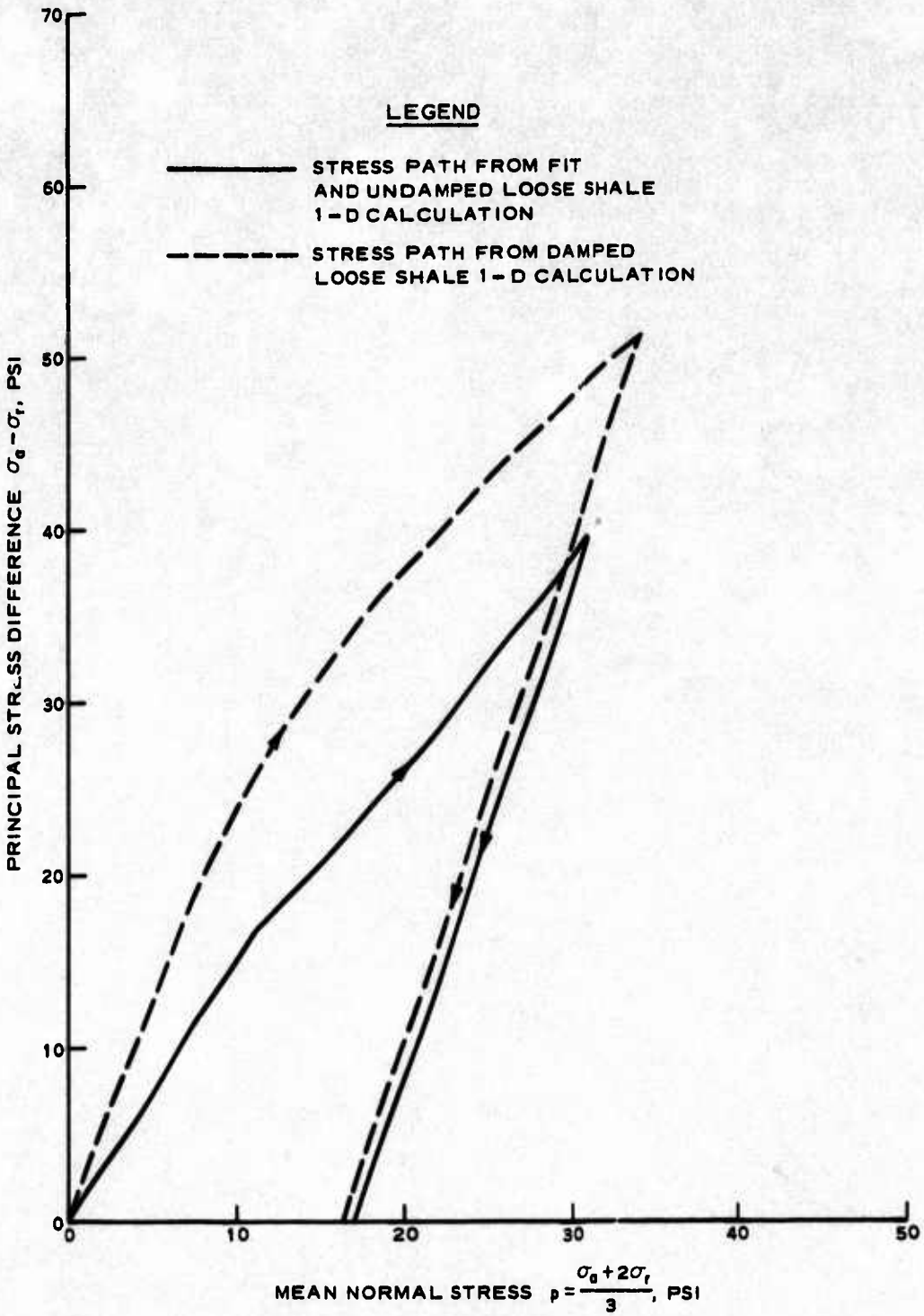

Figure B3. Comparison of UX stress-path cap fit with stress-path output from loose shale 1D calculations with and without artificial viscosity

In accordance with ER 70-2-3, paragraph 6c(1)(b), dated 15 February 1973, a facsimile catalog card in Library of Congress format is reproduced below.

Windham, Jon Enrique
Effect of backfill compaction on design criteria for hardened facilities: results of soil-structure interaction calculations for dry types I and II backfill materials, by Jon E. Windham. Vicksburg, U. S. Army Engineer Waterways Experiment Station, 1976.
1 v. (various pagings) illus. 27 cm. (U. S. Waterways Experiment Station. Technical report S-76-4)
Prepared for Office, Chief of Engineers, U. S. Army.
Project AT60, Task 01, Work Unit 001.
Includes bibliography.

1. Backfills. 2. Compaction (Soils). 3. Constitutive properties. 4. Dynamic loads. 5. Finite element method. 6. Protective structures. 7. Soil-structure interaction. 8. Underground structures. I. U. S. Army. Corps of Engineers (Series: U. S. Waterways Experiment Station, Vicksburg, Miss. Technical report S-76-4)
TA7.W34 no.S-76-4